

A!

**Aalto University
School of Chemical
Engineering**

Katarzyna Wojdalska

FABRICATION OF WEARABLE PRESSURE AND STRAIN SENSORS

Master's Programme in Chemical, Biochemical and Materials Engineering
Major in Functional Materials

Master's thesis for the degree of Master of Science in Technology submitted
for inspection, Espoo, 18 June, 2021.

Supervisor

Asst. Prof. Jaana Vapaavuori

Instructor

D.Sc. Fevzihan Basarir



Author Katarzyna Wojdalska

Title of thesis Fabrication of wearable pressure and strain sensors

Degree Programme Master's programme in Chemical, Biochemical and Materials Engineering

Major Functional Materials

Thesis supervisor Asst. Prof. Jaana Vapaavuori

Thesis advisor(s) / Thesis examiner(s) D.Sc. Fevzihan Basarir

Date 18.06.2021

Number of pages 98

Language English

Abstract

Wearable sensors attract significant attention due to their potential applications especially in personal health monitoring, health data collection and wearable electronics integrated in smart clothing. Breathable, biocompatible, stretchable sensors are easily skin-mountable and together with sensors embedded in fabrics, open up possibilities for real-time measurements of health and wellness without hindering comfort of the users. Thus, it comes as no surprise that within the next four years, the global wearable sensors market size is predicted to be worth \$2.9 billion. Commonly recognized main classes of pressure sensors are capacitive, piezoelectric and piezoresistive sensors. It has to be acknowledged that among these categories, capacitive pressure sensors exhibit smaller temperature drift, higher accuracy, lower consumption, usually a more robust structure, and less sensitivity to environmental effects like humidity. What is more, capacitive sensors provide a promising solution towards highly sensitive pressure sensors. In this report, introduction, fabrication, and characterization of three classes of wearable capacitive pressure sensors and two classes of wearable capacitive strain sensors are present. The following categories of the sensors were distinguished: yarn-based, textile-sandwiched, and silver nanowire (AgNW)-based sandwich-type. As a dielectric layer, polydimethylsiloxane (PDMS) was utilized and as conductive component silver-coated nylon yarns or AgNWs were used. In the first approach, 8 iterations before the final pressure sensor prototype were completed. The leading prototype exhibits overall change in capacitance of 18% and sensitivity of 0.02 kPa^{-1} upon applying pressure in the range from 0.2 kPa to 9.5 kPa. In the second approach, 14 pressure sensing devices iterations were assembled, and the top-notch prototype shows 37% of capacitance change and 0.12 kPa^{-1} of sensitivity. Lastly, two pressure sensors were created in the third category and the surpassing iteration demonstrates increase of capacitive response of 22% and sensitivity of 0.04 kPa^{-1} . Consequently, two proof of concept (POC) strain sensors complementary to the two first classes were fabricated. Together with aforementioned pressure sensing devices, realization of multifunctional sensors becomes achievable. Obstacles and insights from all experiments were collected, and finally recommendation and future vision were suggested. Further research focusing mostly on scaling up the samples, selection and impact of other dielectric materials, like wool, and their porosity caused by template choice, e.g., PDMS foam based on a nickel template, should be carried out.

Keywords multifunctional capacitive sensors, wearable pressure sensor, wearable strain sensor, textile-integrable sensor, yarn-based sensor, sandwich-type sensor, AgNW-based sensor, cellulose hydrogel, nanocellulose film, Spandex, PDMS, silver-coated nylon yarns, weaving

Table of Contents

Preface.....	
Symbols and Abbreviations	
1 Introduction.....	1
2 Literature review.....	3
2.1 Wearable pressure sensors.....	3
2.1.1 Pressure regimes	3
2.1.2 Key parameters associated with pressure sensors	4
2.1.3 Categories	4
2.1.3.1 Capacitive pressure sensors.....	5
2.1.3.2 Piezoresistive pressure sensors.....	7
2.1.3.3 Piezoelectric pressure sensors.....	8
2.1.3.4 Others	9
2.2 Literature review of reported capacitive pressure sensors.....	9
2.2.1 Approach 1 – Wearable yarn-based pressure sensors	10
2.2.1.1 Example 1 – Graphene oxide (GO)-doped polyurethane (PU) nanofiber core-spun yarns wounded around an elastic thread.....	10
2.2.1.2 Example 2 – PU yarn coiled with silk fibers and coated with silver nanowires encapsulated with Ecoflex.....	13
2.2.2 Approach 2 – Wearable textile-sandwiched pressure sensors.....	16
2.2.2.1 Example 1 – Photo-curable ion-enhanced fluorinated elastomers	16
2.2.2.2 Example 2 – Porous Ecoflex-multi-walled carbon nanotube (MWCNT) composite (PEMC) sandwiched in fabric electrodes	19
2.2.3 Approach 3 – Wearable AgNW-based sandwich-type pressure sensor	23

2.2.3.1 Example 1 – Ecoflex sandwiched in between PDMS layers patterned with AgNWs.....	23
2.2.3.2 Example 2 – Porous acrylic elastomer layer sandwiched between PU films patterned with AgNWs.....	26
2.3 Strain sensors.....	28
2.3.1 Key parameters	28
2.3.2 Categories	28
2.3.2.1 Capacitive strain sensors	28
2.3.2.2 Resistive strain sensors	29
2.3.2.3 Piezoelectric strain sensors	29
2.3.2.4 Others	30
2.4 Literature review of reported capacitive strain sensors	31
2.4.1 Approach 1 – Wearable yarn-based strain sensors	31
2.4.1.1 Example 1 – Silver-coated nylon fibers wrapped with cotton fibers	31
2.4.1.2 Example 2 – Rubber fibres wrapped with multiwall carbon nanotube sheet (NTS) layers	34
2.4.2 Approach 2 – Wearable textile-sandwiched strain sensors	36
2.4.2.1 Example 1 – PDMS sandwiched between CNTs films	36
2.4.2.2 Example 2 – Genus structures with metallic seeds on cotton fabrics	38
2.5 Textile environment.....	41
3 Experimental	45
3.1 Sample preparation.....	45
3.1.1 Wearable pressure sensors.....	45
3.1.1.1 Approach 1 – Wearable yarn-based pressure sensors	46

3.1.1.2	Approach 2 – Wearable textile-sandwiched pressure sensors	49
3.1.1.3	Approach 3 – Wearable AgNW-based sandwich-type pressure sensor	51
3.1.2	Wearable strain sensors	53
3.1.2.1	Approach 1 – Wearable yarn-based strain sensors.....	53
3.1.2.2	Approach 2 – Wearable textile-sandwiched strain sensors	54
3.2	Weights	54
3.3	Characterization methods.....	57
4	Results and Discussion.....	58
4.1	Wearable pressure sensors.....	58
4.1.1	Approach 1 – Wearable yarn-based pressure sensors	58
4.1.1.1	Comparison of the suitability of 1-ply versus 4-ply silver-coated nylon yarns and summary of all coating attempts.....	58
4.1.1.2	1 st and 2 nd prototypes – Thick PDMS coated yarns by using brush painting	64
4.1.1.3	3 rd , 4 th , and 5 th prototypes – Contact point made of two yarns coated with PDMS of different thicknesses.....	64
4.1.1.4	6 th prototype – Thin PDMS coated yarns by using brush painting woven into a fabric	65
4.1.1.5	7 th , 8 th , and 9 th prototype – Thin PDMS coated yarns by using brush painting paired with silver-coated nylon yarns	66
4.1.2	Approach 2 – Wearable textile-sandwiched pressure sensors.....	69
4.1.2.1	1 st , 2 nd and 3 rd prototype – Creating simple 2x2 matrixes with the desired amount of yarns.....	69
4.1.2.2	4 th prototype – Pre-curing PDMS and placing the fabric on top to improve the stability of the device	72

4.1.2.3	5 th prototype – Creating a more stable fabric by adding yarns of another material in between the silver coated nylon yarns	74
4.1.2.4	6 th , 7 th and 8 th prototype – Introducing a porous PDMS layer ..	76
4.1.2.5	9 th , 10 th and 11 th prototype – Influence of the number of yarns utilizing PDMS foam as the dielectric layer.....	78
4.1.2.6	12 th , 13 th and 14 th prototype – Influence of the number of yarns utilizing PDMS as the dielectric layer.....	79
4.1.3	Approach 3 – Wearable AgNW-based sandwich-type pressure sensor	81
4.1.3.1	Substrate materials.....	81
4.1.3.2	Prototypes	84
4.2	Wearable strain sensors	86
4.2.1	Approach 1 – Wearable yarn-based strain sensors	86
4.2.2	Approach 2 – Wearable textile-sandwiched strain sensors	87
5	Conclusions.....	89
6	References	91

Preface

Before you lies the dissertation “Fabrication of wearable pressure and strain sensors”, the basis of which is design, assembly and characterization of three capacitive wearable pressure and proof-of-concepts of two capacitive wearable strain sensors. The thesis has been written to fulfil the graduation requirements of the Functional Materials major in the Chemical, Biochemical and Materials Engineering study program at Aalto University. I was engaged in conducting research from the middle of January to the end of May 2021 in the Multifunctional Materials Design research group in the School of Chemical Engineering. Other elements of the process like writing, revising, and delivering the oral presentation proceeded until June 2021. This work made use of Aalto University A Grid, OtaNano, and RawMatters infrastructure. Essential components required in the experiments were delivered by the School of Arts, Design and Architecture and Aalto Bioproduct Centre.

My research question was formulated together with my supervisor, Asst. Prof. Jaana Vapaavuori, and advisor, D.Sc. Fevzihan Basarir. The research was challenging in its complexity, but the extensive investigation allowed me to identify the crucial problems, answer the identified questions, and propose a vision for future iterations. Fortunately, both my supervisor and advisor were always available and willing to answer my queries.

I would like to thank Asst. Prof. Jaana and D.Sc. Fevzihan for their excellent guidance and support during the process. Asst. Prof. Jaana is an extraordinary professional who believed in me and significantly boosted my development. In truth, I could not have achieved my current level of success without a strong reliance on my advisor and supervisor. I am grateful for my grandmother Bozena who acted as a wise counsel and thus, lent a helping hand to the choice of this stimulating topic that ignited my passion towards wearable technology. At this

point, I would extend thank to my whole family: my mother, uncle, and grandfather. I was privileged to receive from my family members financial support that not many Polish students can secure. I also wish to thank Maija Vaara for help in weaving structures and sharing her knowledge in handcraft, and D.Sc. Joice Kaschuk for preparation of cellulose hydrogels. I want to show appreciation to all members of the Multifunctional Materials Design research group and especially Yujiao Dong, who I benefitted from debating issues with. Aalto University employees, and particularly School of Chemical Engineering employees, deserve a particular note of thanks: Without your thoughtful actions during the coronavirus pandemic, I would not be able to carry out the research at all. Finally, I would like to thank my Polish friends Adrian, Karol, Magdalena, Marek, and international friends Anhelina, Arunima, Madina, Meghna, Rachhek, Rafael, Shreya, and Waliyah for keeping me motivated.

Symbols and Abbreviations

2D = Two dimensional

3D = Three dimensional

A = Area of electrodes

AC = Alternating current

Ag = Silver

AgNW = Silver nanowire

Al = Aluminum

BP = Blood pressure

C = Capacitance

C_0 = Initial capacitance value (without the applied pressure)

Ca = Calcium

CNT = Carbon nanotube

Cu = Copper

d = Dielectric layer thickness

d' = Dielectric layer thickness after compression

DBP = Diastolic blood pressure

ECG = Electrocardiogram

EGaIn = Eutectic gallium-indium

ELD = Electroless deposition

ϵ_0 = Dielectric constant of vacuum

ϵ_r = Dielectric constant of relative permittivity of dielectric media

f = Frequency

FBG = Fiber Bragg Grating

GaN = Gallium nitride

GF = Gauge factor

HR = Heart rate

ICSS = Interdigitated capacitive strain sensor

LOD = Limit of detection
MEMS = Micro Electro Mechanical Systems
MWCNT = Multi-walled carbon nanotube
-NCO = Isocyanate functional group
NFC = Nanofibrillar cellulose
-NHCOO = Carbamate functional group
NP = Nanoparticle
NTS = Carbon nanotube sheet
OFET = Organic field-effect transistor
OM = Optical microscopy
P = (Quantitative) Applied pressure
P(VDF-TrFE) = Poly(vinylidene fluoride-co-trifluoro-ethylene)
PAMD = Polymer-assisted deposition
PDMS = Polydimethylsiloxane
PEDOT = Poly(3,4-ethylenedioxythiophene)
PEMC = Porous Ecoflex-multi-walled carbon nanotube composite
POC = Proof of concept
PP = Polypyrrole / Polypropylene
PS-b-P2VP = Polystyrene-b-poly(2-vinylpyridine)
PU = Polyurethane
PUD = Polyurethane Dispersion
PUU = Polyurethane urea elastomer
PVDF = Polyvinylidene fluoride
PVDF-HFP = Poly(vinylidene fluoride-cohexafluoropropene)
S = Sensitivity
SAW = Surface Acoustic Wave
SBP = Systolic blood pressure
SEM = Scanning Electron Microscopy
SEM-EDS = Scanning Electron Microscopy-Energy Dispersive X-Ray Spectroscopy
SEMC = Solid part of the Ecoflex-multi-walled carbon nanotube composite

Si = Silicon

SWNT = Single-walled nanotube

TBAP = Tetrabutylammonium perchlorate

TEMPO-CNF = 2,2,6,6-tetramethylpiperidine-1-oxyl radical-cellulose nanofibers

X = Quantitative output signal

Z = Strain sensitivity

ZnO = Zinc oxide

ϵ = Strain

1 Introduction

During the recent years, robotic systems, prosthetics, and wearable medical devices attracted significant interest due to their potential in realization of highly sensitive and skin-mountable sensors.¹ Especially, breathable, biocompatible and stretchable sensors became desired, because of their efficient applications in personal health monitoring, health data collection and wearable electronics integrated in smart clothing.^{2,3} Such wearable sensors embedded into fabrics can easily meet the afore-mentioned requirements and thus, open up possibilities for real-time measurements of health and wellness like detection of running or jumping movements and body functions like heart rate.^{1,2} Therefore, it should not feel surprising that the wearable sensors market is predicted to be worth \$2.86 billion by 2025.⁴

Upon now, capacitive, piezoelectric, and piezoresistive sensors are commonly recognized as three main classes of pressure sensors. Among these types of pressure sensors, capacitive pressure sensors exhibit smaller temperature drift, higher accuracy, lower power consumption, more robust structure, and less sensitivity to environmental effects like humidity.^{5,6} In comparison, piezoelectric sensors are less suitable for health monitoring applications and wearable electronics as they are not sensitive enough to gentle touch. At this point, it is necessary to highlight that in wearable applications detection of low pressure regime (<10 kPa) and medium pressure regime (10-100 kPa) corresponding to mild touch, suited for object manipulation and human body circulation, is particularly needed for a broad range of applications.⁷ On the other hand, piezoresistive sensing devices, which can detect both low- and high-pressure regimes, show high sensitivity and their fabrication is facile. Nevertheless, multiple factors like temperature and humidity affect changes in electrical resistance what results in lower reliability and higher susceptibility to electrical resistance

hysteresis.³ Therefore, capacitive sensors provide a promising solution towards highly sensitive pressure sensors.

In this work, three wearable capacitive pressure sensors were fabricated and characterized. Taking this opportunity, it is important to briefly describe the working principle of this class of sensors. A typical capacitive device requires a dielectric layer sandwiched between two electrodes. The distance between these electrodes influences the capacitance value. Thus, when pressure or strain is applied, and electrodes come closer, the capacitance increases.⁷ Another possible manipulation method of capacitance is alternation of the contact area size. To broaden the research scope of the thesis and to enable potential fabrication of wearable multifunctional sensors, two POC prototypes of wearable capacitive strain sensors were developed. All the aforementioned sensing devices were categorized into three classes: yarn-based, textile-sandwiched, and AgNW-based sandwich-type. Literature review of the current state-of-the-art in both pressure and strain sensors was presented and their working principles including key parameters were described. Furthermore, textile environment was depicted. All prototypes exhibit reasonable sensitivity, large overall increase in capacitance, and allow realization of multifunctional and highly sensitive in the low weight region sensors leaving space for development.

2 Literature review

2.1 Wearable pressure sensors

To understand the topic of pressure sensing devices thoroughly and contextualize the current work, their categories based on the transduction mechanism, key parameters, pressure regimes, and possible applications must be discussed.

2.1.1 Pressure regimes

To gain a better understanding specific pressure distributions and the relevant sensing devices, the pressure regime division into four categories: ultra-low, subtle, low, and medium, and their potential applications is presented in Table 1. Typical object manipulation, normal touch and human body circulation are distributed mainly in low and medium pressure regimes.⁷ For example, pressure generated by human touch varies from 1 to 10 kPa,³ pressure of the carotid pulse (pulse recorded at the neck over the carotid artery)⁸ amounts to around 1.3 kPa, and pressure of butterfly weight to 0.003 kPa.³

Table 1. Classification of pressure regimes and potential applications in each category.⁷

Value	Regime	Application
<1 Pa	<i>Ultra-low pressure</i>	<i>Acoustic pressure, hear aids, microphone</i>
1 Pa – 1 kPa	<i>Subtle pressure</i>	<i>Ultra-sensitive e-skin, touch screens</i>
1 kPa – 10 kPa	<i>Low pressure</i>	<i>Daily activities, medical diagnosis</i>

10 kPa – 100 kPa *Medium pressure* *Health monitoring,
weight and heights
measurement*

2.1.2 Key parameters associated with pressure sensors

In order to evaluate the performance of sensing devices, the following key parameter have to be considered: sensitivity, response time, limit of detection (LOD), stability, and linearity. LOD denotes the lowest pressure which generates a detectable change in signal. This pressure can be referred to as threshold pressure. Linear (%) operation range is preferred in such devices due to their more accurate and reliable responses. Response time describes the amount of time that passed between the input pressure and production of a stable signal output. Sensitivity determines the accuracy of the measurement and effectiveness of the sensor. Eq. 1 shows the calculation of the sensitivity S

$$S = \frac{dX}{dP} \quad \text{Eq. 1}$$

where S is sensitivity, X is the quantitative output signal, and P is the quantitative applied pressure.⁷ Thus, sensitivity S of a capacitive pressure sensor can be also determined by the Eq. 2.

$$S = \frac{d(\frac{\Delta C}{C_0})}{dP} \quad \text{Eq. 2}$$

where C is the value of capacitance of the device with the applied pressure, C_0 is the value of the capacitance without the applied pressure and P is the applied pressure.⁹ This means that sensitivity can be obtained by reading the slope of the regression line of the measured capacitance values.¹⁰

2.1.3 Categories

Conventionally, three main categories of pressure sensors are distinguished, namely capacitive, piezoresistive, and piezoelectric pressure sensors. Schematic explanation of their working principles is presented in Figure 1.⁷ In this

subchapter, working mechanisms and material examples of these three categories are described.

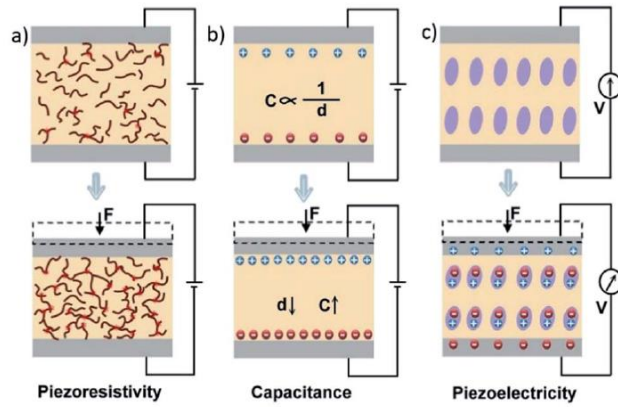


Figure 1. Schematic illustrations of working purposes of the main pressure-sensors classification into a) piezoresistive, b) capacitive, c) and piezoelectric type. Figure reprinted from the article “Advances of flexible pressure sensors toward artificial intelligence and health care applications” written by Zang et al.⁷

2.1.3.1 Capacitive pressure sensors

The ability to store electrical charge is referred to as capacitance.⁷ Eq. 3 shows the calculation of the capacitance C value

$$C = \epsilon_0 \cdot \epsilon_r \cdot \frac{A}{d} \quad \text{Eq. 3}$$

where C is capacitance, ϵ_0 is the dielectric constant of a vacuum, ϵ_r is the dielectric constant of the relative permittivity of dielectric media, A is the area of electrodes, and d is the dielectric layer thickness.¹¹ In this equation, ϵ_0 and ϵ_r are constants, whereas A and d can be altered by external forces, like applied pressure, and thus, their values change. Eq. 4 shows the calculation of the value of normalized capacitance change that will be often used in this work

$$\frac{\Delta C}{C_0} = \frac{\epsilon' d}{\epsilon d'} - 1 \quad \text{Eq. 4}$$

where C is capacitance, ϵ and ϵ' are dielectric constants, d is the distance between electrodes before compression, and d' is the distance between electrodes after compression.

Tracking of changes in capacitance is widely utilized in pressure sensors based on organic field-effect transistors (OFETs), controlling the oscillator's frequency, and varying the alternating-current (AC) coupling.⁷ Exemplary capacitance pressure sensors including materials and key parameters like sensitivity, LOD, response time, and operating voltage are shown in Table 2. For instance, sensitivity of alumina ceramic amounts to 0.0035 kPa^{-1} , whereas sensitivity of PDMS/polyvinylidene fluoride (PVDF) amounts to 30.2 kPa^{-1} . On the other hand, LOD of alumina ceramic amounts to 100 kPa which is much higher than LOD of PDMS/PVDF amounting to 0.7 Pa .^{12,13} The highest response time of 250 ms from the presented examples shows the sensor consisting of silk coiled yarns/AgNWs.² The lowest response time that is less than 10 ms shows PDMS/rubrene.¹⁴

Table 2. Examples of capacitance pressure sensors.

Material	Sensitivity	LOD	Response time / relaxation	Operating voltage	Ref.
Alumina ceramic	0.0035 kPa^{-1} ¹	100 kPa	-	-	12
Gallium nitride (GaN)	0.0086 kPa^{-1} ¹	-	-	-	15
Graphene/porous nylon networks	0.33 kPa^{-1}	3.3 Pa	$<20 \text{ ms}$	5 kV	16
PDMS/PVDF	30.2 kPa^{-1}	0.7 Pa	25 ms	-	13
PDMS/rubrene	0.55 kPa^{-1}	3 Pa	$<10 \text{ ms}$	50 V	14
Polystyrene-<i>b</i>- poly(2- vinylpyridine) (PS- <i>b</i>-P2VP)	1.76 kPa^{-1}	-	$<17 \text{ ms}$	50 V	17
Silk coiled yarns/AgNWs	0.136 kPa^{-1}	-	0.25 s	-	2

2.1.3.2 Piezoresistive pressure sensors

Piezoresistive is defined as a resistivity change upon strain or deformation. Such change in contact resistance between two materials is responsible for generation of electrical signal change. Piezoresistive sensors are characterized by an uncomplicated device structure, quick response speed, high sensitivity, achievable high pixel density, and a simple read-out mechanism in a large pressure range.⁷ Examples of piezoresistive pressure sensors including materials they were made of and their key parameters are presented in Table 3. An interesting case is polypyrrole (PPy) which exhibits sensitivity of 133.1 kPa^{-1} , LOD of 0.8 Pa and response time of 50 ms. Such high sensitivity was achieved due to patterning the surface of the elastic microstructured conducting polymer of interconnected PPy hollow-sphere structures.¹⁸ In contrary, the lowest sensitivity value presents PDMS/carbon nanotube (CNT).¹⁹ The longest response time shows PDMS/poly(3,4-ethylenedioxothiophene) (PEDOT) : Polystyrene sulfonate (PSS)/polyurethane dispersion (PUD) and the shortest PDMS/single-walls nanotubes (SWNTs) that also show the smallest LOD.^{20,21} The largest LOD shows graphene.²²

Table 3. Examples of piezoresistive pressure sensors.

Material	Sensitivity	LOD	Response time / relaxation	Operating voltage	Ref.
Graphene	-	100 Pa	9 s	2.5 V	²²
Nanohair	$11.35 \mu\text{S}$ kPa^{-1}	5 Pa	50 ms	-	²³
PDMS/CNT	0.23 kPa^{-1}	50 Pa	$\leq 125 \text{ ms}$	-	¹⁹
PDMS/PEDOT : PSS/PUD	10.32 kPa^{-1}	23 Pa	200 ms	-	²⁰
PDMS/SWNTs	1.8 kPa^{-1}	0.6 Pa	$< 10 \text{ ms}$	-	²¹
PPy	133.1 kPa^{-1}	0.8 Pa	50 ms	-	¹⁸

2.1.3.3 Piezoelectric pressure sensors

Piezoelectricity refers to generation of electrical charges upon mechanical stress. Such appearance of electric dipole moments occurs in certain solid materials like crystals and particular ceramics. Piezoelectric materials exhibit fast response time and high sensitivity. Thus, they are commonly applied in detection of dynamic pressures e.g., in identification of sound vibrations. Moreover, piezoelectrics are suitable for sensing devices that consume low amounts of power and are self-propelling.⁷ However, these materials are not the most facile to apply into textiles where some deformation capacity is required. Examples of piezoelectric pressure sensors can be found in Table 4. Table 4 lists a few material types of such piezoelectric sensors and presents the following key parameters: sensitivity, LOD, response time, and operating voltage. The longest known response time from the presented examples shows zinc oxide (ZnO) whereas the shortest – nanowires/graphene.^{24,25} The highest LOD of titanate/P(VDF-TrFE) amounts to 200 kPa whereas the lowest LOD of polypropylene (PP) amounts to 2 Pa.^{26,27} Most values of sensitivity are much lower than in previously described sensor classes.

Table 4. Examples of piezoelectric pressure sensors.

Material	Sensitivity	LOD	Response time / relaxation time	Operating voltage	Ref.
Nanowires/graphene	9.4×10^{-3} <i>kPa⁻¹</i>	-	5-7 ms	-	25
Poly(vinylidene fluoride-co-trifluoro- ethylene) (P(VDF- TrFE))	-	13.3 Pa	-	1 V	24

PP	0.001 kPa^{-1}	2 Pa	-	-	27
PVDF	2 V kPa^{-1}	1 kPa	-	-	28
Titanate/P(VDF-TrFE)	6.7×10^{-4}	200	-	15 V	26
ZnO	$2.1 \mu\text{S kPa}^{-1}$	3.5 kPa	0.15 s	1 V	24

2.1.3.4 Others

Besides the prior transduction methods, there are also optical, pressure-induced frequency change, and triboelectric mechanisms. However, these classes are rarer on the market due to their lower efficiency, higher price, or less suitable working mechanisms.

An optical sensor constitutes of the transmission media, the detector, and the light source. Main signals of the applied pressure are light intensity and wavelength. This category is envisioned to be applied in touch screens of tablets and smart phones. In resonant pressure sensors, pressure-induced resonant frequency change plays the most important role. The resonant frequency is determined by the media density of the resonating object. This technology can be used in combination with force collectors. For triboelectric sensors, contract electrification is used to produce a voltage signal as a reaction to physical contact without reliance on an external power supply.⁷

2.2 Literature review of reported capacitive pressure sensors

In this subchapter, exemplary wearable capacitive pressure sensors are presented. Previously developed capacitive sensors that were integrated into textiles have adopted mainly woven or parallel plate capacitor structures. To fulfill the requirement of a sufficient surface area, textile yarns are often embedded in planar polymer matrixes what hinders integration with fabrics and clothing.

Additionally, planar devices are often better suited for sensing of pressure than strain.¹¹ This review focuses on yarn-based and sandwich-structured types of capacitive pressure sensors. In the reported examples, researchers wove shell-insulated conductive yarns or sandwiched dielectric layers between two pieces of conductive fabrics or created Ag-NW-based sandwich-type sensors.

2.2.1 Approach 1 – Wearable yarn-based pressure sensors

2.2.1.1 *Example 1 – Graphene oxide (GO)-doped polyurethane (PU) nanofiber core-spun yarns wounded around an elastic thread*

You *et al.* developed a stretchable capacitive electronic skin by weaving Ni-coated cotton yarns coated with GO-doped PU nanofibers around an elastic thread. In this example, the Ni-coated cotton yarn acts as the conductive electrode and the nanofiber coating serves as a dielectric. The developed sensing device shows sensitivity of 1.59 N^{-1} under 0.3 N, short response time below 50 ms, sensing range from 0-5 N and a low LOD of 0.001 N. It can be applied as an electronic fabric suitable for voice recognition, finger and wrist muscle movements, monitoring of airflow and noncontact proximity of fingers. Thus, it has potential to be used in humanoid robots and wearable electronic devices. Figure 2 presents the fabrication process steps needed to obtain such electronic skin and the final outcome. The manufacturing steps include: electroless deposition of nickel on Pristine cotton yarns, electrospinning of the conductive GO-doped PU nanofibers, wounding the core-spun yarns around an elastic thread, and weaving.²⁹

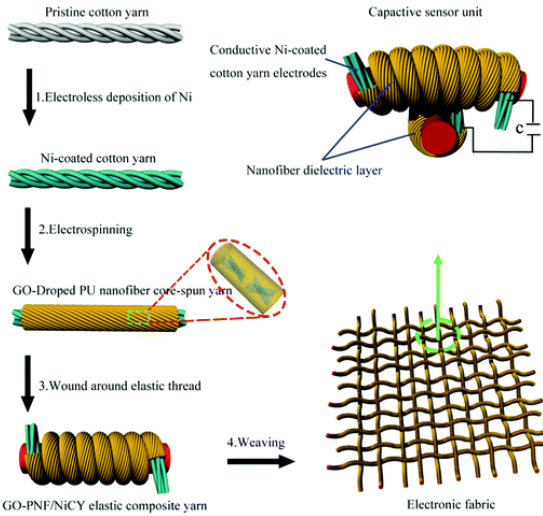


Figure 2. Fabrication steps of the capacitive pressure sensors consisting of a composite fiber coated with nanofibers wound helically around an elastic thread reprinted from the article “Stretchable capacitive fabric electronic skin woven by electrospun nanofiber coated yarns for detecting tactile and multimodal mechanical stimuli” written by You et al.²⁹

Figure 3a presents the capacitance change as a function of loading force of the fabricated sensor and two reference materials: PU nanofiber/copper (Cu) core-spun yarn and PU nanofiber/Ni-coated cotton yarns core-spun yarn. The resulting change in capacitance is largest in case of the reported sensing device. Its sensitivity in the lower loading force region until 0.3 N amounts to 1.59 N^{-1} what can be explained by increase in the contact area between two crossed yarn electrodes. In the loading-force region until 2 N the sensitivity value decreases to 0.54 N^{-1} as a result of simultaneous change in the distance between the electrodes and the permittivity due to driving out air of the gaps, whereas in the region above 2 N, the sensitivity was stable and low what was caused by the permittivity increase as the air was driven out between the coated nanofibers and the conductive cotton yarns by compression deformation. Figure 3b shows the capacitance change upon loading and unloading force. It can be concluded that the hysteresis is negligible. Figure 3c illustrates the capacitance changes as a function of time upon applying the following loads: 0.05 N, 0.1 N and 5 N. The

response of the sensing device is stable, continuous and there is no noise. Capacitance returned to 98% of the initial state after unloading.²⁹

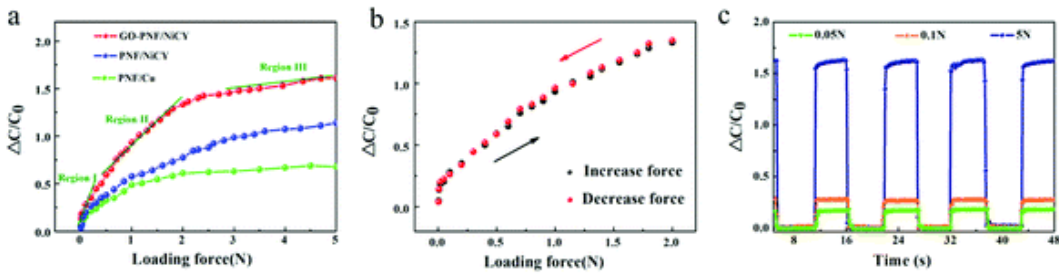


Figure 3. a) Changes in capacitance ($\Delta C/C_0$) presented as a function of loading force of the fabricated sensor and two other elastic composite yarns. b) Results from the loading-unloading force cycle test of the sensor unit. c) Capacitive response because of loading and unloading of 0.05 N, 0.1 N and 5 N force. All figures were reprinted from the article “Stretchable capacitive fabric electronic skin woven by electrospun nanofiber coated yarns for detecting tactile and multimodal mechanical stimuli” written by You et al.²⁹

Figure 4a presents changes in capacitance over time before and after repeated finger proximity to varying distances of 0, 3 and 7 cm from the surface of the electronic fabric. The value of capacitance for the 0 cm distance is 3 times larger than in case of 3 cm. Interestingly, Figure 4b illustrates the phenomenon of reduced capacitance, marked as black dotted box, resulting from electrical field disturbances upon approaching the fabric by the finger and applying pressure. Thus, the capacitance values increase upon physical pressing.²⁹

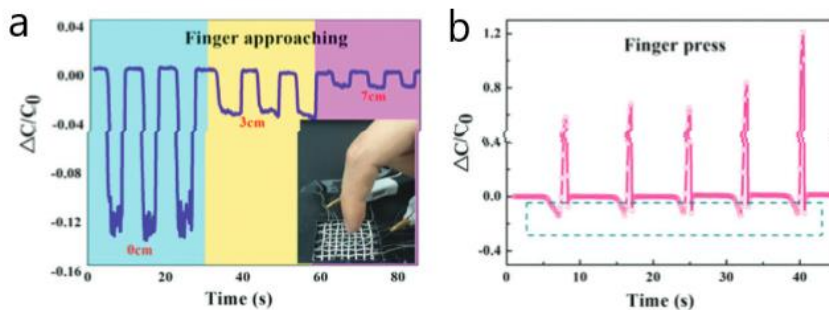


Figure 4. a) Capacitive responses at 0, 3 and 7 cm of a distance from the surface of the electronic fabric. b) Changes in capacitance of the fabricated sensor unit due to finger pressing. All figures were reprinted from the article

“Stretchable capacitive fabric electronic skin woven by electrospun nanofiber coated yarns for detecting tactile and multimodal mechanical stimuli” written by

You et al.²⁹

To study the pressure mapping function of the electronic fabric, experiments visible in Figure 5 were conducted. Figure 5 illustrates the photographs and force distributions of the fabricated electronic fabric upon placing a weight (20 g) and a C-shaped metal letter (6 g) on top of a 4 cm x 4 cm fabric. In the resulting 8 x 8 pixel sensor unit arrays, blue color indicates no change in capacitance, whereas red color corresponds to the largest growth. The array represents accurately the capacitive response arising from applying the weights.²⁹

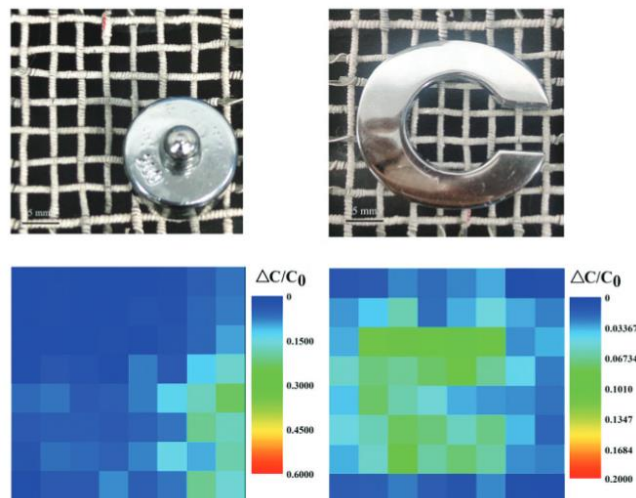


Figure 5. Photographs of an electronic fabric upon placing a weight (left) and a C-shaped metal letter (right) on top of it and their corresponding two-dimensional (2D) intensity profiles reprinted from the article “Stretchable capacitive fabric electronic skin woven by electrospun nanofiber coated yarns for detecting tactile and multimodal mechanical stimuli” written by You et al.²⁹

2.2.1.2 Example 2 – PU yarn coiled with silk fibers and coated with silver nanowires encapsulated with Ecoflex

Wu *et al.* reported a silk composite electronic textile sensor for both temperature and pressure sensing. In their work, PU yarns were coiled with silk fibers, coated with AgNWs, and afterwards with the elastomer called Ecoflex. The detailed

fabrication steps are shown in Figure 6. The AgNW layer acts in this case as an electrode, whereas Ecoflex as a dielectric layer. This setup comprise high sensitivity of 0.136 kPa^{-1} , low relaxation time of 0.25 s and high recycling rate of 5000.²

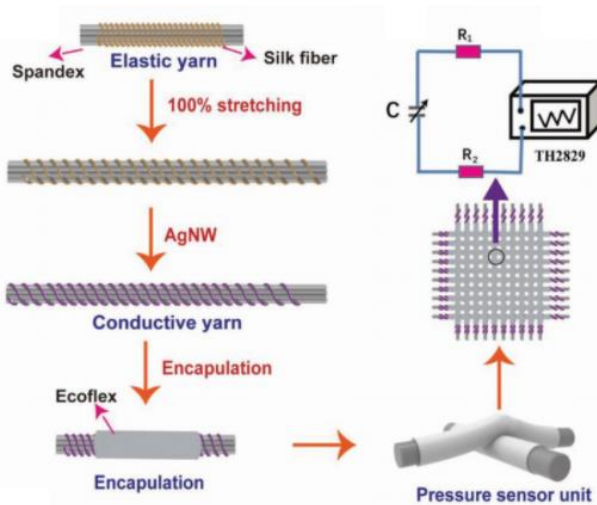


Figure 6. Fabrication steps of the pressure sensor based on AgNW. Spandex yarn was coiled with silk fibers, stretched, coated with AgNW for conductivity purposes, and eventually encapsulated with an Ecoflex layer. Figure was reprinted from the article “Silk Composite Electronic Textile Sensor for High Space Precision 2D Combo Temperature–Pressure Sensing” written by Wu et al.²

The fabricated pressure sensor was subjected to 5 cycles of the following forces: 0.005, 0.006, 0.02, 0.2, and 0.8 cN. Responses to these forces, which are stable and continuous, are presented in Figure 7.²

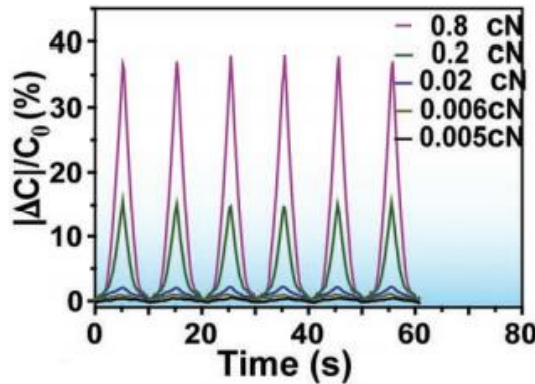


Figure 7. Capacitive changes in placing and removing of 0.005, 0.006, 0.02, 0.2, and 0.8 cN of the sensing device reprinted from the article “Silk Composite Electronic Textile Sensor for High Space Precision 2D Combo Temperature–Pressure Sensing” written by Wu et al.²

In this work, a textile combining both temperature and pressure sensors was created and tested. Figure 8 shows the response of this setup upon application of certain pressure and temperature. Each of the sensing units was affected mainly by its specific signal.²

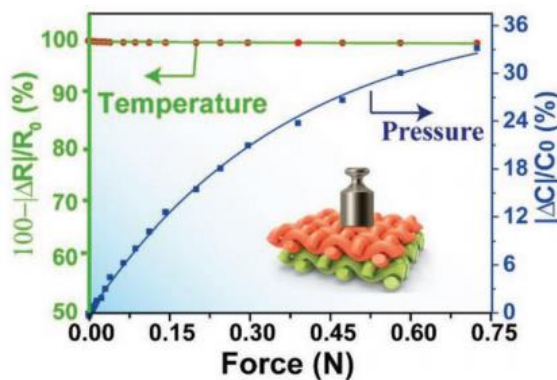


Figure 8. Responses of the temperature and pressure sensor due to touching and lifting a hot stage and applying different weights reprinted from the article “Silk Composite Electronic Textile Sensor for High Space Precision 2D Combo Temperature–Pressure Sensing” written by Wu et al.²

Figure 9 clearly illustrates the distribution of position-related three-dimensional (3D) pressure sensing due to loading of a heavy object. The detected force amounted up to 0.32 N. The higher the bar in the upper graph and the brighter the color in the bottom matrix, the higher the value of the applied pressure.²

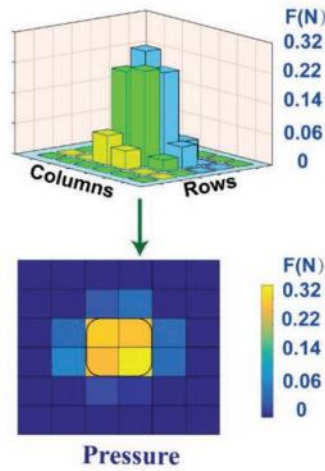


Figure 9. Illustration of weight distribution upon placing a cup on the pressure sensor reprinted from the article “Silk Composite Electronic Textile Sensor for High Space Precision 2D Combo Temperature–Pressure Sensing” written by Wu et al.²

2.2.2 Approach 2 – Wearable textile-sandwiched pressure sensors

2.2.2.1 Example 1 – Photo-curable ion-enhanced fluorinated elastomers

Chen *et al.* reported photo-curable ion-enhanced fluorinated elastomers for pressure-sensitive textiles. To fabricate a highly sensitive pyramid array of poly(vinylidene fluoride-co-hexafluoropropene) (PVDF-HFP) on textile visible in Figure 10, photo-cured PVDF-HFP and a transparent PDMS mold were used. A more detailed description of the fabrication process of the pressure sensor is visible in Figure 11. Ionic additive called tetrabutylammonium perchlorate (TBAP) further improved the sensitivity of the sensor as a result of enhanced dielectric constant of PVDF-HFP. Especially the addition of 2 wt% of the TBAP ions, improved the PDMS sensitivity significantly from 0.19 kPa^{-1} to 0.73 kPa^{-1} .³

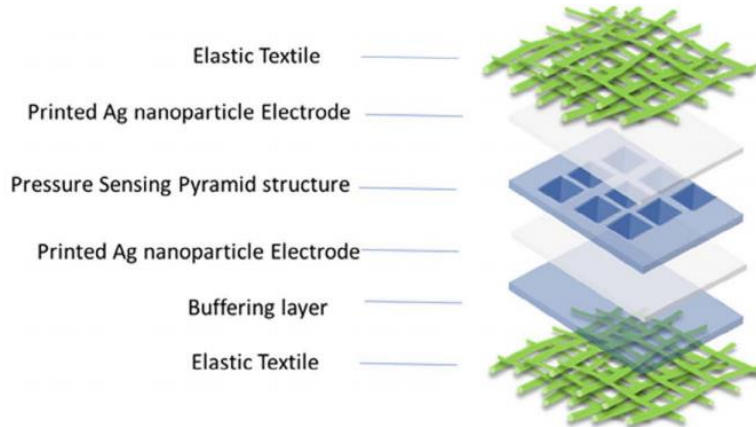


Figure 10. Scheme of the layers of the fabricated capacitive sensing device reprinted from the article “Photo-Curable Ion-Enhanced Fluorinated Elastomers for Pressure-Sensitive Textiles” written by Chen et al.³

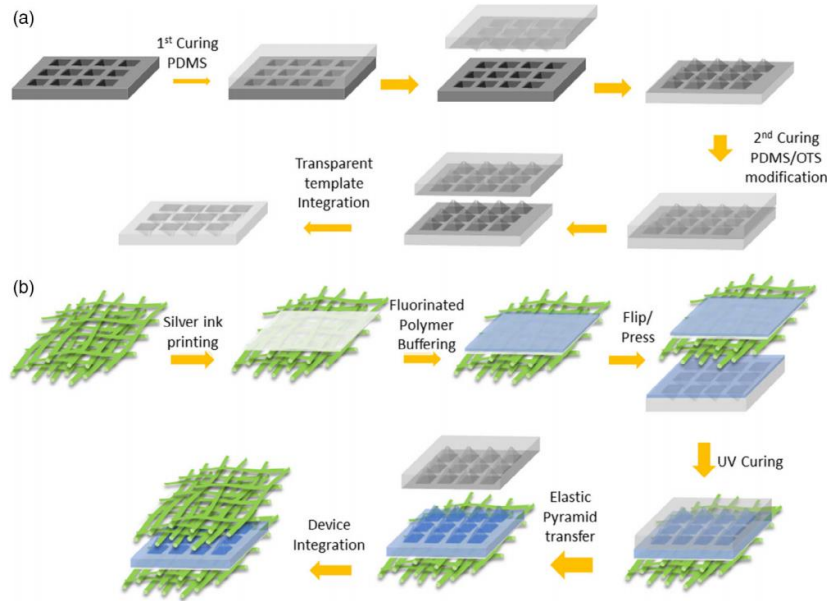


Figure 11. Schematic illustration of the manufacturing steps of a) the PDMS mold and b) pressure-sensing textile reprinted from the article “Photo-Curable Ion-Enhanced Fluorinated Elastomers for Pressure-Sensitive Textiles” written by Chen et al.³

To compare the most promising PVDF-HFP / TBAP pressure-sensitive textile, three different pressure-sensing textiles consisting of PDMS, PVDF-HFP and PVDF-HFP / TBAP were fabricated and studied. Figure 12 shows capacitive responses after loading and unloading of pressures from 0.01 kPa to 4.9 kPa. As expected, the ion-doped pressure sensor exhibited the best performance. All

devices showed a stable response to the applied pressures. The PVDF-HFP / TBAP sensor can detect low pressures like even 9.8 Pa (=100 mg loaded on 1x1 cm²). On the contrary, by 2 kPa the signal remains stable without showing any noteworthy hysteresis nor degradation. In all cases, the capacitive response below 0.4 pF was poor.³

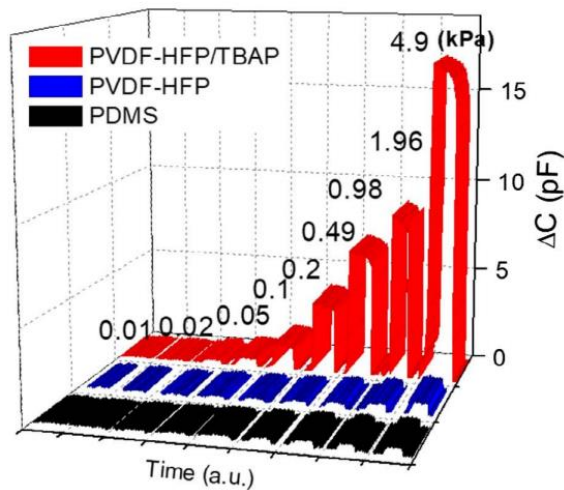


Figure 12. Capacitance curves of pressure-sensing textiles devices consisting of PDMS, PVDF-HFP, and ionic-doped (2 wt%) PVDF-HFP pyramids measured during a few seconds upon various pressures reprinted from the article “Photo-Curable Ion-Enhanced Fluorinated Elastomers for Pressure-Sensitive Textiles” written by Chen et al.³

The fabricated device was tested in real life applications like measuring of pulse on neck and wrist what is visible in Figure 13. The experiment was done in real-time and the recorded pulses varies from 60 to 80 beats per minute. Reported results are a good validation of potential usage of the sensor for health monitoring purposes.³

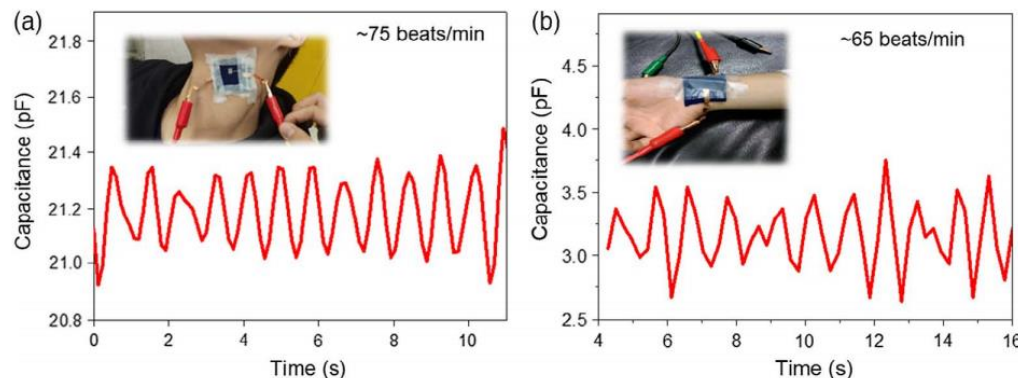


Figure 13. Pulses recorded a) on the neck, b) of the radial artery on the wrist by the attached to human skin pressure-sensing textile reprinted from the article “Photo-Curable Ion-Enhanced Fluorinated Elastomers for Pressure-Sensitive Textiles” written by Chen et al.³

2.2.2.2 Example 2 – Porous Ecoflex-multi-walled carbon nanotube (MWCNT) composite (PEMC) sandwiched in fabric electrodes

Choi et al. fabricated a capacitive pressure sensor by sandwiching porous Ecoflex-MWCNT composite in two conductive fabric electrodes and presented it as a part of a prosthetic robot finger and a healthcare wristband for blood pressure and heart rate monitoring. A schematic of the fabricated device is presented in Figure 14. The manufacturing process itself includes mixing of Ecoflex and MWCNTs, infiltration of the solution into a sugar template, dissolution of the sugar template in water, and lastly PEMC fabrication. The template was used to obtain highly porous (80%) PEMC with pores distributed randomly throughout the volume and pore size amounting to 288 μm in average, which are well visible in the Scanning Electron Microscopy (SEM) image in Figure 14. The composite structure is flexible and compressible what enables trouble-free stretching up to 70%, bending, or pressing.

Sensitivity of this PEMC-based sensor in 0-2 kPa amounts to 6.42 kPa^{-1} and in 2-10 kPa - 1.72 kPa^{-1} . These enhanced values are due to a synergic effect of the porous elastomer and percolation of CNT fillers which reduce the stiffness.³⁰

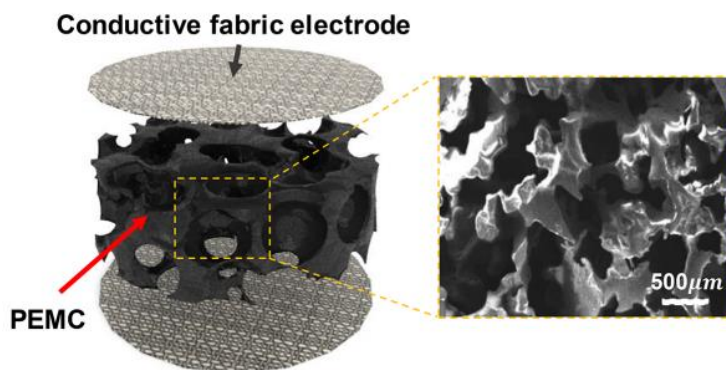


Figure 14. a) Schematic illustration of the PEMC-based pressure sensor and b) SEM image of its porous composite reprinted from the article “Synergetic Effect of Porous Elastomer and Percolation of Carbon Nanotube Filler toward High Performance Capacitive Pressure Sensors” written by Choi et al.³⁰

Figure 15 presents dynamic responses of the fabricated pressure sensor for pressure amounting to 10 kPa and the following frequencies: 0.01, 0.1, 1, and 10 Hz. The PEMC-based sensor shows a negligible hysteresis in these frequencies what can be justified by reducing the elastomer volume fraction due to pores in PEMC. The appearance of pores reduces the solid part of the Ecoflex-multi-walled carbon nanotube composite (SEMC) viscoelastic property. Thus, a reversible sensor response without notable hysteresis can be obtained.³⁰

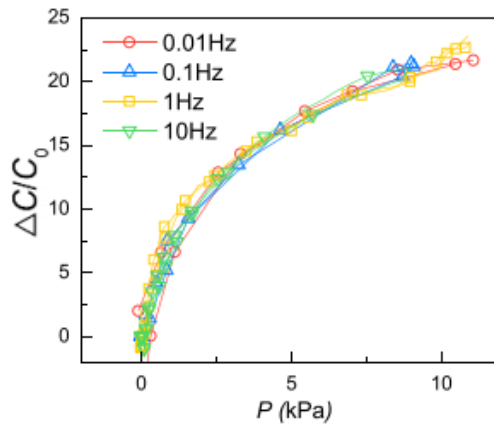


Figure 15. Dynamic responses of the fabricated sensor for 10 kPa of pressure and 0.01, 0.1, 1, and 10 Hz frequencies reprinted from the article “Synergetic Effect of Porous Elastomer and Percolation of Carbon Nanotube Filler toward High Performance Capacitive Pressure Sensors” written by Choi et al.³⁰

Figure 16 presents pressure sensing performance of the fabricated PEMC-based sensor for varying thicknesses (0.5, 1.5, 3 mm) and radii (2.5, 5, 10 mm). It was concluded that the sensing device gives a similar response regardless of its dimensions. Both Figure 16a and Figure 16b show comparable results with an insufficient winning margin in case of 0.5 mm of thickness and 2.5 mm in radius. The sensor dimensions are important to consider in order to achieve better wearability and less interference with diverse human motions.³⁰

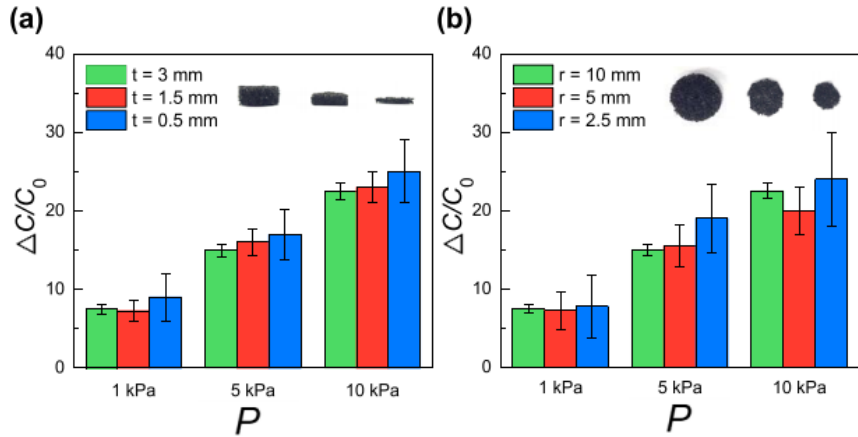


Figure 16. Capacitive responses of the PEMC-based pressure sensing device with a) the following thicknesses: 0.5, 1.5, 3 mm and b) the following radii: 2.5, 5, 10 mm reprinted from the article “Synergetic Effect of Porous Elastomer and Percolation of Carbon Nanotube Filler toward High Performance Capacitive Pressure Sensors” written by Choi et al.³⁰

An exemplary application as a health monitoring wristband is visible in Figure 17. The human subject is presented while standing and squatting and the measured epidermal pulse rate in both positions is showed in Figure 18. Figure 19a presents the determined heart rate (HR), and Figure 18b the blood pressure (BP). To obtain these results, the wristband was integrated with an electrocardiogram (ECG) sensor and the PEMC-based pressure sensor. Moreover, Figure 18b shows the systolic blood pressure (SBP) that varied from 100 to 140 mmHg and the diastolic blood pressure (DBP) values that were about 80 mmHg.³⁰ The determined blood pressure change was confirmed by the medical fact in the literature.³¹

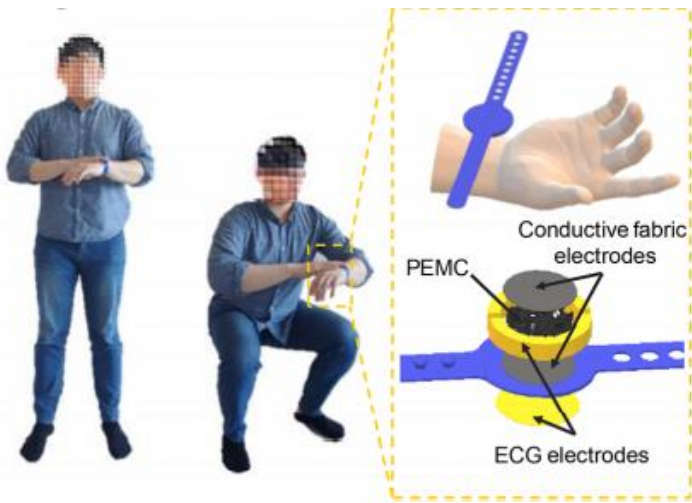


Figure 17. Photographic images of the user wearing the fabricated healthcare wristband and schematic illustration of its components reprinted from the article “Synergetic Effect of Porous Elastomer and Percolation of Carbon Nanotube Filler toward High Performance Capacitive Pressure Sensors” written by Choi et al.³⁰

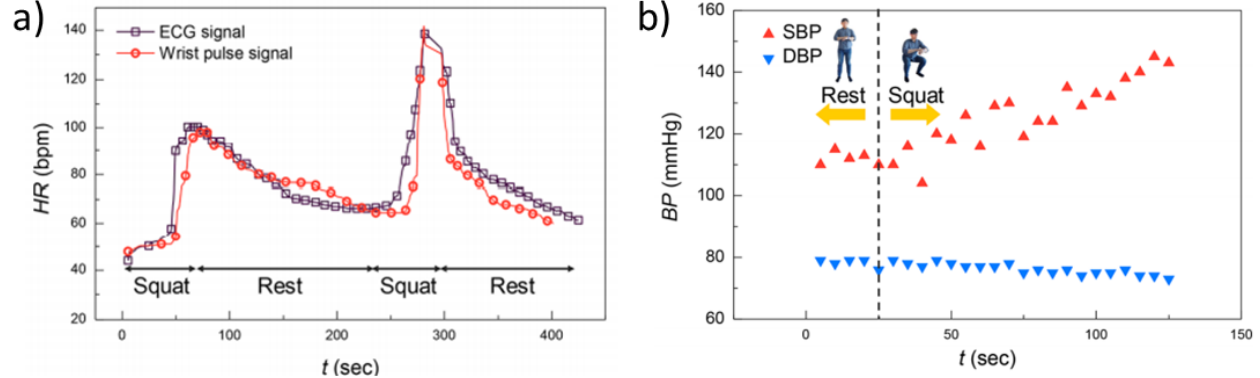


Figure 18. Measured hear rate values before and after performing the squat of the user reprinted from the article “Synergetic Effect of Porous Elastomer and Percolation of Carbon Nanotube Filler toward High Performance Capacitive Pressure Sensors” written by Choi et al.³⁰

2.2.3 Approach 3 – Wearable AgNW-based sandwich-type pressure sensor

2.2.3.1 Example 1 – Ecoflex sandwiched in between PDMS layers patterned with AgNWs

Yao *et al.* developed a multifunctional capacitive sensor with printed stretchable conductors based on AgNWs that is able to detect pressure up to 1.2 MPa. The fabrication process showed in Figure 19a consists of printing patterned by screen printing AgNW conductors (2 mm wide, 5 mm thick, 2 mm of spacing in between), drop casting liquid PDMS to achieve 0.2 mm of thickness and curing, peeling off the AgNW/PDMS from the silicon (Si) substrate, dropping liquid metal (eutectic gallium-indium, EGaIn), positioning of AgNW/PDMS films and laminating them with Ecoflex (0.5 mm thick), embedding copper wires and covering liquid metal with liquid Ecoflex, and finally curing the whole sample at room temperature. Figure 19b presents the cross-section of the prepared device. The sensor can be applied in monitoring of thumb flexing, knee jerking, and other human motion like walking or jumping. Furthermore, the fabrication steps are relatively simple and easy what enables scaling up of the sensor area.¹

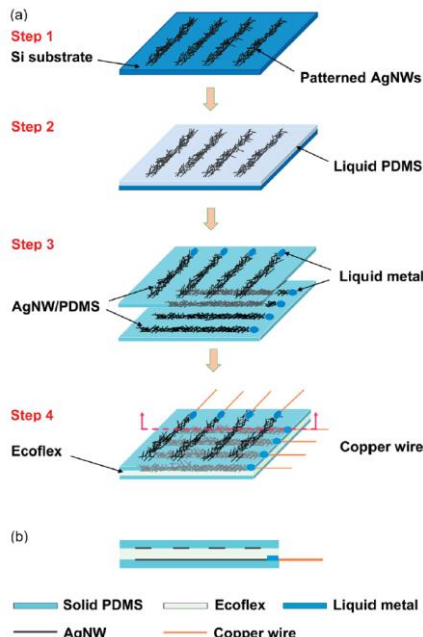


Figure 19. (a) Fabrication steps AgNW/PDMS/Ecoflex multifunctional capacitive sensor and (b) its cross-section reprinted from the article “Wearable multifunctional sensors using printed stretchable conductors made of silver nanowires” written by Yao et al.¹

The changes in capacitance as a response to strong finger press (pressing mode) and gentle finger touch (proximity mode) were measured and evaluated. Figure 20 compares the capacitance changes of these two different modes. In the pressing mode, the capacitance value increases as a result of physical pressing. However, the finger causes also an opposing effect as a grounded conductor – the capacitance value decreases. This decrease is much larger than the physical pressing. Moreover, the interacting area in this mode is larger in comparison to the proximity mode what causes larger capacitance decrease. The results indicate that the sensor can be applied as a touch sensor under both gentle and strong touch. For some purposes, a variety of forces from finger touch is inevitable and thus, it is handier to design a sensor which can respond to any force the users apply. Furthermore, it could be useful in robotics when contacts between robots and humans should be avoided, because of an injure risk.¹

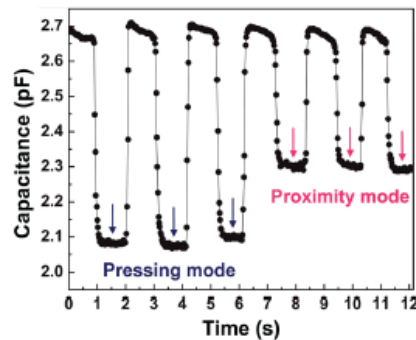
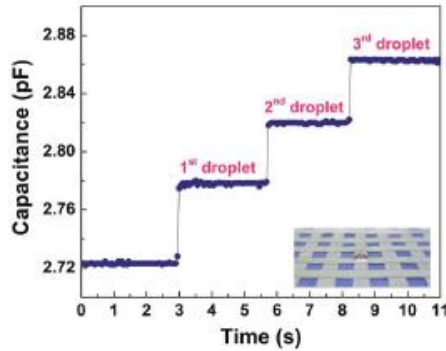


Figure 20. Capacitance changes upon pressing (large force applied) and proximity (gentle force applied) modes reprinted from the article “Wearable multifunctional sensors using printed stretchable conductors made of silver nanowires” written by Yao et al.¹

Three water droplets (0.06 g each) were applied in the middle of the sensor array in order to prove fast response time in real-time monitoring. The time responses, also referred to as rise time, are described as the time interval between 10% and

90% of the steady state values. The rise time values are shown in Figure 21. The research estimated 40 ms to be the response time, which is relatively short in comparison to other reported pressure sensors.¹ For instance, the sensor made of a PDMS membrane and an Au film developed by Liu *et al.* exhibits a response time of 200 ms and the flexible foam based capacitive sensor designed by Metzger *et al.* - several seconds.^{32,33}



*Figure 21. Time responses after dispersing three water droplets onto the sensor array reprinted from the article “Wearable multifunctional sensors using printed stretchable conductors made of silver nanowires” written by Yao *et al.*¹*

Figure 22 demonstrates an experiment, in which a mold shaped as the letter “I” was placed onto the fabricated sensor. Spatial distribution of pressure was measured and presented as a map of relative capacitance changes by using colors from dark purple, through bright purple to white. Dark purple corresponds to no changes in capacitance, whereas white to a high capacitive response.¹

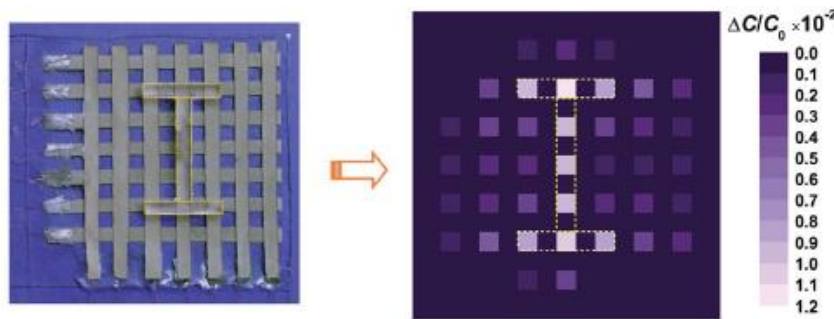


*Figure 22. Sensor array with a mold placed onto its surface (right) and mapping of the corresponding relative capacitance changes (left) reprinted from the article “Wearable multifunctional sensors using printed stretchable conductors made of silver nanowires” written by Yao *et al.*¹*

2.2.3.2 Example 2 – Porous acrylic elastomer layer sandwiched between PU films patterned with AgNWs

Hu et al. created an elastomeric capacitive sensor made of interpenetrating AgNW/PU composite able to detect pressure and deformation visible in Figure 23. The transparent capacitive array consists of a porous acrylic elastomer layer (3 M Scotch 924 ATG Tape), which acts as the dielectric spacer, sandwiched between two transparent AgNW-PU composite electrodes. Each of the electrodes consisted of 3 parallelly deposited and 1.5 mm wide AgNWs spaced at 1mm. Overall, the capacitance of the sensor increases linearly upon externally applied transverse pressure (1 MPa down to 1 kPa) and upon uniaxial stretching up to 60%.³⁴

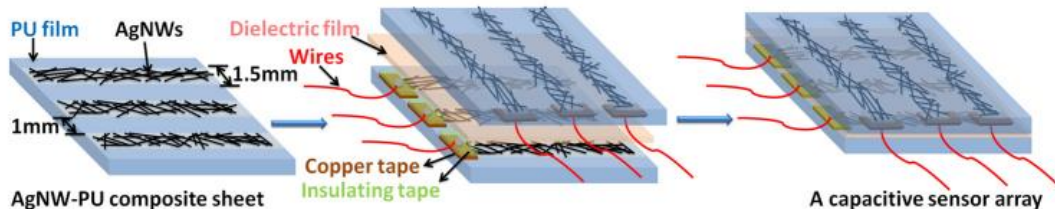


Figure 23. Fabrication steps of the AgNW/PU-based multifunctional sensor reprinted from the article “Elastomeric transparent capacitive sensors based on an interpenetrating composite of silver nanowires and polyurethane” written by Hu et al.³⁴

Figure 24 illustrates the change in capacitance of one sensor pixel as a response to transversely applied pressure up to 100 KPa. The curve shows a characteristic behavior, it is linear, and the standard deviation amounts to 0.995 what makes the sensor a perfect fit for tactile robotics applications. The lowest noticeable pressure is around 1 kPa. Values this range match fingerprint sensing.³⁴

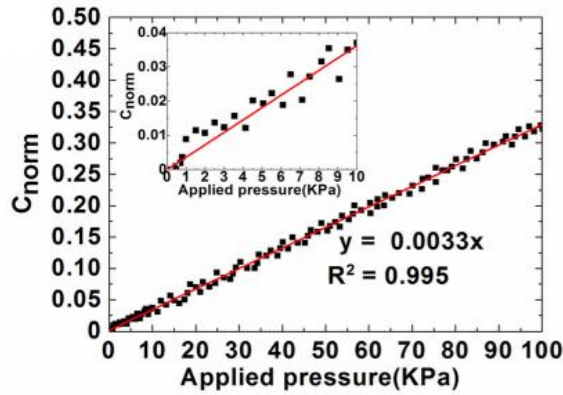


Figure 24. Change in capacitance of one sensor pixel versus applied pressure reprinted from the article “Elastomeric transparent capacitive sensors based on an interpenetrating composite of silver nanowires and polyurethane” written by Hu et al.³⁴

To investigate the crosstalk between adjacent pixels of the 10x10 pixel pressure sensor fabricated by patterning the composite electrodes into X-Y addressable passive matrix, 30 KPa of pressure was applied to the central pixel and capacitance change of all pixels was measured. Figure 25 illustrates the distribution of capacitance changes. The capacitance value of the addressed pixel is at least eight times higher than of the neighboring pixels. In general, the fabricated sensor can identify pressures in the range from 1 kPa up to 100 KPa what enables sensing of gentle touch, finger press, and firm hand grip.³⁴

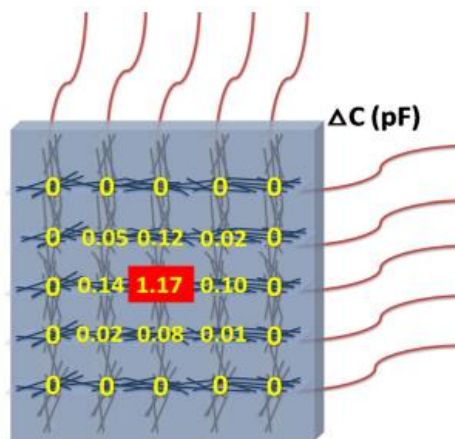


Figure 25. Mapping of the capacitance changes after applying 30 KPa of pressure on the pixel in the middle of the fabricated sensor reprinted from the

article “*Elastomeric transparent capacitive sensors based on an interpenetrating composite of silver nanowires and polyurethane*” written by Hu et al.³⁴

2.3 Strain sensors

The main sensing mechanisms of strain sensors are classified into capacitive, resistive, and piezoelectric.³⁵ This subchapter provides a brief description of the above-mentioned methods and covers less frequently used mechanisms like Surface Acoustic Wave (SAW), Fiber Bragg Grating (FBG), and resonant-type strain sensors. Furthermore, key parameters of strain sensors, e.g., the gauge factor, are presented.

2.3.1 Key parameters

To evaluate the performance of capacitive strain sensors, mainly gauge factor (or sensitivity), response time and linearity have to be taken into account.³⁶ Response time and linearity were covered already in the subchapter about key parameter of pressure sensor.

Gauge factor GF is the most significant parameter, which informs about sensitivity of the strain sensor.³⁷ Gauge factor is determined by the Eq. 5.

$$GF = \frac{\Delta C}{C_0 \cdot \varepsilon_{mech}} \quad \text{Eq. 5}$$

where C is the initial capacitance, ΔC is the capacitance change, and ε is strain.¹⁰

2.3.2 Categories

2.3.2.1 Capacitive strain sensors

Capacitive strain sensors are usually shaped as a 3D multilayer structure made of a dielectric layer and two parallel-plate electrodes on its top and bottom. The capacitance change depends highly on the geometric structure variation of all three elements. However, both pressure and strain can induce capacitance

changes in such sensor what causes a cross-talk issue between sensing of these two stimuli. Typically, capacitive strain sensors show a linear sensitivity-strain relationship with the maximum GF of 1 in theory and no hysteresis. The sandwich-type structure impedes minimization of the sensor thickness for conformal contact of wearable devices. Moreover, it is difficult to conform such parallel-plate-type sensor to irregular surfaces like human skin. Thus, interdigitated capacitive strain sensors (ICSSs) consisting of in-plane electrodes that are parallel to substrates exhibit better strain sensitivity, linearity, and lower hysteresis than parallel-plate-type strain sensors.³⁵

2.3.2.2 Resistive strain sensors

Resistive strain sensors detect the strain value variations due to electrical resistance changes in relation to deformation of the given material. These changes are dependent on the geometric structure and how it alters and create a function of electrical resistivity that differentiates upon the applied stress. The relationship of resistive strain sensors with the applied strain values is nonlinear and a severe hysteresis is for them characteristic.³⁵ Resistance-based strain sensing devices are the largest part of commercially available foil strain-gauge sensors.³⁸

2.3.2.3 Piezoelectric strain sensors

Piezoelectric strain sensors utilize the direct piezoelectric effect to detect structural deformation and the converse piezoelectric effect to actuate the structure.³⁹ They have the ability of converting the mechanical energy into electrical energy. Commonly used materials for such sensing devices are piezoceramics and piezoelectric polymers, e.g. zirconate titanate (PZT) that is typically used for piezoelectric actuators and sensors.³⁸ Piezoelectric strain sensors have the advantage of being compact, easily embeddable, and sensitive over a large strain bandwidth.³⁹ This class of devices has the lowest power

requirements and their charge output lies within the measurement capabilities range of commercially available digital and analog sensors.³⁸

2.3.2.4 Others

Other transduction methods consist of Surface Acoustic Wave (SAW), Fiber Bragg Grating (FBG), and resonant mechanisms. The main effect used by SAW strain sensors is called the piezoelectric effect which transduces an electric signal into a mechanical wave. This wave propagates in the material to another transducer what leads to conversion of the wave back to an electrical signal. In this case, the Rayleigh wave is exploited as a transverse and the surface wave in operation. Piezoelectric substrates applied in SAW sensors are typically relatively expensive, but the resulting sensitivity is exceptionally attractive. SAW devices are insensitive to electrical interference caused by magnetic fields, rugged, small-sized, and can be operated wirelessly.⁴⁰

FBG strain sensors utilize fiber photosensitivity as the primary phenomenon. When light passes through a FBG fiber, numerous Frensel reflections occur along the entire grating length because of refractive index variations. If the propagating light wavelength in the fiber doubles the grating pitch and thus, the Bragg condition is fulfilled, constructive interference takes place. As a result, narrow band light back-reflection appears. The reflected wavelength is referred to as the Bragg wavelength.⁴¹ FBG exhibit several advantages over other types of fiber optic sensors like wavelength-encoded measurand information and excellent multiplexing capability.⁴² They are usually non-conductive, light weight, immune to electromagnetic noise and radio frequency interference, and show a fast response.⁴¹

Resonant-type strain sensors measure the resonant frequency in a function of the quantity.⁴³ For example, Micro Electro Mechanical Systems (MEMS) resonant strain sensors are often used for direct measurement of structural strain on

materials like aluminum and steel and are a great fit for ultra-high resolution strain detection.⁴⁴

2.4 Literature review of reported capacitive strain sensors

In this subchapter, examples of so far fabricated wearable yarn-based and sandwich-type capacitive strain sensors were described. Over the last few years, strain sensors shaped as one-dimensional (1D) yarns or fibers, 2D sheets or films, and 3D architectures have been developed and applied in detection of subtle and large deformation of human activities, like walking and breathing respectively. It is crucial to integrate strain sensors with clothes substrate for comfortable wearing and broader adoption of the technology. Currently, most strain sensors bond on the inner surface of clothes or are adhered directly onto human skin what makes the wearing experience uncomfortable.⁴⁵

2.4.1 Approach 1 – Wearable yarn-based strain sensors

2.4.1.1 Example 1 – Silver-coated nylon fibers wrapped with cotton fibers

Zhang *et al.* developed a textile-only capacitive sensor based on silver-coated nylon fibers wrapped with cotton fibers that can be easily integrated with fabric without compromising the wearability and can act as a strain sensor. Silver fibers, which act as electrodes, are flexible and antibacterial what indicates their desirability for application in smart clothing. The double-ply yarns (0.6 mm in diameter, 10 cm long) were fixed by spraying a PU adhesive, which is visible in Figure 26. Together with cotton fibers, they formed a dielectric layer. The PU adhesive contains polar groups called carbamate (-NHCOO) and isocyanate (-NCO) that impact the durability positively.¹¹

The reported sensor can be embedded into fabrics by knitting, weaving, and sewing by using typical sewing needles and its maximum elastic elongation amounts to 18.5%. Figure 26 shows that higher elongation values are possible

and upon 20% of strain there is no significant rupture noticeable. The measured ultimate strain amounts to 34%. However, movements of elbows, knees or knuckles in this experiment did not exceed 14% of strain.¹¹

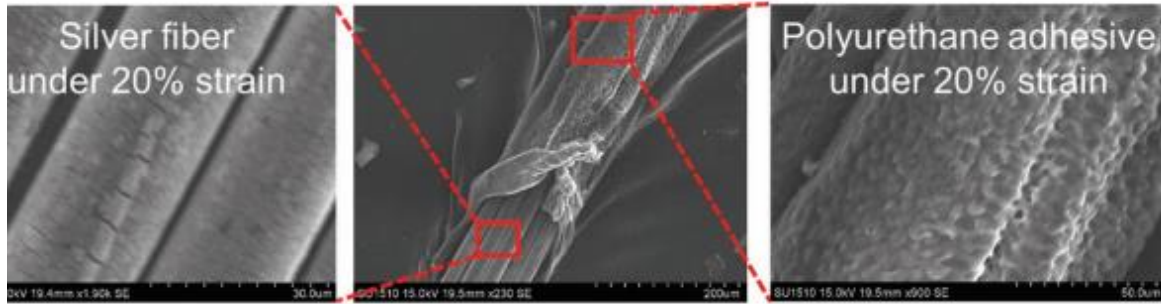


Figure 26. SEM images of silver-coated fibers wrapped with cotton fibers coated with a PU adhesive under 20% of strain reprinted from the article “Textile-Only Capacitive Sensors for Facile Fabric Integration without Compromise of Wearability” written by Zhang et al.¹¹

The sensing mechanism works as follows: External strains generate cracks in silver coating what ruptures the conductive paths. Thus, resistance increases. This behavior illustrates Figure 27a. After 1000 cycles, most cracks do not recover what leads to more fragile electrical paths and sensitivity drifts. Poor stability and high hysteresis limit usage of such resistive sensors. On the opposite, capacitive sensors are stable due to the dielectric structure and reliable what is proven by Figure 27b showing minor hysteresis in a stretch-release cycle. The double-ply yarn sensor can identify strains below 1% and its estimated detection limit amounts to 0.5%.¹¹

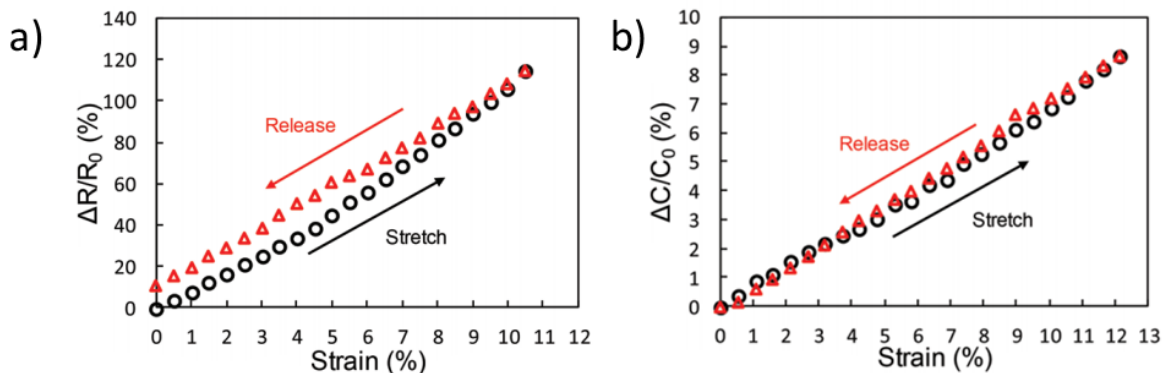


Figure 27. Relative a) resistance and b) capacitance changes upon external strains in a single cycle applied at 1% per second reprinted from the article “Textile-Only Capacitive Sensors for Facile Fabric Integration without Compromise of Wearability” written by Zhang et al.¹¹

Figure 28 presents this strain sensor when sewn into a kneepad. No movement restriction was reported by the tested subject while stretching the device by bending and bulging the knee. Human motions like standing, jumping, walking, rising, squatting, sitting down, walking up and down stairs, standing up, and running were recognized by the device. Some of these movements with related to them capacitance values are shown in Figure 29. The sensor was used also in a second study case – detection of finger motion in a glove.¹¹



Figure 28. Photograph of the fabricated strain sensor embedded in a kneepad reprinted from the article “Textile-Only Capacitive Sensors for Facile Fabric Integration without Compromise of Wearability” written by Zhang et al.¹¹

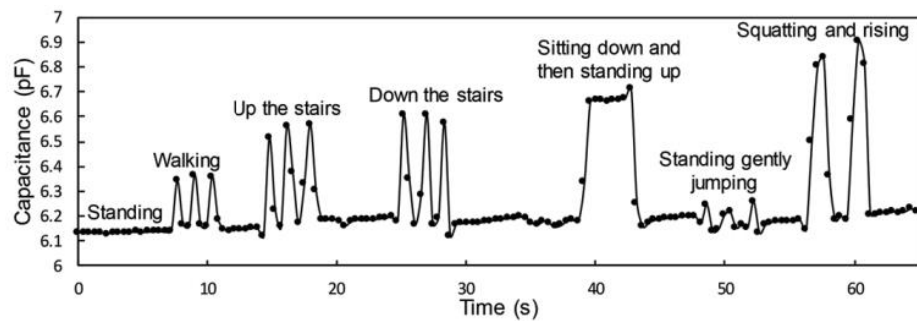


Figure 29. Changes in capacitance according to movements detected by the fabricated kneepad reprinted from the article “Textile-Only Capacitive Sensors for Facile Fabric Integration without Compromise of Wearability” written by Zhang et al.¹¹

2.4.1.2 Example 2 – Rubber fibres wrapped with multiwall carbon nanotube sheet (NTS) layers

Wang *et al.* reported superelastic conducting fibers that can be applied in strain sensors, superelastic wires, supercapacitors, and biosensors. The fabrication steps are visible in Figure 30. First, NTS layers were wrapped around a stretched rubber fiber of a 2 mm diameter. Then, the stretch was released, applied again, and eventually released forming a hierarchically buckling sheath–core structure. Figure 31 shows the NTS₂@fibers₅₀₀ integrated into stretchable textile.⁴⁶

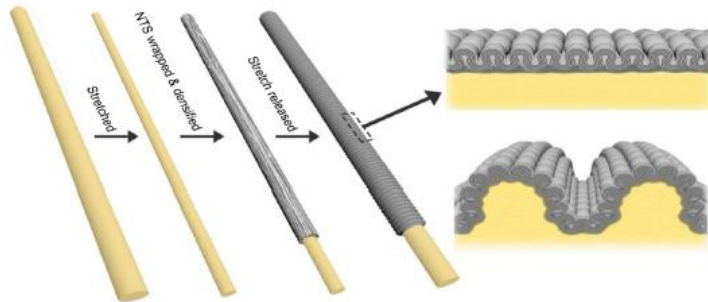


Figure 30. Fabrication steps of the superelastic conducting NTS/rubber fibers reprinted from the article “Downsized Sheath–Core Conducting Fibers for Weavable Superelastic Wires, Biosensors, Supercapacitors, and Strain Sensors” written by Wang *et al.*⁴⁶

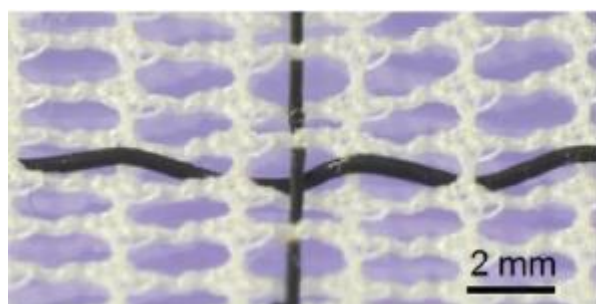


Figure 31. NTS₂@fibers₅₀₀ integrated into a stretchable textile reprinted from the article “Downsized Sheath–Core Conducting Fibers for Weavable Superelastic Wires, Biosensors, Supercapacitors, and Strain Sensors” written by Wang *et al.*⁴⁶

The 4 cm long NTS₁₀@rubber@NTS₆@fiber₃₀₀ strain sensor with a 160 µm diameter was characterized. Numeric values in NTS₁₀ and NTS₆ indicate the

number of NTS layers wrapped around a rubber fiber, and the number in fiber³⁰⁰ refers to the core diameter in micrometers at zero strain. The dependence of sensor capacitance on strain and displacement was determined and visualized in Figure 32. The black squares refer to stretched state of the device and the white circles to the non-stretched state. The hysteresis value is negligible. The strain sensor was stretched to 200% what is equal to 80 mm of length.⁴⁶

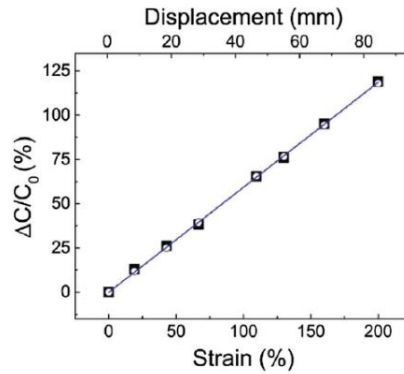


Figure 32. Capacitance changes dependent on strain and displacement of a NTS₁₀@rubber@NTS₆@fiber₃₀₀ upon stretching (black squares) and stretch release (white circles) reprinted from the article “Downsized Sheath–Core Conducting Fibers for Weavable Superelastic Wires, Biosensors, Supercapacitors, and Strain Sensors” written by Wang et al.⁴⁶

Figure 33 presents the capacitance values of the strain sensor in the non-stretched strain and upon elongation from 0% to 40%, from 0% to 70%, and from 0% to 100% during thousands stretch-release cycles. The results indicate a decent reversibility.⁴⁶

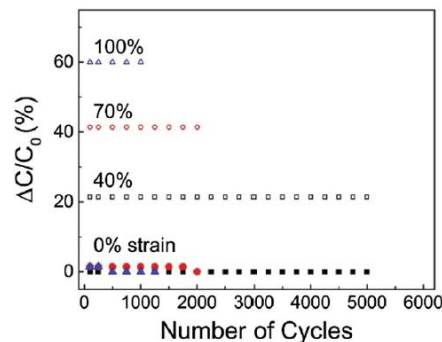


Figure 33. Cycling test demonstrating changes in capacitance upon applying strain from 0% to 40%, 70%, and 100% reprinted from the article “Downsized

Sheath–Core Conducting Fibers for Weavable Superelastic Wires, Biosensors, Supercapacitors, and Strain Sensors” written by Wang et al.⁴⁶

2.4.2 Approach 2 – Wearable textile-sandwiched strain sensors

2.4.2.1 Example 1 – PDMS sandwiched between CNTs films

Cai *et al.* developed capacitive strain sensors based on CNTs for detecting human motion visible in Figure 34. To fabricate the strain gauge alike a parallel plate-like capacitor, two layers of CNT films acting as electrodes and two sides of silicone elastomer lamina were used. The sensor is capable of measuring strain up to 300%, its sensitivity is close to 1, the delay time is below 100 ms which indicates a fast response speed, and it shows an excellent stability. It is durable (1000 cycles at 100% strains) and highly transparent (80% at 550 nm). There is no hysteresis or relaxation.⁴⁷

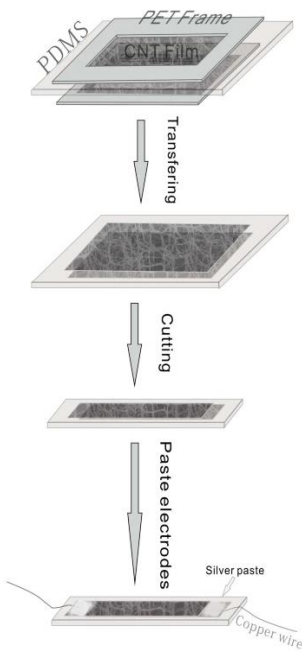


Figure 34. Fabrication steps of the capacitive strain gauge based on CNT reprinted from the article “Super-stretchable, Transparent Carbon Nanotube-Based Capacitive Strain Sensors for Human Motion Detection” written by Cai et al.⁴⁷

Capacitive responses of the fabricated CNT/PDMS sensor are visible in Figure 35. The sensor was stretched up to 100% of strain at 5%/s speed and next released. The experimental data fit the linear model almost perfectly at 0.9999. The slope amounts to 0.97. No hysteresis was observed between the unloading and loading phase what underlines the deterministic characteristic od capacitive sensors.⁴⁷

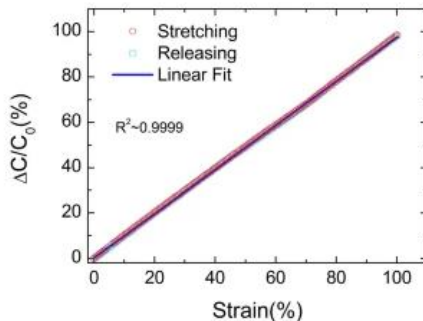


Figure 35. Relative changes in capacitance of the fabricated CNT/PDMS sensor upon loading and uploading to 100% of strain reprinted from the article “Super-stretchable, Transparent Carbon Nanotube-Based Capacitive Strain Sensors for Human Motion Detection” written by Cai et al.⁴⁷

Figure 36 presents relative changes in capacitance in response to random strain values generated by a random number generator during the measured time. The strains were applied at 20 mm/s with a holding time of 10 s. The capacitance changes match the strain values well what indicates that the sensor response is fast and stable even despite the silicone elastomer viscoelasticity and frictions between polymer molecules and CNTs.⁴⁷

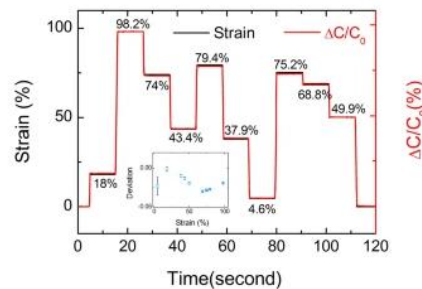


Figure 36. Relative capacitance changes as a function of strain and time reprinted from the article “Super-stretchable, Transparent Carbon Nanotube-

Based Capacitive Strain Sensors for Human Motion Detection” written by Cai et al.⁴⁷

The strain gauge was integrated onto a rubber glove in order to create a data glove able to detect finger movements without constraining the hand motions. Upon folding the finger, the capacitance values increased gradually what is visible in stages I to V in Figure 37. Every single slight bending was easily detected. Capacitance values were constant when the finger was kept at a certain angle. Stages VI to VIII present unfolding of the finger. During this movement, capacitance restored its initial value.⁴⁷

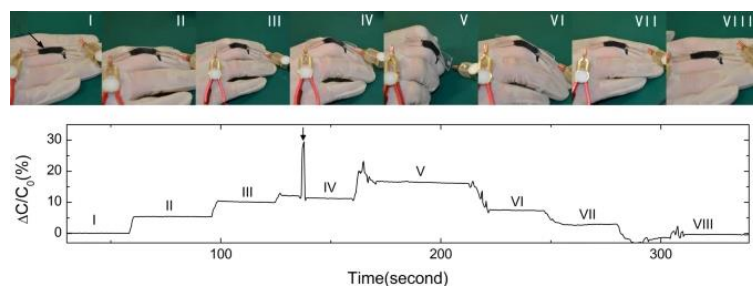


Figure 37. Prototype of a data glove used to detect folding and unfolding of a finger and the corresponding capacitive responses reprinted from the article “Super-stretchable, Transparent Carbon Nanotube-Based Capacitive Strain Sensors for Human Motion Detection” written by Cai et al. The arrow indicates an accidental disrupt of the copper wire.⁴⁷

2.4.2.2 Example 2 – Genus structures with metallic seeds on cotton fabrics

Chen *et al.* designed a capacitive sensor for physical rehabilitation by using genus structures that trap metallic seeds and a cotton fabric. Genus is a term used to describe the p orbital named by mathematician Clebsch.⁴⁸ The sensor was tested during real-time monitoring of speaking, blinking, human breathing, and joint motions carried out in a physical rehabilitation session.

Figure 38 illustrates different genus surfaces acting as cages of catalyst-based nickel seed crystal and the manufacturing steps of the polymer-assisted metal deposition (PAMD). PAMD fabrication procedure involves polymer grafting on the cotton fibers surface, loading of the catalyst into the polymer network, and the

electroless deposition (ELD) of metal nanoparticles (NPs). PAMD is a controllable chemical reaction process with robust interaction bonds what is highly desired. Genus-0 represents the traditional materials surface modification approach in which there are no topographical coating-substrate interactions. Topographical modification of cross-linked polymers leads to fabrication of genus-3 and genus-5 surfaces. To increase the conductivity in the deposition process and upsurge the seed crystal density, these two genus surfaces caged catalyst-based nickel seed crystals. The obtained conductive fabric becomes therefore a capacitive sensor.⁴⁹

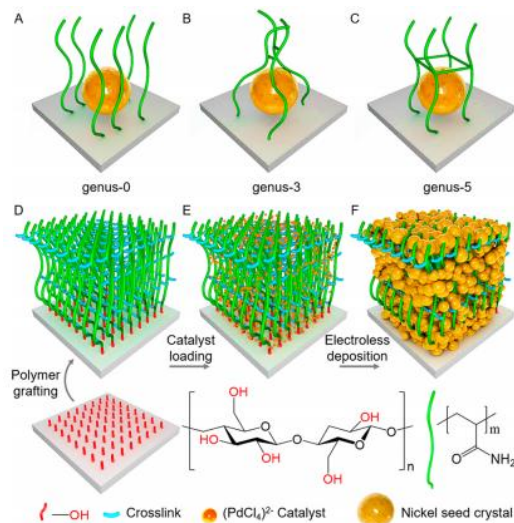


Figure 38. Schematic illustration of a) genus-0, b) genus-3, and c) genus-5 surfaces, and PAMD fabrication steps consisting of d) polymer grafting, e) catalyst loading, and f) metal NPs ELD reprinted from the article “Textile-Based Capacitive Sensor for Physical Rehabilitation via Surface Topological Modification” written by Chen et al.⁴⁹

Figure 39 presents changes in capacitance of the conductive nickel-coated fabric-sandwich sensor with the dimensions of 13 mm x 37 mm as a response to variable from 0 to 20 mm distance between two conductive fabrics and from 0° to 180° rotation angle degree. Figure 39a illustrated the inverse proportionality of the capacitance to the distance what matches the theory. The larger the distance, the smaller the capacitance value. To control the distance, a programmable C scan stage and Arduino-based controller board were used. The data interval amounted

respectively to 1×10^{-4} and 0.5 mm. Capacitance is inversely proportional to the bending angle for nonparallel plate capacitors what was proven in Figure 39b.⁴⁹

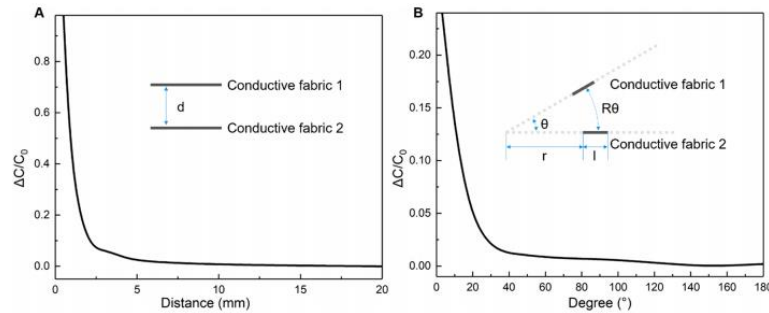


Figure 39. Capacitive response of the fabricated nickel-coated fabrics-based sensor as a function of a) distance and b) bending angle reprinted from the article “Textile-Based Capacitive Sensor for Physical Rehabilitation via Surface Topological Modification” written by Chen et al.⁴⁹

As mentioned above, the capacitive sensor was implemented by integrating the fabric electrode into tights and fixing it inside of a belt to monitor fast and slow breathing upon rehabilitation. Figure 40a represents the second application. While inhaling, the distance between two fabrics reduces due to relaxation of the abdominal muscle and the capacitance value decreases. In contrary, exhaling restores the initial state of the sensor, the abdominal muscles contract, and thus, the capacitance value decreases. Figure 40b and Figure 40c show the generated signal during 5 breaths within 27 seconds of measurements preformed on a person standing, and Figure 40d during 12 breaths within 35 seconds. The breathing cycle while standing is much slower (5.4 s) in comparison to sitting (3 s) or lying (3.4 s) presented in Figures 40e and 40f. However, the normal diaphragmatic respiratory rate is the fastest upon standing, and the slowest when lying which corresponds to respectively the lowest and highest capacitance values.⁴⁹

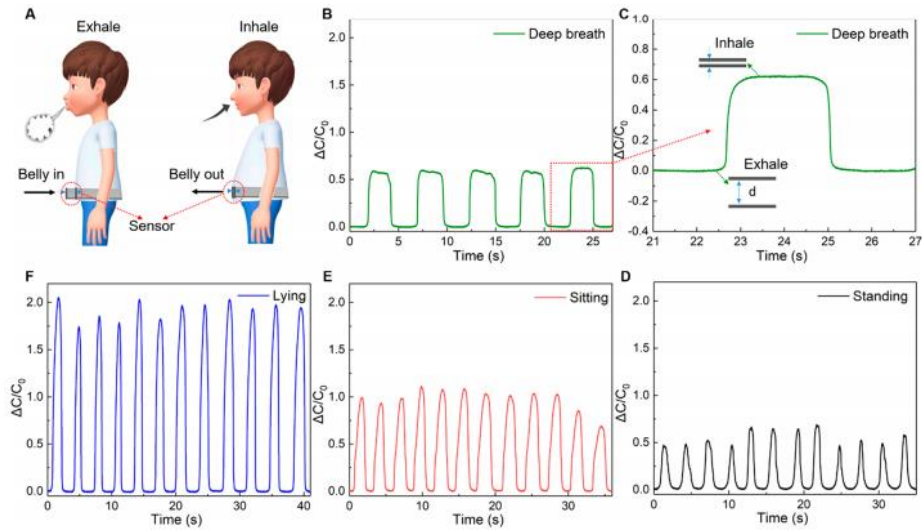


Figure 40. a) Schematic illustration of the fabricated sensor integrated in a belt and worn by the user. b) Capacitive response of the belt-based sensor as a result of deep breath. c) One breathing cycle with corresponding changes in the dielectric layer thickness. Changes in capacitance during the breathing cycles when the user is d) lying, e) sitting, f) standing reprinted from the article “Textile-Based Capacitive Sensor for Physical Rehabilitation via Surface Topological Modification” written by Chen et al.⁴⁹

2.5 Textile environment

To realize dynamic and timely health assessments and medical diagnosis of potential diseases in daily life, it is necessary to develop breathable, highly sensitive, energy-sustainable, and wearable flexible sensors able to monitor body motion and pulse wave continuously. A potential solution is usage of textiles which can withstand versatile complex mechanical deformations during wearing. Furthermore, textiles allow to construct intrinsically shape adaptive sensors and ensure good breathability due to incorporating air inside inherent pores. Air permeability is an important factor desired for patient comfort and long-term wearing convenience.⁵⁰ Another advantages of textiles are their cost-effectiveness, washability and dyability.⁵¹

However, the progress of wearable textile devices is challenging as sensing capabilities of most textile-based sensors are worse than of the commercial sensor products and secondly, due to smooth and curved surface structure which hinders the area of effective contact.⁵⁰ It is significant to consider air resistance, water vapor transmission, effects of washability and different performances resulting from chosen manufacturing technique in the development of textile-based sensors.⁵² In order to overcome low stretchability and wearing unease, common approaches include embedding of electronic functions into pristine fabrics and direct coating of conductive materials such as AgNWs and graphene onto commercialized fibers.⁵³

Figure 41 presents three traditional textile manufacturing technologies: stitching, weaving, and knitting as well as photographs of the sensors fabricated by each of the techniques. The stitched device showed the highest air resistance, whereas the woven sensor the lowest. The water vapor transmission values were similar for all devices, however, the stitched structure showed the highest transmission. The performance of each device was evaluated by recording the pressure as output voltage. All devices exhibited a stable response by showing an increase in the output level, but the output levels values were different. The largest signal was produced by the woven structure. Under large pressure values, sensors made of woven and knitted structures showed saturation (observed as flattened peaks).⁵²

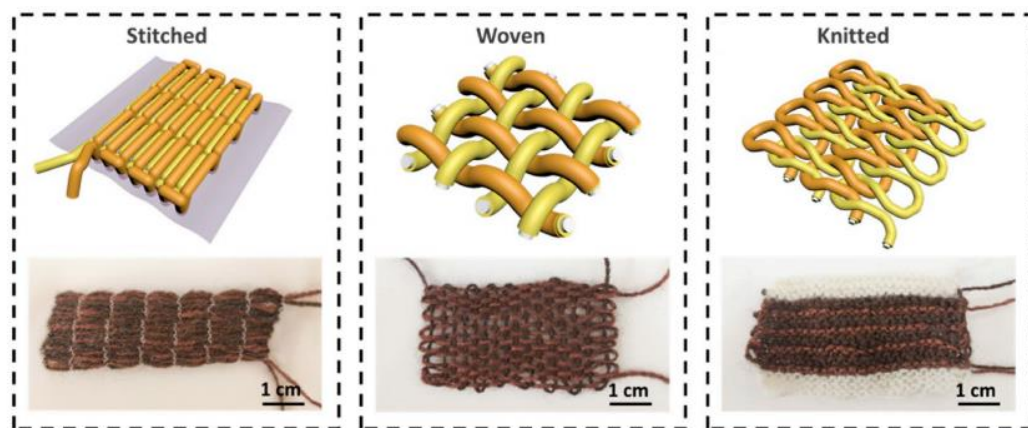


Figure 41. Photographs and graphical illustrations of stitched, woven and knitted structures reprinted from the article “Machine-washable and breathable pressure

sensors based on triboelectric nanogenerators enabled by textile technologies”
written by Zhao et al.⁵²

Besides the traditional textile manufacturing technologies, many other examples of sewing processes can be found in the literature. For instance, Agcayazi et al. reported a bobbin thread. In this approach, the fabric was used as a dielectric and the conducting yarn acting as an electrode and interconnecting route to external front-end circuits was sewn into it. The schematic illustration of this idea is presented in Figure 42.

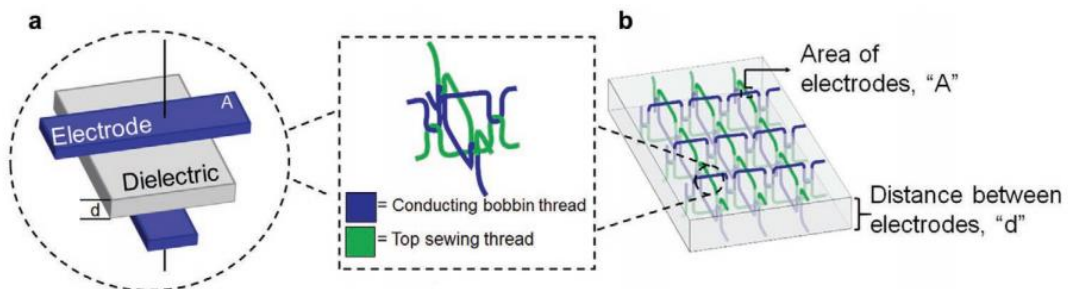


Figure 42. Schematic illustration of the a) parallel plate capacitor created by the fabric and thread and b) the distributed sensor network throughout the fabric
reprinted from the article “Fully-Textile Seam-Line Sensors for Facile Textile
Integration and Tunable Multi-Modal Sensing of Pressure, Humidity, and
Wetness” written by Agcayazi et al.⁵⁴

The textile structure and its construction are significant and determine conversion of external pressure into internal effective contact area change. Figure 43 illustrates cross-sections of yarns in each structure and how the contact area between them changes upon applying pressure. For the stitched structure, the relative positions of the two yarns are parallel what indicated a relatively large contact area. In the woven structure, the relative position of the yarns is perpendicular in the contact region. In this example, the diameter of yarns and their mechanical stiffness are similar. Thus, the deformation of the yarns at the crisscross intersection is the same and the contact area can be illustrated as a circle. For the knitted structure, contacts exist at multiple locations with different characteristics what thwarts the approximation. Nevertheless, Figure 43 presents the chosen contacts as ellipse with two radii along the major and minor axes. Due

to the loose structure, a displacement between the yarn can take place upon applying pressure what is not beneficial to large deformation in the contact area.⁵²

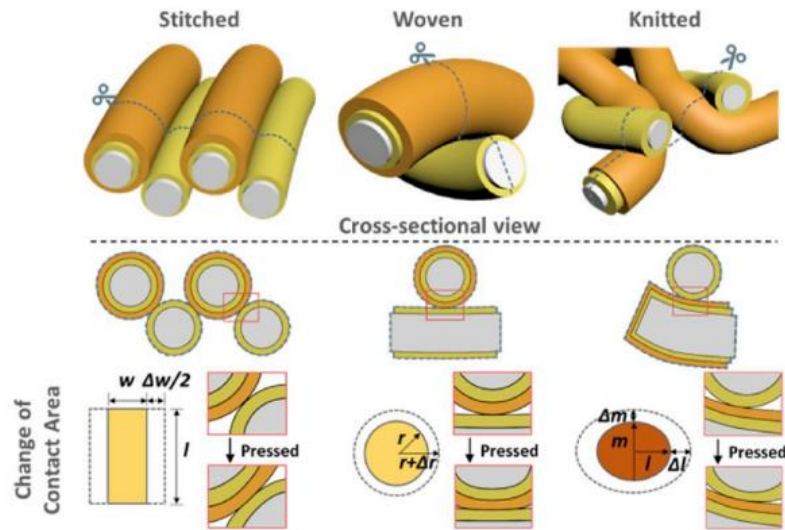


Figure 43. Schematic illustrations of stitched, woven and knitted structures reacting to applied pressure reprinted from the article “Machine-washable and breathable pressure sensors based on triboelectric nanogenerators enabled by textile technologies” written by Zhao et al.⁵²

3 Experimental

The experimental part of the research includes fabrication processes of five sensing devices, namely three pressure sensors and two strain sensors. The sensors were categorized into wearable yarn-based, wearable textile-sandwiched and wearable AgNW-based sandwich-type sensors. One pressure sensor was fabricated in each of the classes and only one POC strain sensor prototype was manufactured in each of the first two classes - wearable yarn-based and textile-sandwiched sensors. This chapter presents the methodology used in the experiments needed for recreating all the prototypes. Finally, the devices and methods used for characterization purposes are reported.

It is expected that during experiments on the final prototypes, the capacitance value will increase significantly as a response to applied pressure or strain. It is known that the largest capacitance is obtained upon applying the highest pressure or strain. The thickness and porosity of the PDMS layer are going to have an impact on the sensitivity of the sensor as well. The thinner the layer and the more pores it possesses, the higher the awaited capacitive responses at the same applied pressure. Further, higher number of yarns in the woven structure should increase the sensitivity of the structures. The hypothesis goes along with the Eq. 3 that states that capacitance can be manipulated by three factors: dielectric constant, thickness, and overlap area.

3.1 Sample preparation

3.1.1 Wearable pressure sensors

This section depicts manufacturing process of three wearable capacitive pressure sensors. Each of the devices falls under one of the following categories: yarn-based, textile-sandwiched or AgNW-based sandwich-type. The mainly used

materials are silver-coated nylon yarns applied as a conductive component and PDMS acting as a dielectric.

3.1.1.1 Approach 1 – Wearable yarn-based pressure sensors

Figure 44 presents the schematic illustration of the desired 5 cm x 5 cm large capacitive pressure sensor woven into a 2 x 2 matrix. The silver-coated nylon 235/34 dtex 4-ply HC+B yarns marked in gray were purchased from Shieldex Trading. The Silicone Elastomer Base and the Silicone Elastomer Curing Agent needed for creating the PDMS layer colored in red were purchased from Sylgard. In the experiments, 1-ply silver-coated nylon yarns from Shieldex were used as well.

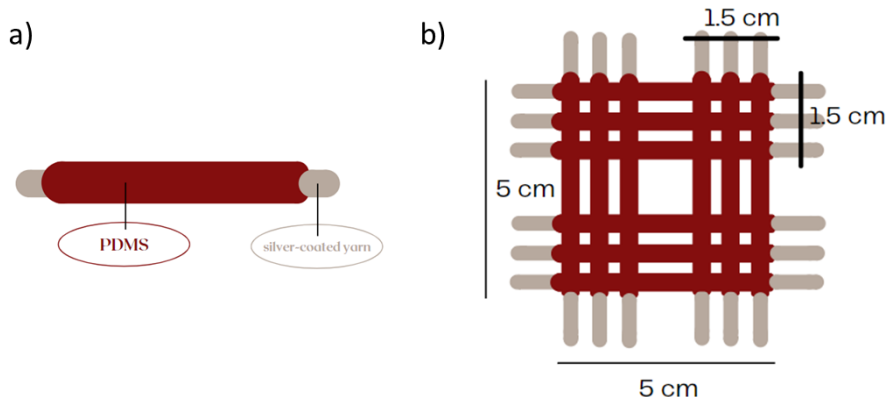


Figure 44. a) Silver-coated nylon yarn coated with PDMS layer and woven into b) the square-shaped textile creating the wearable yarn-based pressure sensor.

- Coating of yarns
 - 1st attempt of coating the yarns – Dip coating

To prepare PDMS, the Silicone Elastomer Base and the Silicone Elastomer Curing Agent purchased from Sylgard were mixed in a beaker in the 10:1 ratio and the yarns were dip coated (Dip coater KSV NIMA) in the mixture at 10 mm/min, kept in the solution for 30 seconds and withdrawn at 10 mm/min. Next, the samples were cured in an oven at 60°C for 2.5 hours.

In the second and third iteration, PDMS mixed like in the afore-mentioned description was diluted with n-hexane purchased from Honeywell International in

1:2 and 1:3 ratio. Silver-coated nylon yarn were dip coated in each of the solutions at 10 mm/min, kept in the solution for 30 seconds and withdrawn at 10 mm/min. Next, the samples were cured in an oven at 60°C for 2.5 hours.

- 2nd attempt of coating the yarns – Dip coating preceded by plasma cleaning

In this attempt, silver-coated yarns were treated with plasma for 1 minute at 50% of power and then dip coated in a non-cured PDMS solution mixed in the above-mentioned procedure. The plasma cleaning device used in the experiment was produced by Henniker. Finally, the yarns were cured in an oven at about 60°C for 2.5 hours.

- 3rd attempt of coating the yarns – Spray coating

The third method consisted of preparation of a 1:3 solution of PDMS : hexane and spray coating of 1 ml of the 10:1 PDMS ratio solution on the about 8 cm long yarns four times on both sides. It is important to prepare the 1:3 PDMS : hexane on the same day. The coating covered only 5 cm of each yarn. Divac KEPT9909 spray coating device with a spray gun produced by Gocheer and another spray gun manufactured by Fengda were used in the experiment. Next, the yarns were cured in an oven at 60°C for 2.5 hours. The action was repeated a few times.

- 4th attempt of coating the yarns – Spin coating

About 1 ml of the afore-mentioned 1:2 PDMS : hexane solution was spin coated at 4000 rpm of spinning speed on a silver-coated nylon yarn and afterwards cured on a heating plate at about 60°C for 2.5 hours. The spin coater was a WS-650MZ-23NPPM 0 Laurell device.

- 5th attempt of coating the yarns – Brush painting

In this attempt, a simple brush bought in Flying Tiger Copenhagen was used. PDMS, 1:2 and 1:3 PDMS : hexane solutions were brush painted on silver-coated yarns hanging vertically from a self-made device. Eventually, the samples were cured in an oven at 60°C for 2.5 hours.

- 6th attempt of coating the yarns – Brush painting on a heating plate of a thick PDMS layer

The last approach requires a heating plate setup at about 60°C, mixed PDMS and brush. PDMS was brush painted on silver-coated nylon yarns from both sides and let for 2.5 hours on the heating plate to cure. The action was repeated until an about 5 mm wide PDMS layer was achieved.

- 7th attempt of coating the yarns – Brush painting on a heating plate of a thin PDMS layer

This attempt is alike the 6th attempt with the exception that only one PDMS layer was brush painted twice on silver coated nylon yarns that were placed on a heating plate. Therefore, just one half of each yarn was coated.

- Prototypes
 - 1st and 2nd prototypes – Thick PDMS coated yarns by using brush painting

Yarns created in the 6th approach were woven into a 1 x 1 matrix with 5 yarns crossing each other in the matrix intersection and 5 yarns laying on top of each other. To be more precise, 5 yarns were places vertically closely to each other and on top of them, 5 yarns were put horizontally. All yarns were stitched to a fabric to stabilize the structure.

- 3rd, 4th, and 5th prototypes – Contact point made of two yarns coated with PDMS of different thicknesses

Here, the yarns from the past prototypes were reused by gradually scrapping off PDMS. The third prototype consists of two yarns from which one is thinner due to cutting off some PDMS (the thickness decreases twice). The fourth prototype consist of one thick yarn and one yarn with PDMS scraped off. The fifth structure is made of two yarns with PDMS scraped off – only a thin layer of PDMS was left.

- 6th prototype – Thin PDMS coated yarns by using brush painting woven into a fabric

Yarns created in 7th approach were woven into a cotton piece of fabric hardened with corn starch. In each intersection, 14 yarns are crossing each other. The structure created a 2 x 2 matrix.

- 7th, 8th, and 9th prototype – Thin PDMS coated yarns by using brush painting paired with silver-coated yarns

In this iteration, yarns created by the 7th coating attempt were utilized. The 8th prototype consists of such one yarn placed on top of the second yarn. The next two prototypes are 5 x 5 matrixes made of the aforementioned yarns either placed under silver-coated nylon yarns used in the experiments or woven together with them.

3.1.1.2 Approach 2 – Wearable textile-sandwiched pressure sensors

Figure 45 illustrates the desired in this approach capacitive textile-sandwiched pressure sensor consisting of a PDMS layer sandwiched in between of two pieces of fabric made of a 2 x 2 matrix of silver-coated nylon 235/34 dtex 4-ply HC+B yarns purchased from Shieldex used in the research. The sensing device is a square of 5 cm x 5 cm and about 0.5-1 cm high.

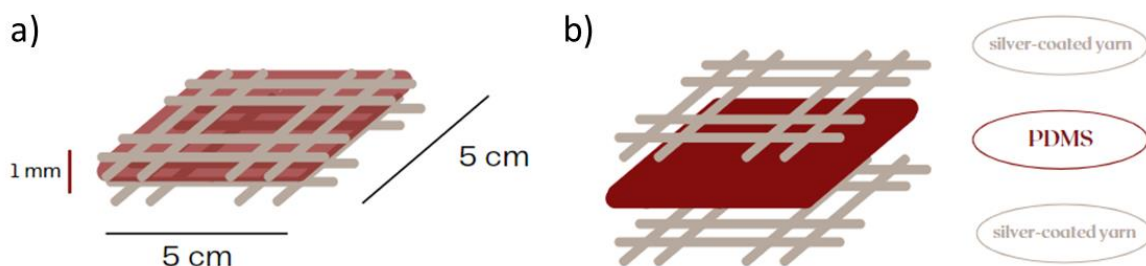


Figure 45. Schematic illustration of the wearable textile-sandwiched pressure sensor including a) its dimensions and b) materials.

- 1st, 2nd and 3rd prototype – Creating simple 2 x 2 matrixes with the desired amount of yarns

The 1 mm thick PDMS layer was fabricated by mixing 10 ml of the Silicone Elastomer Base with 0.1 ml of the Silicone Elastomer Curing Agent purchased from Sylgard in a Petri dish. The sample was left for 30 minutes in a vacuum oven and next, it was cured at 60°C for 2.5 hours in an oven. 5 cm x 5 cm PDMS square was cut and placed in between of two fabric pieces made of silver-coated nylon. The fabric was woven to a 2 x 2 matrix with 6, 10, and 14 silver-coated nylon yarns that would be crossing in each of the four contact points.

- 4th prototype – Pre-curing PDMS and placing the fabric on top to improve the stability of the device

Another approach consisted of pre-curing of about 0.5 mm thick PDMS layer for 30 minutes, placing the silver-coated yarn matrix (14 yarns in the intersection) on top of it, curing it for 2 hours at about 60°C, rotating and next adding a fresh PDMS layer (same thickness), pre-curing it again for 30 minutes and lastly placing the second the silver-coated yarn matrix on top of it and curing for 2 hours at 60°C.

- 5th prototype – Creating a more stable fabric by adding yarns of another material in between the silver coated nylon yarns

This approach is almost identical as the previous method with the exception that the active silver coated nylon yarns were woven into a non-active fabric acquired from Taito Pirkanmaa. The purchased “Penelopekanavakangas” fabric consisted of cotton yarns hardened with starch.

- 6th, 7th and 8th prototype – Introducing a porous PDMS layer

Three sugar templates were prepared, namely two of granulated sugar and one made of sugar cubes. PDMS solution was poured in petri dishes with sugar and the sample was cured for 2.5 hours at 60°C along the standard procedure described in the thesis. Next, the samples were placed in boxes with warm water and left for a week until sugar dissolves. The fabric piece used in this experiment consisted of 7 silver-coated nylon yarns crossing each other in the intersection woven into non-active cotton yarns hardened with starch.

- 9th, 10th and 11th prototype – Influence of the number of yarns utilizing PDMS foam as the dielectric layer

In these iterations, foams based on sugar cubes (1.5 cm x 1.5 cm) fabricated in the last instructions were used as dielectric layers. To understand the influence of different numbers of yarns, fabrics consisting of 7, 14, and 21 yarns crossing each other in the intersections were utilized.

- 12th, 13th and 14th prototype – Influence of the number of yarns utilizing PDMS as the dielectric layer

To understand the influence of different numbers of yarns, fabrics consisting of 7, 14, and 21 silver-coated yarns crossing each other in the intersections were

woven and assembled into sensors. The only divergence from the last case is the dielectric layer material. Here, non-porous PDMS of the same size as the fabrics was used.

3.1.1.3 Approach 3 – Wearable AgNW-based sandwich-type pressure sensor

Figure 46 presents the pressure sensor desired in this approach which consists of AgNWs, two cellulose hydrogel layers and one PDMS layer. AgNWs would be brush painted on one side of each of the two cellulose hydrogel square-shaped samples (3.5 cm x 3.5 cm) and a PDMS layer would be sandwiched in between them. This way, AgNWs would create a 3 x 3 conductive matrix inside the structure.

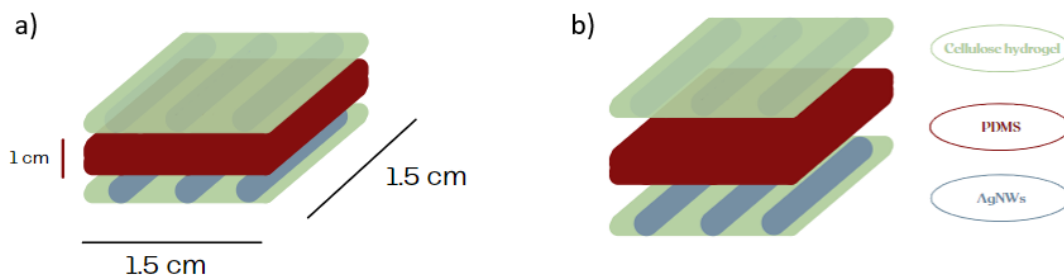


Figure 46. Schematic illustration of the wearable AgNW-based sandwich-type pressure sensor including a) its ready form and b) materials that were used.

- Substrate materials
 - Cellulose hydrogels

The first cellulose hydrogel was prepared according to the procedure described by Dong *et al.*⁵⁵ A 1.8% 2,2,6,6-tetramethylpiperidine-1-oxyl radical-cellulose nanofibers (TEMPO-CNF) suspension was spread in a petri dish and left overnight in a aluminium (Al^{3+}) and calcium (Ca^{2+}) ions.

The second cellulose hydrogel was prepared along the procedure presented in the article written by Lee *et al.*⁵⁶ The only alternative was mixing of 1 mL of epichlorohydrin in TEMPO-CNF (1.8%) and next putting it in a petri dish. The substance was kept overnight and on the next day, an Al^{3+} solution was used to

finalize the crosslinking reaction. The fabrication processes are not essential for understanding of the research and thus, the details were omitted.

- Nanocellulose film

The nanocellulose film was obtained by following the procedure described in the CHEMARTS Cookbook written by P. Kääriäinen *et al.* First, 100 g of nanofibrillar cellulose (NFC) purchased from UPM were mixed in a beaker with 200 ml of water by using a spoon. Next, a magnet was put into the beaker and the beaker was placed on a magnetic stirrer. The solution was mixed at 800 rpm of stirring rate for 24 hours. Then, 100 ml of glycerol purchased from VWR Chemicals was added to the beaker and the solution was mixed for 1 hour. Preferable, the mixture should be poured in a 2.5 cm high petri dish with 15 cm in diameter.⁵⁷ In this case, the mixture was poured into a 2 cm high petri dish with 13 cm in diameter and the leftover solution was poured into a small petri dish. Lastly, the container was left in an oven set up at 35°C for 8 days and 1 day at 60°C.

- Synthesis and deposition of AgNWs

Ultralong AgNWs were synthesized via the multistep growth proposed by Lee *et al.*,⁵⁸ Lee *et al.*,⁵⁹ and Lee *et al.*⁶⁰ by using first grown AgNWs a seed. The process conditions including metal salt injection rate, concentration, stirring speed and environment gas type were carefully controlled. After the synthesis, the were subjected to surface modification via ligand exchange with alkanethiol molecules. AgNWs were deposited by brush painting followed by 30 minutes long annealing at 100°C. The fabrication process is not essential for understanding of the research and thus, the details were omitted. In each of the prototypes, two 1.5 cm x 1.5 cm large pieces of nanocellulose film were used as substrates.

- Prototypes

- 1st prototype – Porous PDMS layer

To obtain porous PDMS, a sugar cube was placed in a tiny container and PDMS solution (prepared as afore mentioned) was poured onto it. Next, the sample was left for 30 minutes in a vacuum oven. Almost the whole height of the sugar cube (1 cm) was covered with PDMS. Only a few millimeters were left out so that after curing for 2.5 hours at about 60°C, when warm water was poured into the

container, the water could dissolve the sugar. The setup was left for a week so that the sugar cube would fully dissolve. Within the week, the water was replaced daily by warm water.

- 2nd prototype – Non-porous PDMS layer

In the second iteration, 0.5 mm high non-porous PDMS was created by using the same technique as described in the previous example. No vacuum oven treatment was used. Instead, the sample was left for 15 minutes so that all air bubbles could escape. The aim of creating this prototype is to obtain a comparable data set to discuss the influence of pores on the capacitive response.

3.1.2 Wearable strain sensors

3.1.2.1 Approach 1 – Wearable yarn-based strain sensors

In this approach, Spandex yarns purchased from Kinetic were twisted with the afore-mentioned silver-coated nylon yarns with a self-made device. Ideally, they would be coated with PDMS afterwards. The schematic representation of the desired yarns and their woven 2 x 2 matrix structure are presented in Figure 47. The POC prototype created for the experiments consists of twisted yarns (1 cm x 2 cm) woven into a 1 x 1 matrix embedded in a fabric made of cotton hardened with corn starch (total size: 5 cm x 5 cm). The stretchability percentage of the setup amounts to more than 50%.

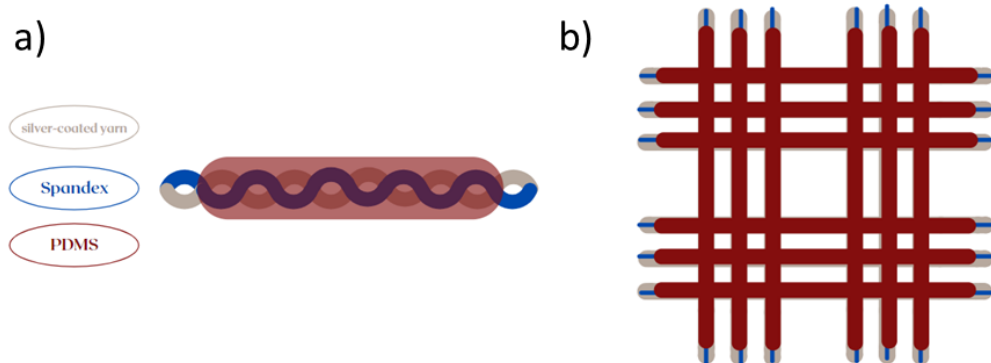


Figure 47. a) Silver-coated nylon yarn twisted with Spandex and coated with PDMS layer and woven into b) the square-shaped textile creating the wearable yarn-based strain sensor.

3.1.2.2 Approach 2 – Wearable textile-sandwiched strain sensors

Figure 48 illustrates the strain sensor desiderated in this approach. Again, silver-coated nylon yarns and Spandex used in past examples would be twisted with a self-made device and woven into two 2×2 matrixes. A PDMS layer would be sandwiched between the fabric pieces. The fabricated POC prototype of a strain sensor consists of a small 1×1 matrix ($1 \text{ cm} \times 2 \text{ cm}$) made of Spandex and silver-coated nylon yarns based on a cotton fabric hardened with corn starch (total size: $5 \text{ cm} \times 5 \text{ cm}$).

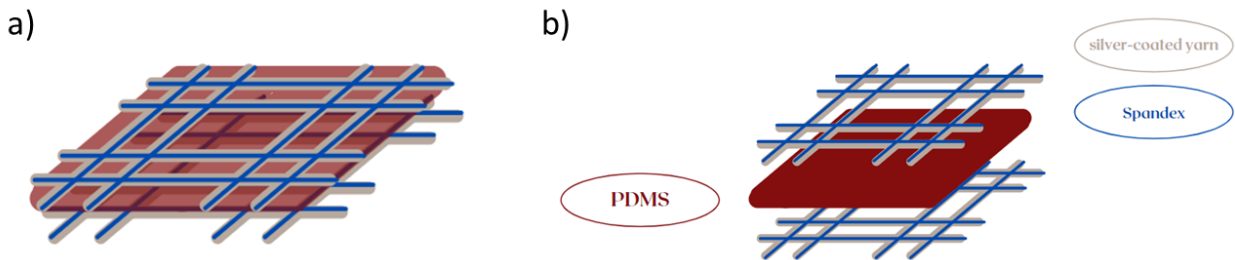


Figure 48. Schematic illustration of the wearable textile-sandwiched strain sensor including a) its ready form and b) materials that were used.

3.2 Weights

To apply pressure on the fabricated sensors, six vials were used. Five of the vials had screw caps. The applied pressure was determined by the Eq. 6.

$$P = \frac{W}{A} \quad \text{Eq. 6}$$

where P is pressure, W is weight, and A is the area where the weight is applied and next converted into Pascals knowing that 1gcm^{-2} equals 98.0665 Pa .^{61,62} Figure 49 presents a photography of all vials and Table 5 summarizes their weights based on sizes, their areas and the resulting pressure values. The largest vial weights about 25 grams what equals to 4.99 g/cm^2 , whereas the smallest 3 g

what equals to 3.04 g/cm^2 . It is worth noticing that the pressure value does not depend on the weight of the vials. The highest pressure can be applied by placing the 20 g heavy vial, whereas the lowest pressure by the 7 g heavy vial.

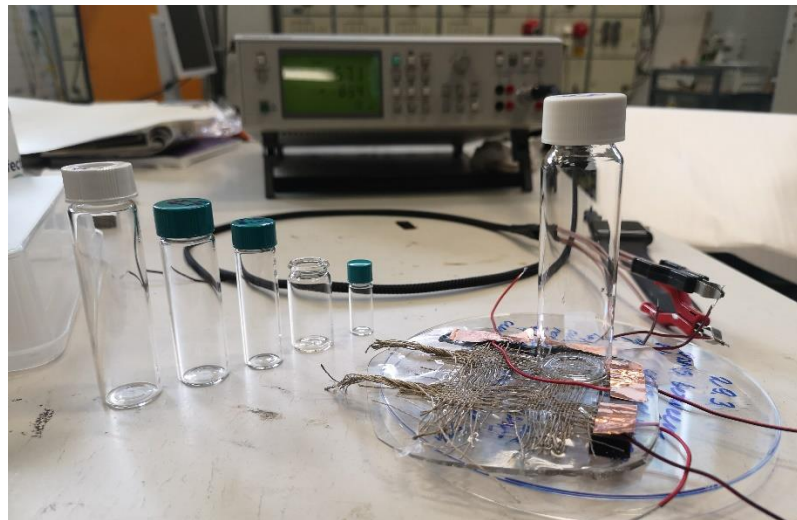


Figure 49. Photograph of all weights used in the experiments during one of the capacitance measurements.

Table 5. Summary of vials used in the experiment as weights and their actual and approximated weight values.

Weight size	Weight [g]	Approximation [g]	Area [cm²]	Pressure [Pa]
Smallest height	2.9	3	0.95	0.298
	6.9	7	2.84	0.238
	9.4	10	2.01	0.463
	14.0	15	3.14	0.437
	19.2	20	3.80	0.495
Largest height	24.5	25	4.91	0.489

Calibration weights purchased from Sartorius were used in the experiments as well. Figure 50 presents a photograph of exemplary weights (100 g - 1 g) and Table 6 summarized their areas and respectively their pressure values. The

highest pressure can be applied by using the 50 g heavy weight, whereas the lowest pressure value can be applied by the 0.005 g heavy weight.



Figure 50. Photograph of exemplary calibration weights (100 g, 50 g, 20 g, 10 g, 5 g, 2 g, 1g) used in some of the experiments.

Table 6. Summary of weights used in the experiment and their weight values.

Weight [g]	Area	Pressure [kPa]	Weight [g]	Area	Pressure [kPa]
	[cm ²]			[cm ²]	
0.005	0.211	0.0023	1	0.283	0.3468
0.010	0.100	0.0098	2	0.283	0.6937
0.020	0.250	0.0079	5	0.503	0.9755
0.050	0.348	0.0141	10	0.785	1.2490
0.100	0.333	0.0327	20	1.327	1.4780
0.200	0.723	0.0272	50	1.539	3.1850
0.500	0.968	0.0507	100	3.801	2.5800

Figure 51 shows a photograph of self-made copper weights used in a few experiments. It is important to note that these weights have the same surface areas. Table 7 summarizes information about the area, weights, and corresponding pressure values. The largest weight of 40 g shows the largest pressure value of 9.55 kPa, which is even larger than in past two sets of weights. Pressure of four weights is lower than 1 kPa. The surface area of all copper weights amounts to 0.41 cm².



Figure 51. Photograph of copper weights (40 g, 25 g, 20 g, 15 g, 10 g, 7g, 5 g, 3 g, 2 g, 1.5 g, 1g) used in several experiments.

Table 7. Summary of information about copper weights used in several experiment and their corresponding weight values.

Area [cm²]	Weight [g]	Pressure [kPa]	Weight [g]	Pressure [kPa]
0.410881	1.0	0.24	10.0	2.39
	1.5	0.36	15.0	3.58
	2.0	0.48	20.0	4.77
	3.0	0.72	25.0	5.97
	5.0	1.19	40.0	9.55
	7.0	1.67		

3.3 Characterization methods

Samples were characterized with the Tabletop SEM-Energy Dispersive X-Ray Spectroscopy (EDS) Hitachi TM4000Plus, Tescan Mira3 SEM, and the Olympus BH-2 Optical Microscope. A metal sputter (Ag/Cu) was utilized to coat samples for 30 s with a conductive layer before SEM imaging. Capacitance measurements were conducted with Keysight 34465A Digital Multimeter and Fluke PM6306 RCL meter. The voltage used in reading of the capacitance amounted to 1 V (AC) and the frequency 100 Hz, 1 kHz, and 100 kHz. These parameters were chosen based on the literature review of similar works.^{2,3,30,54} Silver paste or copper tape and copper wires were used to connect the sensors with the multimeters.

4 Results and Discussion

This chapter called “Results and Discussion” is the most essential part of the research as it describes the main findings of the experiments and interprets the results. All three categories of devices were manufactured and characterized. Five final devices and the insights from trials before achieving the desired outcomes were explained and evaluated critically. The results were compared to the literature review and their meaning, importance and relevance discussed.

4.1 Wearable pressure sensors

First, three approaches in the wearable pressure sensor class, namely wearable yarn-based, textile-sandwiched, and AgNW-based sandwich-type pressure sensors, are described and discussed.

4.1.1 Approach 1 – Wearable yarn-based pressure sensors

4.1.1.1 Comparison of the suitability of 1-ply versus 4-ply silver-coated nylon yarns and summary of all coating attempts

To compare which silver-coated yarns are more suitable for the experiments, 1-ply and 4-ply yarns were dip coated in PDMS. Photographs of these yarns after dip coating are visible in Figure 52. The difference between these yarns is that in the 4-ply structure, 4 twisted yarns create the final yarn, whereas in the 1-ply structure, it is only 1 yarn. Thus, 1-ply yarn looks alike a spiral. The thickness of the 4-ply yarns amounts to 0.46 mm, and the thickness of the 1-ply yarn is 0.32 mm.

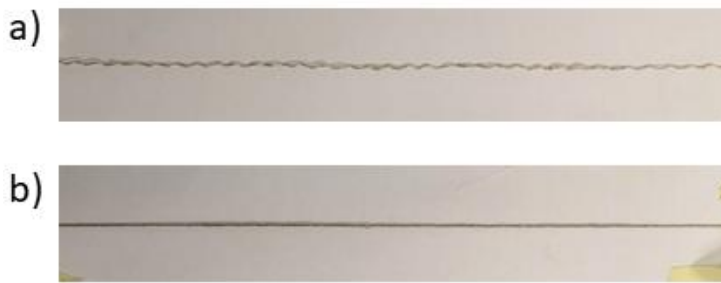


Figure 52. Photographs of a) 1-ply and b) 4-ply silver coated nylon yarns dip coated in PDMS.

The PDMS coating is not visible in the above photograph. Thus, optical microscopy images shown in Figure 53 were taken. Figure 53a presents a non-coated 4-ply silver-coated yarn. Figures 53b and 53c illustrate coated 4-ply and 1-ply yarns. The thin white smudges in Figure 53b correspond to PDMS. However, the amount of PDMS is incredibly little and thus, the coating method (without using any adhering support layer) is not sufficient for the scope of the experiment. In Figure 53c the PDMS layer seems to have entered inside of the yarn what is not the desired behavior of coating. Because of this reasoning and because of better availability due to a lower price, it was decided to pursue the research with the 4-ply silver-coated yarns. From the conductivity point of view, 1-ply might be less optimal as less contact points are possible.

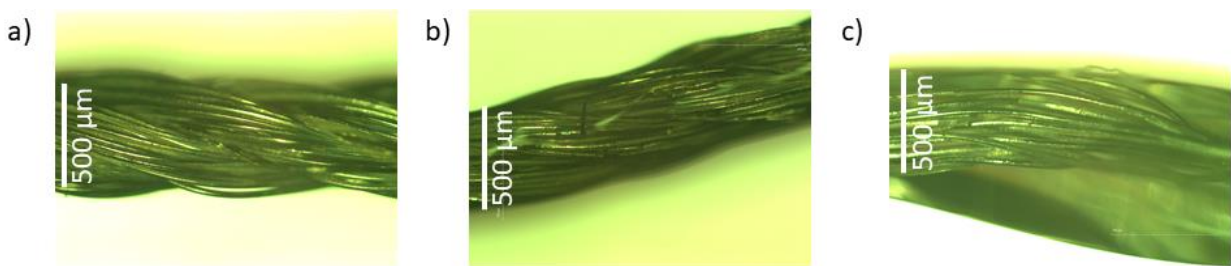


Figure 53. Optical microscopy images of a) non-coated 4-ply yarn, b) PDMS coated 4-ply yarn, c) PDMS coated 1-ply silver-coated nylon yarn

Next, the method was alternated to achieve a thicker coating by adding an additional step. Plasma cleaning was applied before dip coating the yarns. Nevertheless, the only visible difference, most likely addressed to the plasma cleaning process, was the color change from the initial silver to black. The amount of coating was still insufficient. Another method that was tested was dip coating

in two different mixtures of PDMS and hexane. The SEM image visible in Figure 54 shows that one of the resulting coating is negligible. Same results were obtained for the second solution.

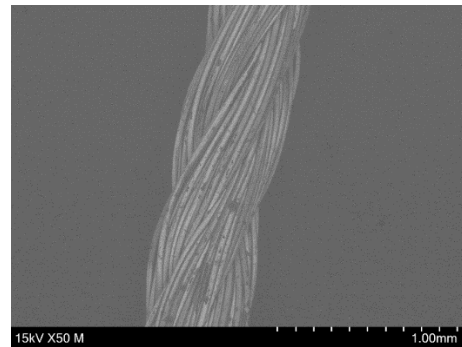


Figure 54. SEM image of a silver-coated yarn dip coated in 3:1 hexane:PDMS solution.

One last alternation was tested – dipping the yarn in PDMS and curing it for 30 minutes. Then, the yarn was taken out from PDMS. The outcome coating is much thicker than in all previous cases, but it is non-uniform. However, this method has a potential to be improved.

Therefore, a new approach was introduced – spray coating. Two layers (instead of one like in the past examples) were spray coated on the yarns by using a solution of PDMS in hexane that is shown in optical microscopy images in Figure 55. The resulting PDMS layer is better visible throughout the whole length of the yarns, but its amount is still low.

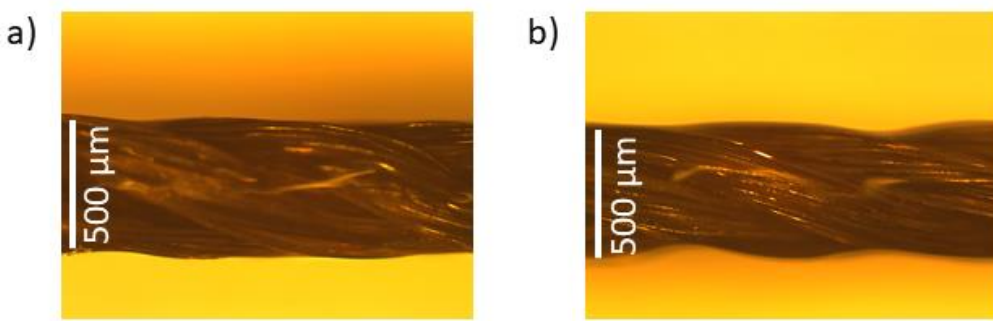


Figure 55. Optical microscopy images of spray coated silver-coated yarns.

To confirm the presence of PDMS after spray coating, SEM images were taken. A clear, shown in Figures 56a, 56b and 56c, difference is visible between the initial non-coated yarn. Spray coating was concluded to be a better approach and

experiments continued as at least 1 mm thick coating was desired. Unfortunately, the total duration of the coating process (4 layers from both sides) started extending from 2.5 hours to 13 h hours as the spray gun was gradually getting more clogged even though it was cleaned every day. After ending of a daily coating procedure, the spray gun was placed in a beaker with hexane, put into an ultrasonication bath for 10 minutes, and eventually let soaking overnight. To accomplish the desired number of yarns with a thick PDMS layer, a huge number of days would be needed. In addition to that, the resulting coating consisted of bubbles mostly which is not an ideal shape and is not uniform throughout the whole length of a yarn. Thus, spray coating was concluded to be an infeasible solution and would need to be improved by e.g., purchasing a new spray gun with a larger nozzle.

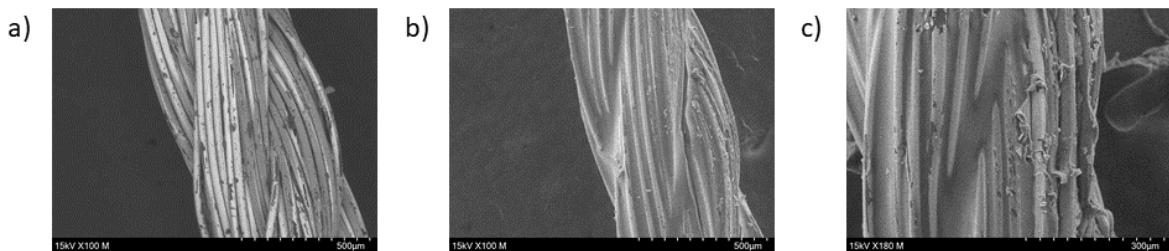


Figure 56. SEM images of a) a non-coated silver-coated yarn, b-c) spray coated with a PDMS solution in hexane silver-coated yarns.

Afterwards spin coating was tested for its applicability as a deposition method. The resulting PDMS layer (from hexane) was non-uniformly distributed what was clearly visible on a glass slide and the amount of coating was insufficient. Last method that was tested was brush painting. First, PDMS and its mixtures with hexane were applied on yarns hanging vertically from a self-build holder. The coatings were not strongly enough adhering to the yarn, they dripped down and thus, after a few minutes, the yarn was bare again. For this reason, the setup was changed, the yarns were placed on a heating plate and PDMS and its solutions with hexane were applied. Figure 57 presents the outcome – the silver-coated nylon yarn coated multiple times with PDMS by brush coating. The deposited PDMS layer is relatively thick as it has about a few millimeters. Such yarns were

used to create the first prototypes. Yarns that were coated with hexane and PDMS met the needs too, but adding hexane was an unnecessary step.



Figure 57. PDMS layer deposited by brush painting on a 10 cm long silver-coated nylon yarn.

Table 8 presents a summary of all coating methods that were tried in the research and reasons for their poor or decent applicability. Figure 57 presents photographs of yarn coated by using respectively the afore-mentioned approaches. The most feasible solution turned out to be the simple brush painting. However, methods like dipping in pre-cured PDMS or spray coating can be further worked on.

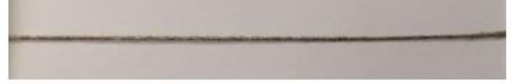
Table 8. Summary of all coating methods and their applicability for creating a 1 mm thick PDMS layer on silver coated nylon yarns.

Coating method	Applicability	Reason
Dip coating	-	Poor adhesion of the PDMS coating to the yarn.
Dip coating after plasma cleaning	-	Poor adhesion of the PDMS coating to the yarn. The yarn changed its color from silver to black.
Dipping in pre-cured PDMS	-	The outcoming coating is too non-uniform. The difference in thickness is too large.
Spray coating	-	The spray gun is getting more stuck with every experiment. Thus, the final average time is too long what makes the approach infeasible.
Spin coating	-	Poor adhesion of the coating to the yarn and its non-uniform distribution.

<i>Brush painting</i>	-	<i>Poor adhesion of the PDMS coating to the yarn when applied vertically.</i>
<i>Brush painting</i>	+	<i>The method is effective. The coating was created successfully.</i>
<i>on a heating plate</i>		



a)



g)



b)



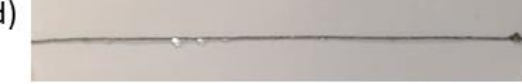
h)



c)



i)



d)



j)



e)



k)



f)

Figure 57. Coating achieved upon a) dip coating of yarns in PDMS for 30 seconds, b) dip coating of yarns in PDMS for 30 seconds after plasma cleaning treatment, c) dip coating of yarns in PDMS and curing it for about 30 minutes, d) spray coating of one layer of PDMS:hexane solution mixed in 1:3 ratio, e) spray coating of multiple layers of PDMS:hexane solution mixed in 1:3 ratio, f) spin coating on a glass slide (photograph includes the non-uniform coating visible on the glass slide), g) spin coating on a glass slide, h) brush painting of PDMS on the yarns hanging vertically from a self-build holder, i) brush painting of PDMS:hexane (1:2) solution on the yarns hanging vertically from a self-build holder, j) brush painting of PDMS:hexane (1:3) solution on the yarns hanging vertically from a self-build holder, k) brush painting of one layer of PDMS applied on a heating plate.

4.1.1.2 1st and 2nd prototypes – Thick PDMS coated yarns by using brush painting

The created PDMS coated yarns were woven into a one cell large matrix visible in Figure 58a. No capacitance change was recorded. Thus, the device structure was altered by placing 5 yarns vertically on top of 5 yarns placed horizontally on the bottom what is shown in Figure 58b. The variation did not influence the output and again no capacitance change was observed. It was concluded that the coating is too thick.

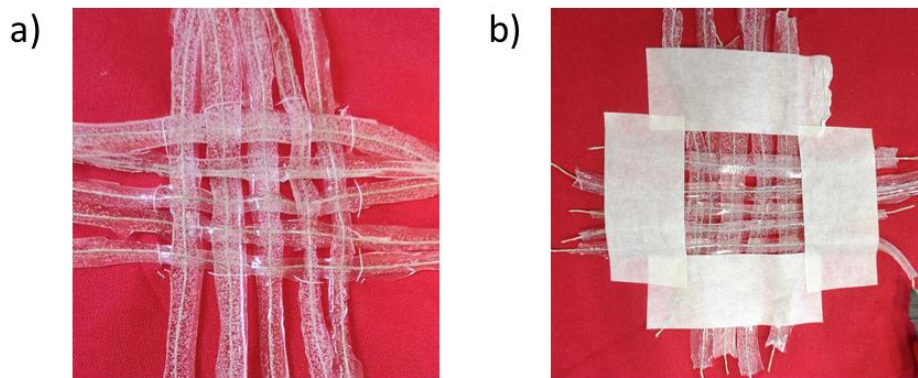


Figure 58. The single cell matrix made of 5 yarns crossing each other in the intersection created by a) weaving and b) placing 5 yarns vertically on top of 5 yarns placed horizontally.

4.1.1.3 3rd, 4th, and 5th prototypes – Contact point made of two yarns coated with PDMS of different thicknesses

A contact point made of two yarns only with reduced PDMS thickness showed in Figure 59a was measured and again no capacitive response was recorded. However, the conductivity of the yarns was tested and proved, so the next step was to scrap off PDMS from one of the yarns what is visible in Figure 59b. The frequency values were modified from 100 Hz to 100 kHz to achieve more precise readings. As a result, the capacitance value increased a little upon applying pressure by touching. Figure 59c presents the final step which included scrapping off PDMS from the second yarn leaving only a very thin layer of the dielectric. This setup turned out to be successful as capacitance increased significantly upon

gentle, medium and strong finger touch and it was concluded that the thickness of PDMS plays a crucial role as it must be as thin as possible to obtain decent results. Another learning is that it might be beneficial not to coat the whole yarn, but to keep the coating on its half only. Data was not plotted upon touch as it is too difficult to define the exact pressure generated by a finger and link the responses. The literature review is not helpful in defining the regimes either.^{3,63}

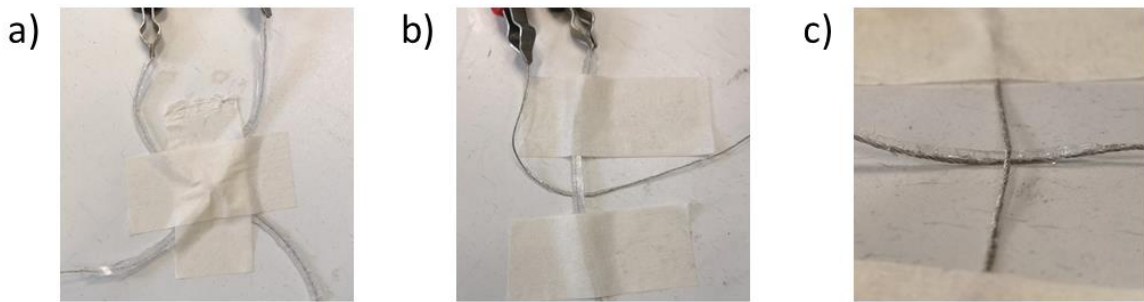


Figure 59. Contact point made of two yarns which a) are both coated with PDMS by brush painting, b) one of them is coated with PDMS and the second one has leftovers of scraped off PDMS, c) both with a thin layer of scraped off PDMS.

4.1.1.4 6th prototype – Thin PDMS coated yarns by using brush painting woven into a fabric

Next, a prototype made of non-conductive cotton yarns, that ensured a higher stability, and conductive silver-coated yarns was created. Figure 60 shows the woven fabric piece with convex center because of a high number of used yarns. The coating is thin, so the capacitance response should be measured easily. Due to weaving, much PDMS was scrapped off and thus, conductive sides of silver-coated yarns were touching each other. As a result, the whole sample was conductive, and no capacitance could be recorded. To better understand the reason why this approach did not work, optical microscopy images visible in Figure 61 were taken. It is difficult to identify conclusions from the images though. An interesting observation is the presence of bubbles in PDMS what can cause higher capacitive response. Nonetheless, the biggest and most important mistake to begin with was weaving. Also, it is inevitable that bare sides of silver-coated

yarns would be touching each other (as the coating was applied only from one side) as can be imagined by using Figure 43 as a reference. This means that the organization of yarns has to be further improved. For example, stitching (Figure 42) or a bobby thread (Figure 43) could be utilized.



Figure 60. Photograph of the sixth prototype made of non-active and active yarns.

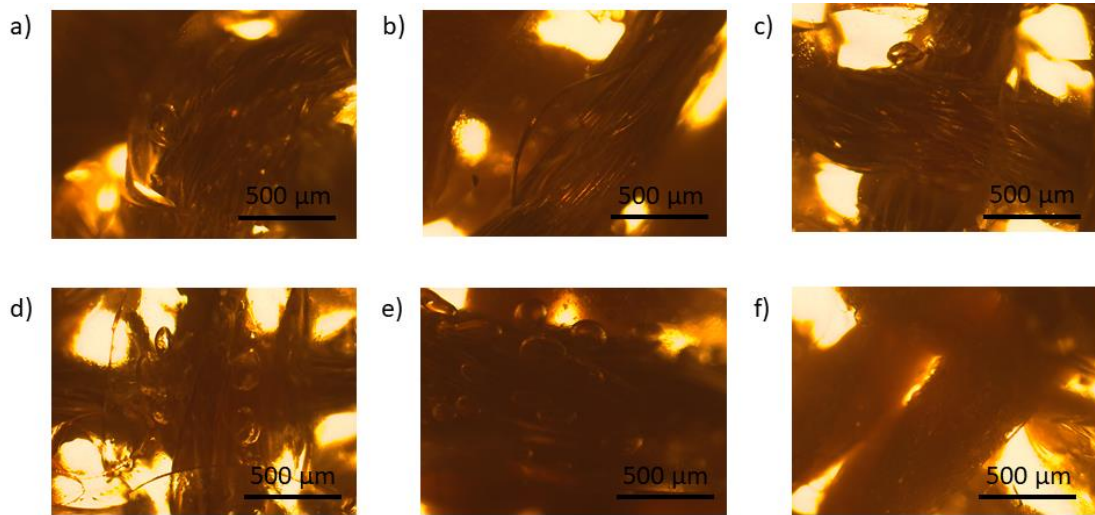


Figure 61. Optical microscopy images taken of the sixth prototype.

4.1.1.5 7th, 8th, and 9th prototype – Thin PDMS coated yarns by using brush painting paired with silver-coated nylon yarns

The next prototype was made of yarns coated from one side only. The photograph of the setup is shown in Figure 62a. Figure 62b presents the measured capacitive

response. The change in capacitance is clearly observed with calibration weights. However, the heaviest weight does not exceed pressures larger than 5 kPa. For the scope of this research, it is preferred to have one weight that exhibits pressure around 10 kPa, and a few weights that can apply pressure under 1 kPa. Thus, copper weights were introduced. The main difference between these two types of weights lies in the surface area. Copper weights have the same surface area, whereas the calibration weights have different surface areas. At this point, it is worth to ask if the material of the weights plays a role in the measurements. It is unlikely, but surely the placement of the weights on the sensor impacts the readings (as when placed in a tilted way, the pressure was not applied on the whole area, but only partly). The prototype is less sensitive towards copper weights over 1 kPa, and more sensitive below 1 kPa. Furthermore, the shape of the plot seems to be more relevant in comparison to literature.⁶ From this experiment on, only copper weights are used in the research.

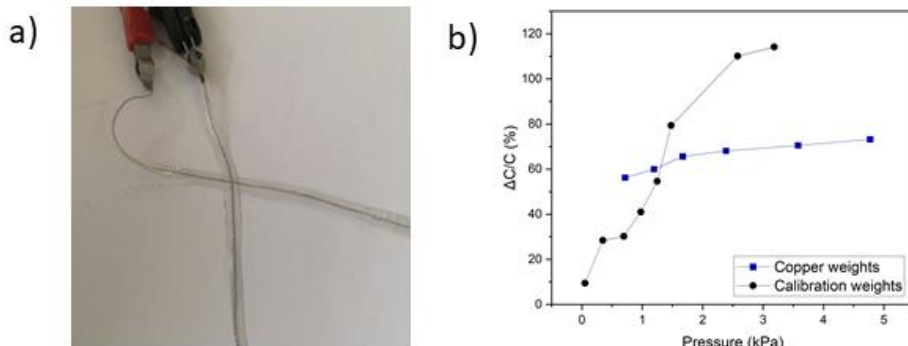


Figure 62. a) Photograph of the 7th prototype consisting of two yarns coated thinly with PDMS. b) Capacitive response measured upon copper and calibration weights.

Due to promising results, a 1 x 1 matrix visible in Figure 63a was created by placing the coated with PDMS yarns vertically and the non-coated silver yarns horizontally. The sensitivity in the low-pressure regime amounts to 0.0209 kPa^{-1} and the capacitive response in Figure 63b is clear. In comparison to Figure 64, the sensitivity is higher. Figure 64a presents an alternative setup in which the yarns are woven. Weaving prevents silver yarns from touching each other what would enable an easier scaling up and mass production. The sensitivity that can

be calculated from the slope in Figure 64b amounts to 0.0129 kPa^{-1} . In addition, it seems that there are three distinguishable pressure regimes.

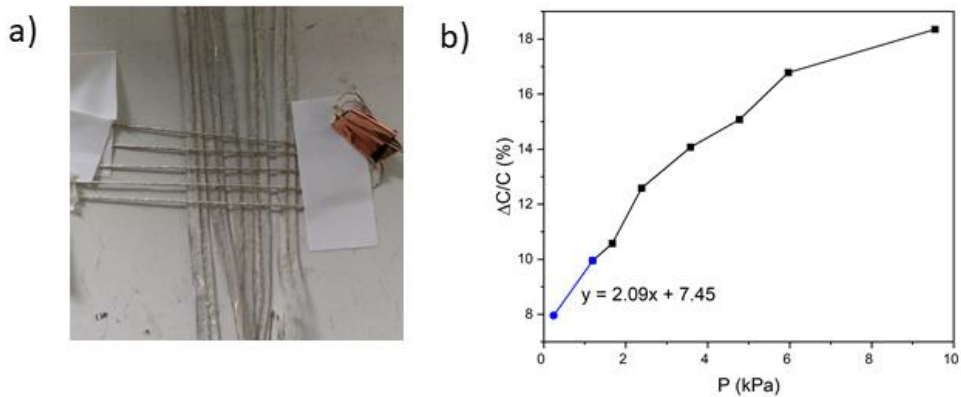


Figure 63. a) Photograph of the 8th prototype composed of non-coated and PDMS-coated yarns placed one of top of the other and b) the corresponding changes in capacitance noted upon application of copper weights.

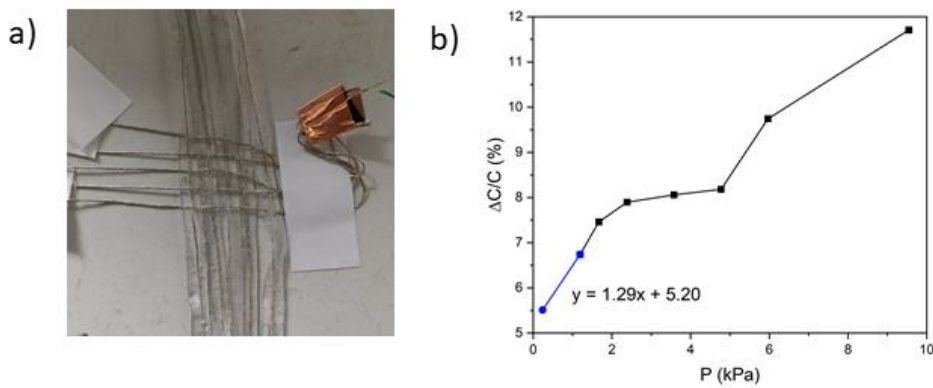


Figure 64. a) Photograph of the 9th prototype composed of non-coated and PDMS-coated yarns woven together and b) the corresponding changes in capacitance noted upon application of copper weights.

To sum up, the main problems encountered in the fabrication process were selection of a coating method, adjusting the thickness of PDMS, assembly issues (occurring of contact points between silver yarns), implementation of weaving, and choice of weights. The leading prototype with top-notch sensitivity (Figure 63) was made of silver-coated yarns placed on top of PDMS- and silver-coated yarns. The change in capacitance amount to almost 20%. The thickness of PDMS is up to 3 mm from each side. A worth-mentioning next step, valid for all fabricated sensors, is introducing a digital array and by creating an Arduino-based setup

mapping the exact locations of touch and linking it to pressure values alike in the reference papers.^{2,64} New coating methods should be experimented with taking into account a uniform deposition and ensuring breathability of the final fabric which should be an upscaled sample. Fabric-related testing should be performed and multifunctionality should be added.

4.1.2 Approach 2 – Wearable textile-sandwiched pressure sensors

4.1.2.1 1st, 2nd and 3rd prototype – Creating simple 2x2 matrixes with the desired amount of yarns

The first three prototype aimed to evaluate the influence of the number of yarns crossing each other in the intersections and the feasibility of the proposed sandwich structure. In the first place, a 2 x 2 matrix was woven with 6 yarns crossing each other in the intersection. When the structure was untapped from the sheet of paper below, the yarns started losing their structure, the matrix became messy what hinders the measurement. Figure 65 presents the matrix before and after untapping the edges of the yarns. Also, the yarns had to be cut at the ends to assure a proper circuit.

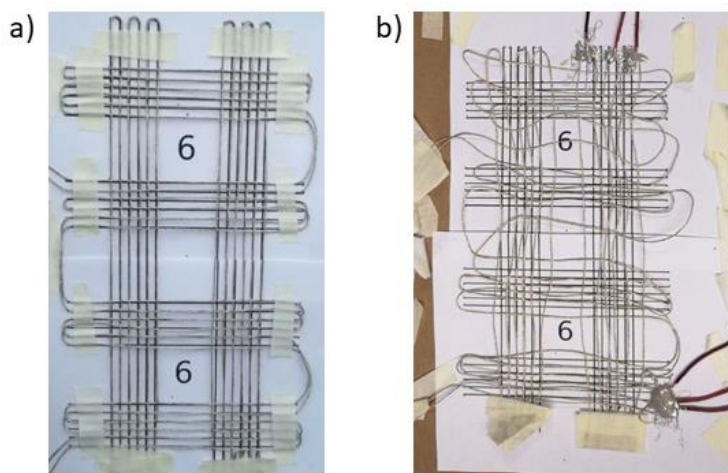


Figure 65. First prototype of the 2 x 2 matrix with 6 yarns crossing each other in each of the contact points a) after weaving, b) after untapping the edges to connect the sensing device with silver paste and copper wires.

Next, the matrix was folded, and a 0.5 mm thick PDMS layer was sandwiched between the two pieces of fabric. The closed device is visible in Figure 66. The setup is not feasible, because after folding, the contact points are not visible anymore and their exact location can be only poorly estimated. However, after drawing a 3 x 3 matrix on the cardboard, a semi-successful measurement was carried out. Figure 67 presents the capacitive responses upon finger pressing of the prototype. The initial capacitance value amounted to about 0.3 pF, what means that the highest change in capacitance amounted to 0.43 pF.



Figure 66. First prototype and the measurement setup including crocodile clips connected to copper wires.

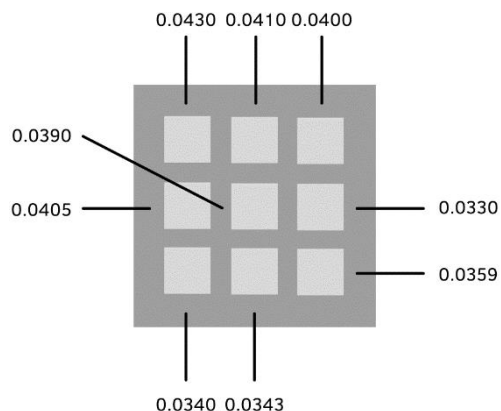


Figure 67. Schematic illustration of the measured values of capacitance in pF.

The second prototype, shown in Figure 68, was made of 10 yarns crossing each other in every of the contact points. Copper wires were connected with the sensing device with copper tape, which turned out to be too less tenacious. The copper tape unstuck very easily. The contact points were marked on the paper sheet which allowed effortless locating after separating the matrixed and putting one of top another. However, the capacitance measurement was unsuccessful with both

weights and finger touch. The air gap between all layers was too large to obtain the initial capacitance values and a proper value of the response. It was concluded that the pressure sensor needs lamination.

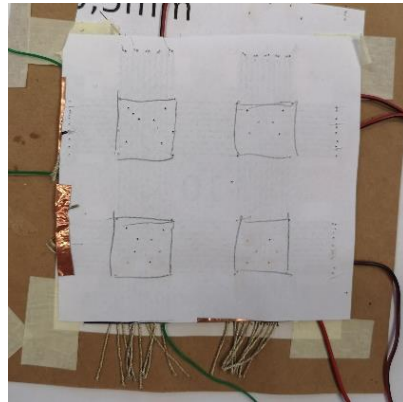


Figure 68. Second prototype with 10 yarns crossing each other in the intersection with copper tape and copper.

In the third attempt, a higher number of yarns - 14 – was used for weaving a more stable fabric, a fabric with a stronger structure. The prototype and the measurement setup are shown in Figure 69. What must be kept in mind is that in order to weave yarns, an even number of yarns has to be utilized. The fabric pieces were separated after weaving and places on top of each other with a PDMS layer sandwiched in between them. Alike in the previous example, the air gap did not allow a noteworthy measurement as only one contact point worked. Nevertheless, the capacitive change seemed too large (a few hundred percent).

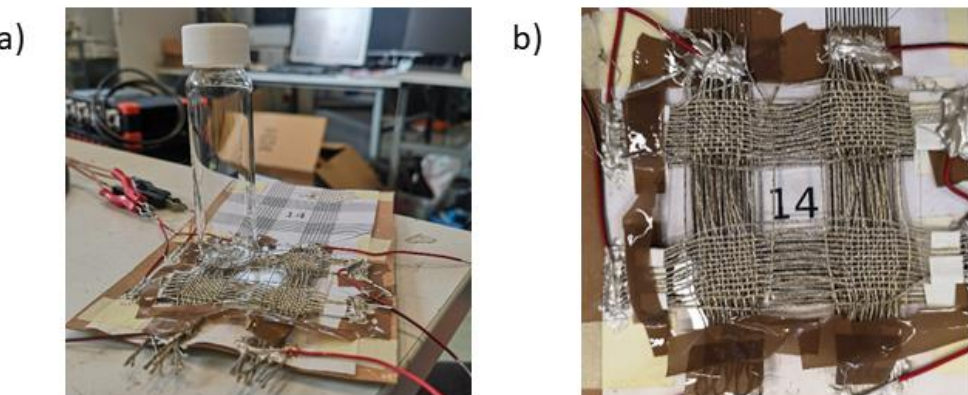


Figure 69. a) Third prototype wires during a measurement and b) its close up on the fabric made of 14 yarns crossing each other in the intersection and a thin transparent PDMS layer in between the fabric pieces.

To summarize, the insights from the first three prototypes include: 1) usage of silver paste instead of copper tape due to better adhesion, 2) avoiding air gaps – need of lamination or placing the fabric on pre-cured PDMS, 3) higher number of yarns creates a stronger structure and thus, 14 yarns is a suitable choice or weaving yarns in between of the silver-coated nylon yarns to create an even more stable structure.

4.1.2.2 4th prototype – Pre-curing PDMS and placing the fabric on top to improve the stability of the device

The fourth prototype created by pre-curing PDMS and placing the fabric made of silver-coated nylon yarns on top and then fully curing the device and repeating the activity by rotating it, placing a fresh PDMS layer on the cured PDMS, pre-curing and placing the second fabric piece is shown in Figure 70. All four contact points of this sensing device worked well. The capacitive responses were measured in each of the contact points by connecting the crocodile clips with copper wires and copper tapes. The only minor flaw of the final result is the fact that some of the extrinsic yarns slipped a little out of the structure. Nevertheless, weaving 14 yarns in the intersection makes the sensor much stronger and the yarns do not come out as much as in previous examples.



Figure 70. Photograph of the third prototype achieved by pre-curing PDMS and placing the fabric on top of it followed by curing and repeating the procedure starting by applying a thin layer of PDMS on PDMS.

Figure 71 presented below shows capacitive change in each of the contact points measured in the experiment by using weights heavy from 3 g to 25 g. The respective sensitivity values amount to 0.00130 kPa^{-1} , 0.00082 kPa^{-1} , 0.00095 kPa^{-1} and 0.00071 kPa^{-1} . The measured data does not align linearly well, thus, the measurements should be repeated with calibration weights by repeating the readings at least 3-5 times and plotting the average values. Figure 72 shows how the capacitive change is distributed upon rising pressure value. Data marked with the darkest green color correspond to the first plot in Figure 71a – first contact point of the sensor. Described in the literature review of the thesis Figure 16 shows that capacitance should increase linearly with higher pressure values. Here, no linear trend is visible what gives another reason to repeat the measurements.

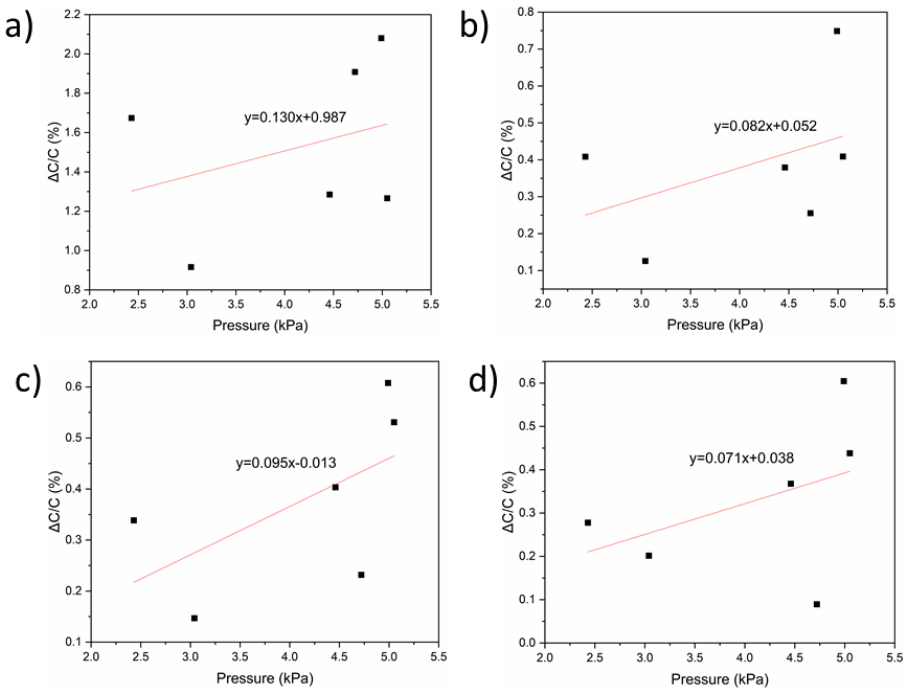


Figure 71. Capacitive responses of each contact points upon applying pressure.

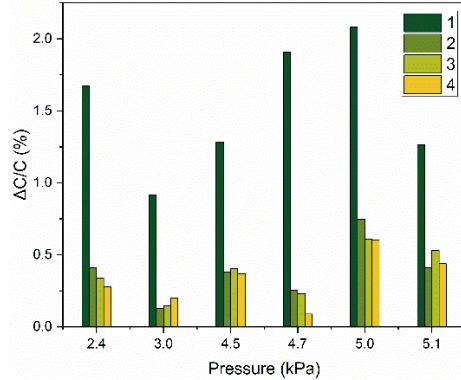


Figure 72. Capacitive changes versus increasing pressure values of each of the four contact points. The darkest green color represents the first contact point which is the same contact point as in Figure 71a.

4.1.2.3 5th prototype – Creating a more stable fabric by adding yarns of another material in between the silver coated nylon yarns

Figure 73 presents the sensor and Figure 74 the observed capacitance changes dependent on applied pressure by calibration weights on each of the contact points. Three pressure regimes regions were distinguished, namely: ultra-low (<0.1 kPa), low (<1kPa) and medium (>1kPa). The first contact point exhibits the following sensitivity values: 1.02 kPa^{-1} , 0.45 kPa^{-1} , and 0.02 kPa^{-1} . The sensitivity values for the second contact point are: 0.35 kPa^{-1} , 0.17 kPa^{-1} , and 0.04 kPa^{-1} , and for the third contact point: 0.56 kPa^{-1} , 0.05 kPa^{-1} , 0.03 kPa^{-1} . The last contact point shows 0.34 kPa^{-1} , 0.05 kPa^{-1} , and 0.06 kPa^{-1} as sensitivity values. The highest sensitivity was recorded in the first contact point, and the lowest in the last contact point. The sensor is most sensitive in the low weight region.

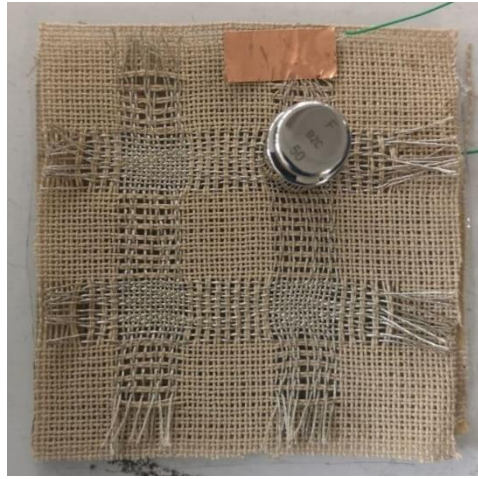


Figure 73. Prototype made of active silver-coated yarns stabilized by weaving into a fabric of non-active cotton yarns.

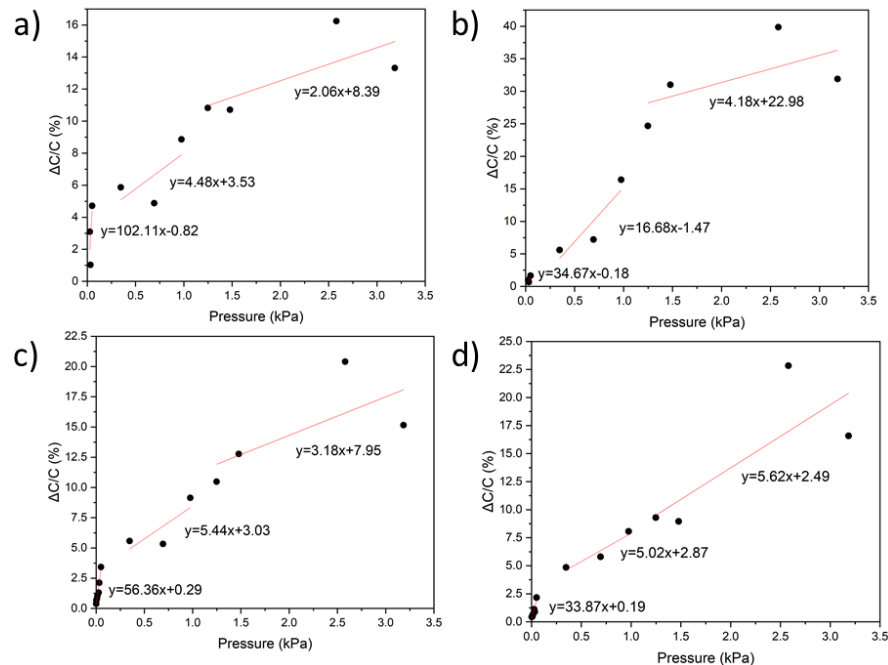


Figure 74. Capacitive responses upon applied pressure on the created prototype made of silver-coated nylon yarns and cotton yarns.

The measurements were repeated by using both copper and calibration weights in contrary to the previous data collected by utilizing only the calibration weights. The results are shown in Figure 75. Even though the capacitive response is higher in case of calibration weights (~2.5% vs ~1%), the results seem more relatable to references in case of copper weights (more appropriate shape of the plot). Thus, next experiments were carried out by using this type of weights.

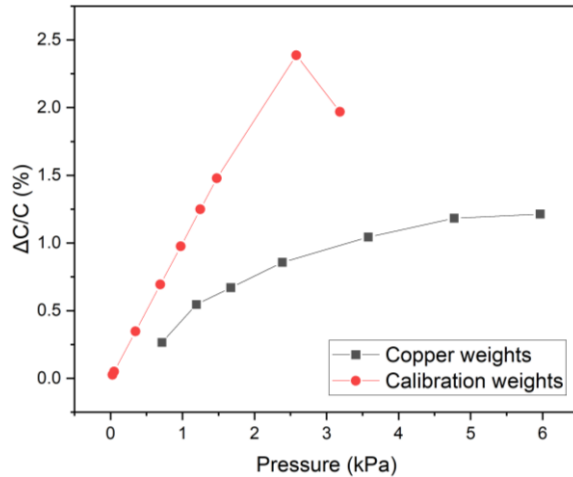


Figure 75. Capacitive responses upon applying two types of weights (calibration and copper weights) on the fabricated pressure sensor.

4.1.2.4 6th, 7th and 8th prototype – Introducing a porous PDMS layer

As the final structure of the desired fabric of the sensor was found, porous PDMS layers were created to compare the sensitivity values of the current and previous sensors. To obtain porous PDMS layers, sugar templates were used. Utilization of a salt or sugar template and their porosity values are described in the literature by, for example, Zhu *et al.* and Dan *et al.*^{65,66} Figure 76 presents photographs of two sugar templated used in the experiment – one with lower sugar content and one with a higher sugar content – and a group of sponges / foams obtained by pouring PDMS on sugar cubes and dissolving the sugar in water.



Figure 76. Sugar templates with a) lower and b) higher content of sugar, and c) foams resulting from pouring PDMS on sugar cubes and dissolving them in water.

Figure 77 present the assembled sensors by using two porous PDMS layers and a PDMS-based foam. The fabric used in these measurements consists of 7 yarns crossing each other in the intersection points. Figure 78 illustrates graphs plotted from the resulting data of capacitive responses. Porous PDMS foam gives the highest change in capacitance ($\sim 18\%$) and the highest sensitivity (0.019 kPa^{-1}). The runner up is the reference sample made of non-porous PDMS with the sensitivity of 0.0092 kPa^{-1} and overall change in capacitance of almost 4%. The layer with a lower number of pores has a smaller overall capacitance change in percentage (1%) and larger sensitivity (0.0023 kPa^{-1}) in comparison to the layer with higher number of pores (1.07% , $S = 0.0009 \text{ kPa}^{-1}$), but the values are very similar to each other, indicating unsuccessful fabrication of porous templates. Likely, sugar was trapped by PDMS, and the granulated particles did not dissolve properly. Thus, sonication was introduced. Nonetheless, the results did not improve significantly. It was decided not to continue experiments with these sugar templates, but only with PDMS foams and non-porous PDMS.

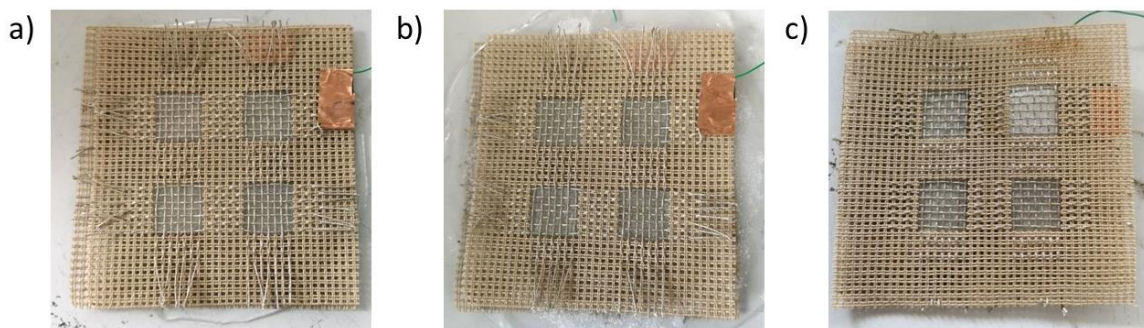


Figure 77. Prototypes with 7 silver-coated yarns crossing each other in the intersections in all 4 contact points utilizing a dielectric PDMS layer with a) the smaller number of pores, b) a higher number of pores, and a c) PDMS foam based on a template made of a sugar cube.

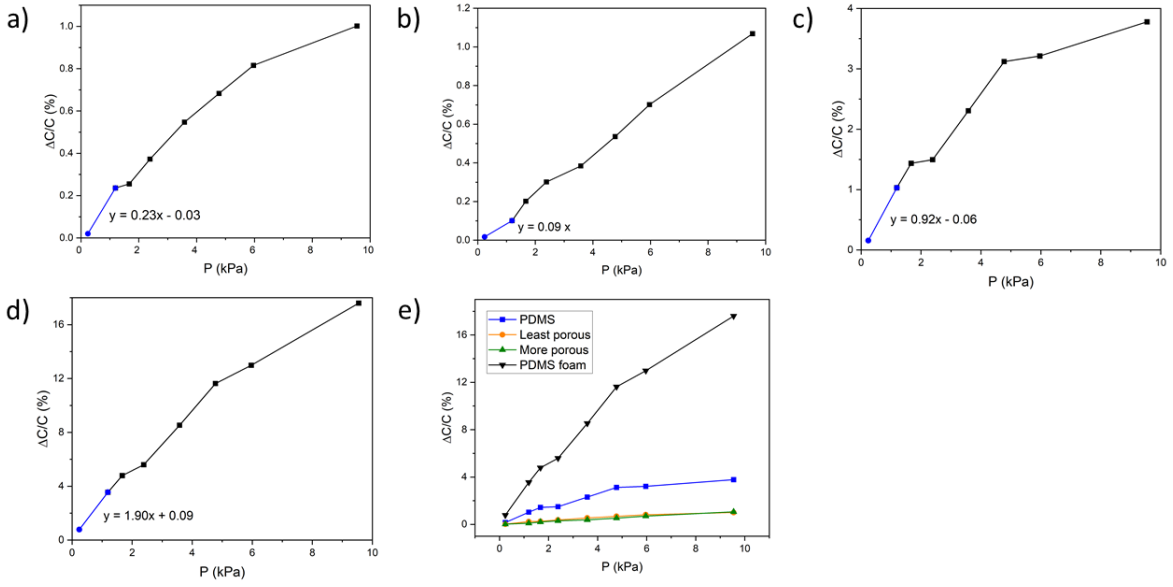


Figure 78. Capacitive responses upon applying pressure on the sensor with a) a less porous PDMS layer, b) more porous PDMS layer, c) non-porous PDMS layer, and d) a PDMS foam. e) Summary of all changes in capacitance values based on the type of the dielectric layer.

4.1.2.5 9th, 10th and 11th prototype – Influence of the number of yarns utilizing PDMS foam as the dielectric layer

After finding the prototype with the highest overall change in capacitance, next experiment aiming to evaluate the impact of different number of yarns on the generated capacitive responses was performed. The hypothesis at this point is that the more yarns, the higher the capacitive response. Surprisingly, the highest change in capacitance (~28%) and the highest sensitivity (0.0432 kPa^{-1}) is exhibited by the fabric with the lowest number of yarns. The second-best result (~20% and $S = 0.0363 \text{ kPa}^{-1}$) was obtained by the fabric with the highest number of yarns. It was concluded that the measurement has to be repeated by utilizing a non-porous PDMS layer. This is because in this setup different PDMS foams were used. Their heights vary, the contraction rate decreases during the passage of time what might influence the data and hinder a reliable comparison.

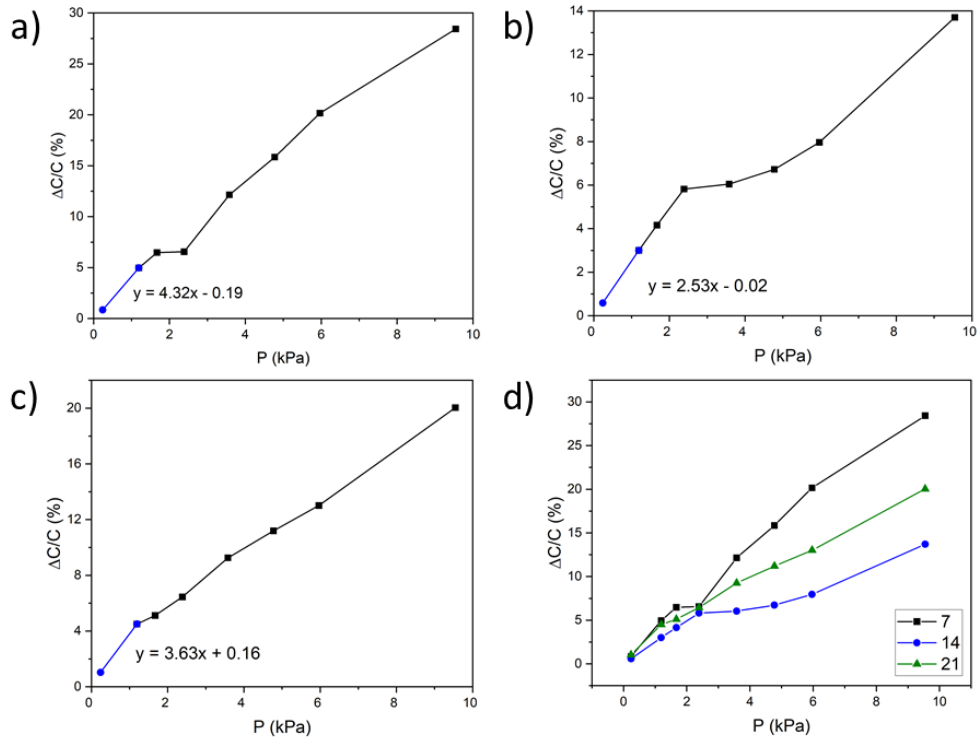


Figure 79. Changes in capacitance detected by applying pressure on sensors fabricated with fabrics having a) 7, b) 14, and c) 21 yarns crossing each other in all intersections of contact points and PDMS foam. d) Summary of capacitive responses of all three sensors.

4.1.2.6 12th, 13th and 14th prototype – Influence of the number of yarns utilizing PDMS as the dielectric layer

The experiment was repeated with a non-porous PDMS layer and a similar dataset was obtained. Again, the fabric with 14 yarns, exhibited the lowest change in capacitance (~23%). The highest capacitance increase showed the fabric with 21 yarns (~37%) and the second highest – fabric with 7 yarns (~31%). This behavior is most probably caused by the number of contact points and by strong, linear alignment. In case of 21 yarns, there are simply the most yarns woven which results in the most dense and highest number of contact points. For 7 yarns, the weaving was strong, there is a lot of tension between the yarns, they aligned parallelly and are the flattest in comparison to other samples. Lastly, the shape of

the curves looks more appropriate for samples with 7 and 21 yarns than for 14 yarns.

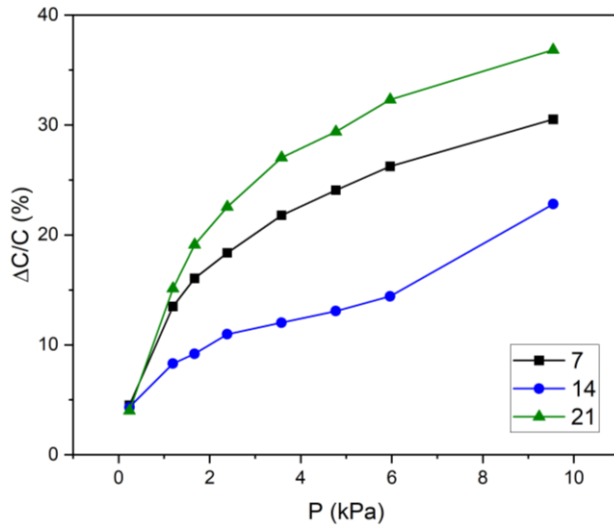


Figure 80. Changes in capacitance measured by applying pressure on sensors fabricated with non-porous PDMS layer and fabrics made of 7, 14, and 21 yarns crossing each other in all intersections of contact points.

In a nutshell, the main obstacles and insights from the fabrication process of the sensors created in this approach include weight selection, stability of the fabrics including the number of yarns used in the contact points, assembly (visibility of contact points, mobile yarns), air gaps (lamination / adhesion between layers), fabrication of porous templates (porosity percentage, heights of the outgoing dielectric layers), impact of different yarn numbers. It is difficult to indicate which prototype is the best as in theory it should consist of porous PDMS foam, but data suggest it to be the non-porous PDMS with 21 yarns ($\Delta C/C_0 = \sim 37\%$, $S = 0.1165 \text{ kPa}^{-1}$) in all contact point intersections. More data should definitely be collected and more thought into the comparison of porous and non-porous PDMS layers based on varying heights should be put.

The future vision of this approach should consider integration in clothing to create a smart fabric, performing wearability-related testing (e.g., breathability), mapping the exact spot of touch by connecting the sensor to an Arduino setup, introducing multifunctionality (e.g., strain sensor), and more. For future iterations, it would be especially beneficial to analyze the state-of-the-art of textile-based capacitive

sensors broader and understand the impact of different number of yarns better. Also, other types of foam templates could be introduced, e.g. nickel template.^{65,67} I believe that it is possible to fabricate a more stable foam (repeatable ability to contract over time) that could be used in multiple iterations.

4.1.3 Approach 3 – Wearable AgNW-based sandwich-type pressure sensor

The last approach consists of fabrication of a wearable AgNW-based sandwich-type pressure sensor on a skin-friendly bio-based substrate. This section is remarkable, because the calculated sensitivity values can be compared to previous prototypes and thus, a conclusion about viability of utilization of AgNWs as a conductive material can be reached. This example broadens the usage range as well.

A significant objective of this method is to manufacture a sensor with low-cost materials that AgNWs are and in an uncomplicated process like microcontact printing. Another advantage of AgNW over a CNT mesh used in similar applications is a higher sensitivity in the low-pressure regime.¹⁹

In opposite to preceding examples, this type of a sensor can be employed as a sticker for continuous monitoring of pressure in the wrist, neck, and eye. The next step to bring this approach to the next level, could be usage of a flexible bio-based substrate which would enable fabrication of multifunctional strain sensors. It is also worth to mention that widely exploited stretchable polymers like PDMS, PU, SR, and polyurethane urea elastomer (PUU), show a poor processability and poor adhesion which opens a wide field for bio-based materials.

4.1.3.1 *Substrate materials*

The optimal substrate material should be bio-based, skin-friendly, and biodegradable. Additionally, it should be flat, and its structure should be stable for weeks at least. These parameters are important because of the next step in prototyping – deposition of AgNWs – as the contact area between the substrate

and the dielectric later should be as large as possible. Lastly, the annealing temperature of AgNWs that has to be performed on a substrate material amounts to about 200°C, but it can be decreased to about 100°C. Thus, the material should be inert during a 30-minute-long treatment at 100°C.

- Cellulose hydrogels

The fabricated cellulose hydrogels were subjected to drying under a fume hood for 4 days. After the first day, the upper surfaces of the samples were relatively dry, the structure was kept well, and there was lots of water left throughout the whole samples. After 4 days, the cellulose hydrogels shrank significantly (about 80%) and became crescentic. The substrate material must keep its original shape for weeks at least and ideally, it must withstand temperatures high as 100°C to enable the required annealing of AgNWs. Having said that, this substrate was concluded not to be appropriate for the purpose.

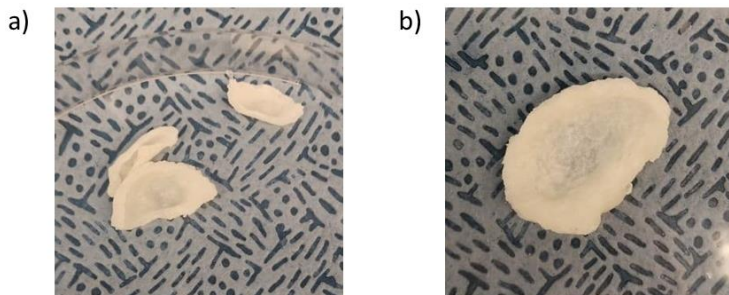


Figure 81. Photograph of the cellulose hydrogels prepared according to two different methodologies after drying in a fume hood for 4 days.

- Nanocellulose film

A more suitable material for the scope of this approach is nanocellulose film. After drying, the film is flexible, flat and it keeps its structure unchanged for weeks. Figure 82 presents how the film looks like after drying in an oven and in room temperature. What is interesting is the number of bubbles that appear upon drying in an oven (air trapping). Degassing might be introduced for the oven-dried sample in the future. In spite of that, such film fits the purpose well.

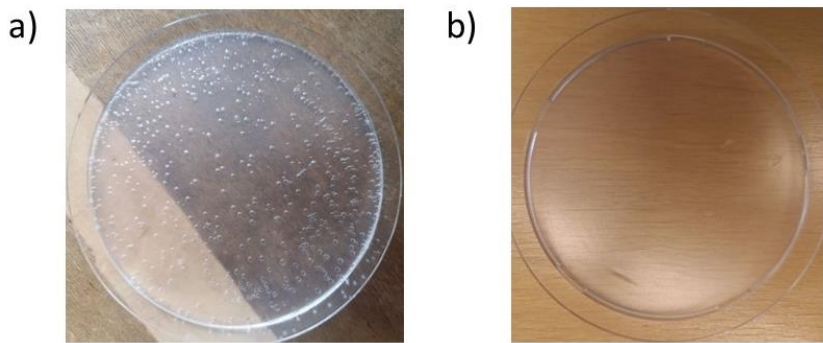


Figure 82. Nanocellulose films after drying in a) an oven and b) in room temperature for some days.

To understand the temperature resistance of this film, a simple test was carried out. Two sections of the same dimension were cut out and subjected to high temperatures – 100°C and 200°C – for 30 minutes. The results are visible in Figure 83. Besides a visible tone shift from transparent to black after placed on a heating plate for 200°C, the second sample became brittle. The hardness of the first sample altered to a higher degree, but the color was only slightly affected. It is important to understand the maximum temperature that can be applied as the AgNWs has to be annealed on the surface of a bio-based substrate. Taking into account that in 100°C the film does not contract nor change its color or properties significantly, surface modification of AgNWs was carried out to decrease the required annealing temperature.

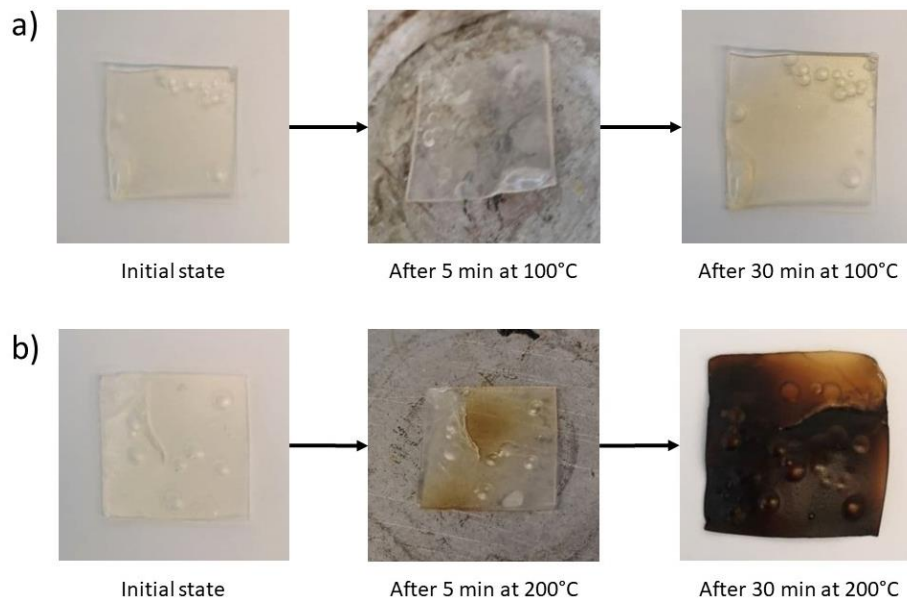


Figure 83. Small sections of the nanocellulose film subjected to 100°C and 200°C for 30 minutes.

4.1.3.2 Prototypes

Two prototypes were created – one with non-porous PDMS layer and the second with a porous PDMS layer. In both cases NFC films coated with AgNWs and annealed in 100°C were utilized. Figure 84 illustrates the sensor with PDMS foam and SEM images of the NFC films surface after coating with AgNWs. The resulting coating is uniform and thick enough to cover the substrate.

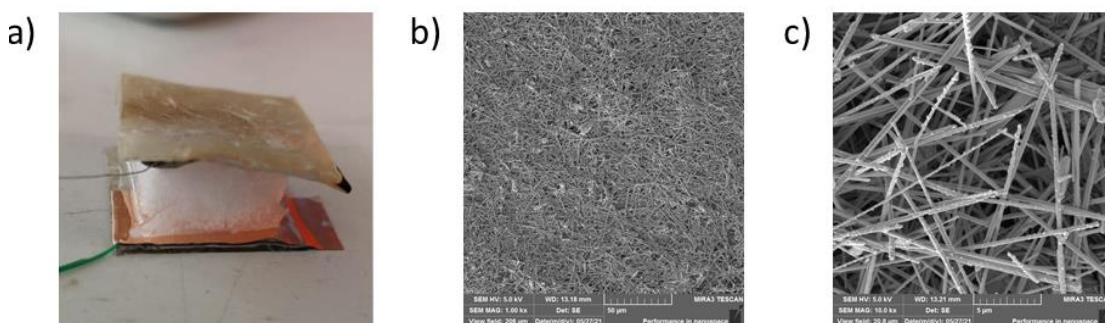
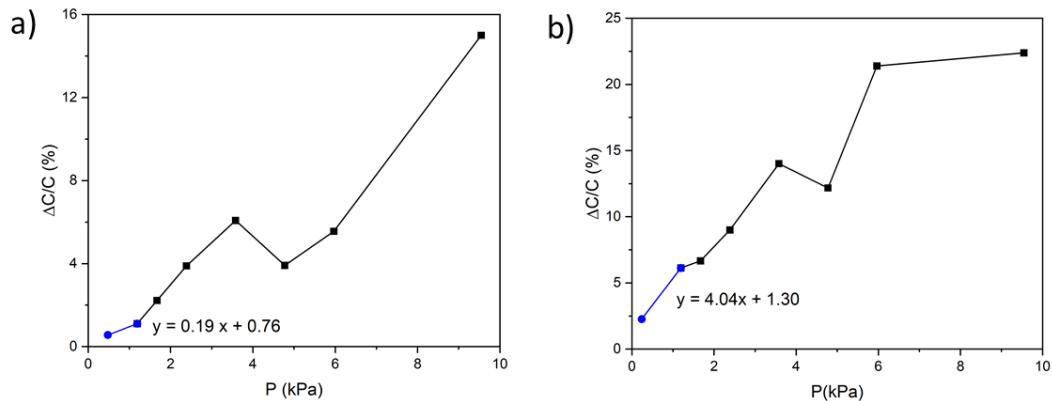


Figure 84. a) Photograph of the sensor made of a PDMS-based foam and NFC films. b-c) SEM images of the NFC films after depositing AgNWs under respectively 1 000 and 10 000 of magnification.

Figure 85 demonstrates the changes in capacitance upon applying pressure with copper weights on both sensors. In the first case of utilization of the PDMS foam, the sensitivity value amounts to 0.0019 kPa^{-1} and the overall increase in capacitance amounts to about 14%. In the second case the sensitivity value is larger and amounts to 0.0404 kPa^{-1} . The overall change in capacitance amounts to more than 20%, and alike sensitivity, it is higher than in the previous example. Oddly, there is a decrease in capacitance around 5 kPa in both cases which in theory should not appear. The non-porous layer works better than the porous foam which might be impacted by assembly issues. Furthermore, the sensitivity value in comparison to Approach 1 is higher, but in contrary to Approach 2 is comparable or lower.



*Figure 85. Capacitive responses of the developed NFC/AgNWs sensor utilizing
a) PDMS foam and b) non-porous PDMS layer.*

There is a potential to develop this approach and reach a higher sensitivity level. However, the most valuable aspect of this system is the application – the sensor can be applied as a sticker on different body parts and pulse might be measured. To achieve this goal, more bio-based materials should be assessed based on their shape stability over time and temperature resistance. Furthermore, the impact of different dielectric layer thickness should be considered, and the assembly process developed.

4.2 Wearable strain sensors

Such fabricated pressure sensors can be enriched in additional materials or measurement techniques and thus, become multifunctional. In this part of research, complementary wearable strain sensors to first two approaches are presented. POC prototypes of wearable yarn-based and textile-sandwich strain sensors were developed, and basic measurements were carried out. In both cases eventually, they would simultaneously act like pressure sensors.

4.2.1 Approach 1 – Wearable yarn-based strain sensors

Figure 86 presents the POC prototype of the first sensor. Upon stretching the resistance changed from 0.73 to 0.79 Ω . Moreover, a single yarn was tested, and the resistance increased from 4.4 to 4.6 Ω . These measurements give the necessary basic information to bring this sensor to the next step and introduce PDMS coating. Intriguingly, based on future needs, the yarn stretchability can be adjusted by changing the length ratio of Spandex to silver-coated nylon yarns. When the tests with PDMS turn out successful, the sample should be upscaled and more data should be gathered. The capacitive responses would be then potentially be linked to various body movements alike in Figure 29 creating interactive digital textiles like those proposed by Poupyrev *et al.*⁶⁸ Finally, wearability-related tests to understanding factors like breathability should be carried out.

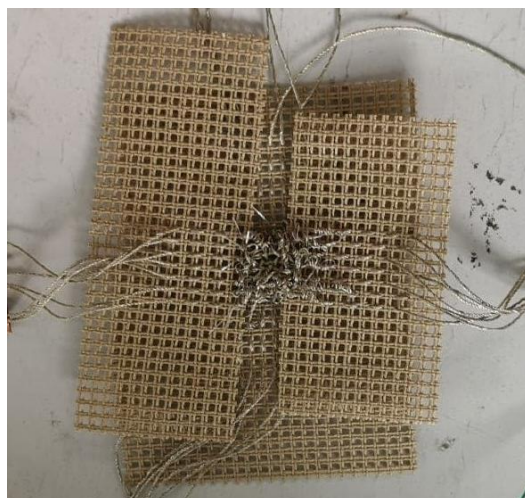


Figure 86. POC prototype of a wearable yarn-based strain sensor.

4.2.2 Approach 2 – Wearable textile-sandwiched strain sensors

Figure 87 presents the POC prototype of a wearable textile-sandwiched strain sensor. The brown fabric pieces on the edges are made of cotton hardened with corn starch, whereas the silver yarns are silver-coated nylon yarns twisted with white elastane yarns. Upon applying force in the vertical direction, the sensor stretches. When the force is released, the material contracts and returns to its original state. The stretchable material in the middle of the picture can change its length from 1 cm to maximum 2 cm. By conducting a simple test, in which the crocodile clips were connected to the fabric and stretching the fabric, it is possible to measure the capacitive response.

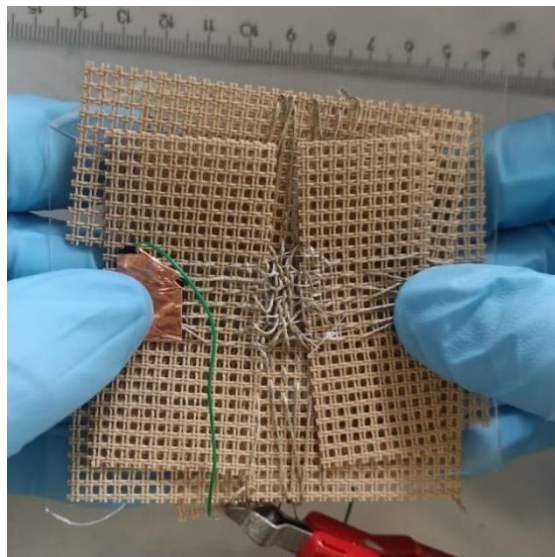


Figure 87. POC prototype of a wearable textile-sandwiched strain sensor.

The changes in capacitance observed at 50% and 100% of strain are presented in Table 9. The values clearly change upon stretching. Nonetheless, the final lengths were measured with a ruler, which is not accurate enough for this purpose. Thus, such large differences in measured capacitance responses at 100% of strain (from 48 pF to 70 pF of change). Moreover, the strain sensor acts simultaneously as a pressure sensor what can be detected as a change in capacitance (e.g., from 4 pF to 12 pF) upon a tighter grip. This experiment should

be scaled up and further measurements should be carried out. For instance, a larger sample could be connected to the multimeter and placed in a tensile tester. This way, a precise length of the sensor could be noted, the initial capacitive response upon pressure of the grip could be detected, and the whole experiment would become more repeatable and reliable. Furthermore, more data should be gathered and evaluated. Ideally as for the previous example, the changes in capacitance could be linked to various body movements and wearability-related tests to understand factors like breathability should be conducted.

Table 9. Capacitive changes upon applying 50% and 100% of strain on the fabricated POC prototype of a strain sensor.

C_0 [pF]	C_1 [pF]	ΔC [pF]	$\Delta C/C$	$\Delta C/C$ [%]	Strain [%]
12.00	38.00	38.00	3.17	316.67	50
12.00	60.00	48.00	4.00	400.00	100
12.00	82.00	70.00	5.83	583.33	
16.00	65.00	49.00	3.06	306.25	

5 Conclusions

The scope of the research was to introduce and fabricate wearable capacitive pressure sensors and complementary strain sensing devices. In the first approach referred to as yarn-based class, 8 iterations before the final pressure sensor prototype and a POC prototype of the strain sensor were completed. The leading pressure sensor exhibits overall change in capacitance of 18% and sensitivity of 0.0209 kPa^{-1} upon applying pressure in the range from 0.2 kPa to 9.5 kPa. Resistance of the POC prototype of the strain sensor in this category alternates from 0.73 to 0.79 Ω ($= 8\%$). In the second approach called textile-sandwiched, 14 pressure sensing devices iterations were assembled, and the top-notch prototype shows 37% of capacitance change and 0.1165 kPa^{-1} of sensitivity. The overall growth of capacitance of the complementing strain sensor amounts to 317% upon 50% strain. Finally, two pressure sensors were created in the third concept (AgNW-based sandwich-type) and the surpassing iteration demonstrates increase of capacitive response of 22% and sensitivity of 0.0404 kPa^{-1} . All sensors are more sensitive in the low weight region. Altogether, the research emerges as successful due to a broad base understanding of the required fabrication process and numerous insights regarding future advancements.

In each category different next steps should be implemented. For instance, in the first approach of pressure sensors, mainly a more agile coating process should be proposed keeping in mind impact of the PDMS thickness. Concerning the second approach, the most crucial obstacles were stability of fabric, assembly because of hindered visibility of contact points and mobile yarns, and air gaps appearance that could be fixed by adjusting the adhesion between layers. Weaving should be more extensively analyzed in both cases. In the last approach, a broader range of bio-based material assortment should be studied by taking into account shape alteration over time and temperature resistance. Pertaining to

strain sensors, current setup must be changed in light of measuring strain and capacitance simultaneously, and noting capacitive response upon grip.

All in all, experiments with other even softer and potentially more sensitive dielectric materials, like Ecoflex silicone, wool or felt, and porosity ratios should be carried out. Wool is especially noteworthy as it would enable realization of comfortably wearable and breathable textiles. In addition, different base fabrics could be taken into consideration. Choice of templates, e.g., nickel template instead of sugar, might lead to higher repeatability and better reliability of results. Besides, more thought into lamination processes of sensors should be put and appropriate wearability-related tests should be performed. Another essential factor that could be addressed is an easier adjustable number of yarns by introducing a thinner yarns, hence, denser network. After the above-mentioned ideas and insights are evaluated and more data is collected, multifunctionality can be implemented in a less burdensome manner. Not only strain sensors can be united, but also farther more abstract functions can be integrated leading to development of enthralling examples of multifunctional sensors.

6 References

1. Yao S, Zhu Y. Wearable multifunctional sensors using printed stretchable conductors made of silver nanowires. *Nanoscale*. 2014;6(4):2345-2352. doi:10.1039/c3nr05496a
2. Wu R, Ma L, Hou C, et al. Silk Composite Electronic Textile Sensor for High Space Precision 2D Combo Temperature–Pressure Sensing. *Small*. 2019;15(31):1-11. doi:10.1002/smll.201901558
3. Chen G-T, Su C-H, Wei S-H, et al. Photo-Curable Ion-Enhanced Fluorinated Elastomers for Pressure-Sensitive Textiles. *Adv Intell Syst*. 2020;2(4):1900180. doi:10.1002/aisy.201900180
4. Grand View Research. Wearable Sensors Market Worth \$2.86 Billion By 2025 | CAGR: 38.8%. <https://www.grandviewresearch.com/press-release/wearable-sensors-market>. Published 2018. Accessed April 2, 2021.
5. Gu C, Chen S, Guo X. Transparent elastic capacitive pressure sensors based on silver nanowire electrodes. *8th Annu IEEE Int Conf Nano/Micro Eng Mol Syst IEEE NEMS* 2013. 2013;1:1183-1185. doi:10.1109/NEMS.2013.6559930
6. Chen S, Guo X. Improving the Sensitivity of Elastic Capacitive Pressure Sensors Using Silver Nanowire Mesh Electrodes. *IEEE Trans Nanotechnol*. 2015;14(4):619-623. doi:10.1109/TNANO.2015.2422993
7. Zang Y, Zhang F, Di CA, Zhu D. Advances of flexible pressure sensors toward artificial intelligence and health care applications. *Mater Horizons*. 2015;2(2):140-156. doi:10.1039/c4mh00147h
8. Subasi A. Introduction and Background. In: *Practical Guide for Biomedical Signals Analysis Using Machine Learning Techniques*. Vol 4. Elsevier; 2019:1-26. doi:10.1016/B978-0-12-817444-9.00001-5
9. Zhang Q, Wang YL, Xia Y, Kirk TV, Chen XD. Textile-Only Capacitive Sensors with a Lockstitch Structure for Facile Integration in Any Areas of a

- Fabric. ACS Sensors. 2020;5(6):1535-1540.
doi:10.1021/acssensors.0c00210
10. Zeiser R, Fellner T, Wilde J. Capacitive strain gauges on flexible polymer substrates for wireless, intelligent systems. *J Sensors Sens Syst.* 2014;3(1):77-86. doi:10.5194/jsss-3-77-2014
 11. Zhang Q, Wang YL, Xia Y, Zhang PF, Kirk T V., Chen XD. Textile-Only Capacitive Sensors for Facile Fabric Integration without Compromise of Wearability. *Adv Mater Technol.* 2019;4(10):1-11.
doi:10.1002/admt.201900485
 12. Tan Q, Li C, Xiong J, et al. A high temperature capacitive pressure sensor based on alumina ceramic for in situ measurement at 600 °C. *Sensors (Switzerland).* 2014;14(2):2417-2430. doi:10.3390/s140202417
 13. Xiong Y, Shen Y, Tian L, et al. A flexible, ultra-highly sensitive and stable capacitive pressure sensor with convex microarrays for motion and health monitoring. *Nano Energy.* 2020;70(September 2019):104436.
doi:10.1016/j.nanoen.2019.104436
 14. Mannsfeld SCB, Tee BCK, Stoltenberg RM, et al. Highly sensitive flexible pressure sensors with microstructured rubber dielectric layers. *Nat Mater.* 2010;9(10):859-864. doi:10.1038/nmat2834
 15. Kang BS, Kim J, Jang S, et al. Capacitance pressure sensor based on GaN high-electron-mobility transistor-on-Si membrane. *Appl Phys Lett.* 2005;86(25):1-3. doi:10.1063/1.1952568
 16. He Z, Chen W, Liang B, et al. Capacitive Pressure Sensor with High Sensitivity and Fast Response to Dynamic Interaction Based on Graphene and Porous Nylon Networks. *ACS Appl Mater Interfaces.* 2018;10(15):12816-12823. doi:10.1021/acsami.8b01050
 17. Kim J, Nga Ng T, Soo Kim W. Highly sensitive tactile sensors integrated with organic transistors. *Appl Phys Lett.* 2012;101(10).
doi:10.1063/1.4751354
 18. Pan L, Chortos A, Yu G, et al. An ultra-sensitive resistive pressure sensor based on hollow-sphere microstructure induced elasticity in conducting

- polymer film. *Nat Commun.* 2014;5. doi:10.1038/ncomms4002
- 19. Lipomi DJ, Vosgueritchian M, Tee BCK, et al. Skin-like pressure and strain sensors based on transparent elastic films of carbon nanotubes. *Nat Nanotechnol.* 2011;6(12):788-792. doi:10.1038/nnano.2011.184
 - 20. Choong CL, Shim MB, Lee BS, et al. Highly stretchable resistive pressure sensors using a conductive elastomeric composite on a micropyramid array. *Adv Mater.* 2014;26(21):3451-3458. doi:10.1002/adma.201305182
 - 21. Wang X, Gu Y, Xiong Z, Cui Z, Zhang T. Silk-molded flexible, ultrasensitive, and highly stable electronic skin for monitoring human physiological signals. *Adv Mater.* 2014;26(9):1336-1342. doi:10.1002/adma.201304248
 - 22. Zhu SE, Krishna Ghatkesar M, Zhang C, Janssen GCAM. Graphene based piezoresistive pressure sensor. *Appl Phys Lett.* 2013;102(16):9-12. doi:10.1063/1.4802799
 - 23. Pang C, Lee GY, Kim T II, et al. A flexible and highly sensitive strain-gauge sensor using reversible interlocking of nanofibres. *Nat Mater.* 2012;11(9):795-801. doi:10.1038/nmat3380
 - 24. Li C, Wu PM, Shutter LA, Narayan RK. Dual-mode operation of flexible piezoelectric polymer diaphragm for intracranial pressure measurement. *Appl Phys Lett.* 2010;96(5):6-9. doi:10.1063/1.3299003
 - 25. Chen Z, Wang Z, Li X, et al. Flexible Piezoelectric-Induced Pressure Sensors for Static Measurements Based on Nanowires/Graphene Heterostructures. *ACS Nano.* 2017;11(5):4507-4513. doi:10.1021/acsnano.6b08027
 - 26. Graz I, Krause M, Bauer-Gogonea S, et al. Flexible active-matrix cells with selectively poled bifunctional polymer-ceramic nanocomposite for pressure and temperature sensing skin. *J Appl Phys.* 2009;106(3). doi:10.1063/1.3191677
 - 27. Buchberger G, Schwödiauer R, Bauer S. Flexible large area ferroelectret sensors for location sensitive touchpads. *Appl Phys Lett.* 2008;92(12). doi:10.1063/1.2903711
 - 28. Joshi AB, Kalange AE, Bodas D, Gangal SA. Simulations of piezoelectric

- pressure sensor for radial artery pulse measurement. *Mater Sci Eng B Solid-State Mater Adv Technol.* 2010;168(1):250-253. doi:10.1016/j.mseb.2010.01.012
- 29. You X, He J, Nan N, et al. Stretchable capacitive fabric electronic skin woven by electrospun nanofiber coated yarns for detecting tactile and multimodal mechanical stimuli. *J Mater Chem C.* 2018;6(47):12981-12991. doi:10.1039/C8TC03631D
 - 30. Choi J, Kwon D, Kim K, et al. Synergetic Effect of Porous Elastomer and Percolation of Carbon Nanotube Filler toward High Performance Capacitive Pressure Sensors. *ACS Appl Mater Interfaces.* 2020;12(1):1698-1706. doi:10.1021/acsami.9b20097
 - 31. Oggioni C, Jakovljevic DG, Klonizakis M, et al. Dietary nitrate does not modify blood pressure and cardiac output at rest and during exercise in older adults: a randomised cross-over study. *Int J Food Sci Nutr.* 2018;69(1):74-83. doi:10.1080/09637486.2017.1328666
 - 32. Liu X, Zhu Y, Nomani MW, Wen X, Hsia TY, Koley G. A highly sensitive pressure sensor using a Au-patterned polydimethylsiloxane membrane for biosensing applications. *J Micromechanics Microengineering.* 2013;23(2). doi:10.1088/0960-1317/23/2/025022
 - 33. Metzger C, Fleisch E, Meyer J, et al. Flexible-foam-based capacitive sensor arrays for object detection at low cost. *Appl Phys Lett.* 2008;92(1):1-4. doi:10.1063/1.2830815
 - 34. Hu W, Niu X, Zhao R, Pei Q. Elastomeric transparent capacitive sensors based on an interpenetrating composite of silver nanowires and polyurethane. *Appl Phys Lett.* 2013;102(8). doi:10.1063/1.4794143
 - 35. Kim SR, Kim JH, Park JW. Wearable and Transparent Capacitive Strain Sensor with High Sensitivity Based on Patterned Ag Nanowire Networks. *ACS Appl Mater Interfaces.* 2017;9(31):26407-26416. doi:10.1021/acsami.7b06474
 - 36. Atalay O. Textile-based, interdigital, capacitive, soft-strain sensor for wearable applications. *Materials (Basel).* 2018;11(5).

- doi:10.3390/ma11050768
- 37. Atalay O, Richard Kennon W, Dawood Husain M. Textile-based weft knitted strain sensors: Effect of fabric parameters on sensor properties. *Sensors (Switzerland)*. 2013;13(8):11114-11127. doi:10.3390/s130811114
 - 38. Gullapalli H, Vemuru VSM, Kumar A, et al. Flexible piezoelectric zno-paper nanocomposite strain sensor. *Small.* 2010;6(15):1641-1646. doi:10.1002/smll.201000254
 - 39. Sirohi J, Chopra I. Fundamental understanding of piezoelectric strain sensors. *J Intell Mater Syst Struct.* 2000;11(4):246-257. doi:10.1106/8BFB-GC8P-XQ47-YCQ0
 - 40. Neverauskas A, Rupkus S, Kacinskas S. Surface Acoustic Wave Sensors. *Elektron ir Elektrotehnika.* 2016;17(4):1-11. doi:10.5755/j01.eie.17.4.16027
 - 41. Chan THT, Yu L, Tam HY, et al. Fiber Bragg grating sensors for structural health monitoring of Tsing Ma bridge: Background and experimental observation. *Eng Struct.* 2006;28(5):648-659. doi:10.1016/j.engstruct.2005.09.018
 - 42. Kang LH, Kim DK, Han JH. Estimation of dynamic structural displacements using fiber Bragg grating strain sensors. *J Sound Vib.* 2007;305(3):534-542. doi:10.1016/j.jsv.2007.04.037
 - 43. Wojciechowski KE. Electronics for Resonant Sensors. 2005.
 - 44. Ferri M, Belsito L, Mancarella F, et al. Fabrication and testing of a high resolution extensometer based on resonant MEMS strain sensors. *2011 16th Int Solid-State Sensors, Actuators Microsystems Conf TRANSDUCERS'11.* 2011:1056-1059. doi:10.1109/TRANSDUCERS.2011.5969171
 - 45. Tian M, Zhao R, Qu L, et al. Stretchable and Designable Textile Pattern Strain Sensors Based on Graphene Decorated Conductive Nylon Filaments. *Macromol Mater Eng.* 2019;304(10):1-12. doi:10.1002/mame.201900244
 - 46. Wang H, Liu Z, Ding J, et al. Downsized sheath–core conducting fibers for

- weavable superelastic wires, biosensors, supercapacitors, and strain sensors. *Adv Mater.* 2016;28(25):4998-5007. doi:10.1002/adma.201600405
47. Cai L, Song L, Luan P, et al. Super-stretchable, transparent carbon nanotube-based capacitive strain sensors for human motion detection. *Sci Rep.* 2013;3:1-9. doi:10.1038/srep03048
48. Hirzebruch FEP, Kreck M. On the concept of genus in topology and complex analysis. *Not Am Math Soc.* 2009;56(6):713-719.
49. Chen L, Lu M, Yang H, et al. Textile-Based Capacitive Sensor for Physical Rehabilitation via Surface Topological Modification. *ACS Nano.* 2020;14(7):8191-8201. doi:10.1021/acsnano.0c01643
50. Lou M, Abdalla I, Zhu M, Yu J, Li Z, Ding B. Hierarchically Rough Structured and Self-Powered Pressure Sensor Textile for Motion Sensing and Pulse Monitoring. *ACS Appl Mater Interfaces.* 2020;12(1):1597-1605. doi:10.1021/acsmi.9b19238
51. Lou M, Abdalla I, Zhu M, et al. Highly Wearable, Breathable, and Washable Sensing Textile for Human Motion and Pulse Monitoring. *ACS Appl Mater Interfaces.* 2020;12(17):19965-19973. doi:10.1021/acsmi.0c03670
52. Zhao Z, Huang Q, Yan C, et al. Machine-washable and breathable pressure sensors based on triboelectric nanogenerators enabled by textile technologies. *Nano Energy.* 2020;70(January):104528. doi:10.1016/j.nanoen.2020.104528
53. Lan L, Zhao F, Yao Y, Ping J, Ying Y. One-Step and Spontaneous in Situ Growth of Popcorn-like Nanostructures on Stretchable Double-Twisted Fiber for Ultrasensitive Textile Pressure Sensor. *ACS Appl Mater Interfaces.* 2020;12(9):10689-10696. doi:10.1021/acsmi.0c00079
54. Agcayazi T, Tabor J, McKnight M, Martin I, Ghosh TK, Bozkurt A. Fully-Textile Seam-Line Sensors for Facile Textile Integration and Tunable Multi-Modal Sensing of Pressure, Humidity, and Wetness. *Adv Mater Technol.* 2020;5(8):1-15. doi:10.1002/admt.202000155
55. Dong H, Snyder JF, Williams KS, Andzelm JW. Cation-induced hydrogels

- of cellulose nanofibrils with tunable moduli. *Biomacromolecules*. 2013;14(9):3338-3345. doi:10.1021/bm400993f
- 56. Lee K, Jeon Y, Kim D, et al. Double-crosslinked cellulose nanofiber based bioplastic films for practical applications. *Carbohydr Polym*. 2021;260(February):117817. doi:10.1016/j.carbpol.2021.117817
 - 57. Kääriäinen P, Tervinen L, Vuorinen T, Riutta N. *The CHEMARTS Cookbook.*; 2020.
 - 58. Lee P, Lee J, Lee H, et al. Highly stretchable and highly conductive metal electrode by very long metal nanowire percolation network. *Adv Mater*. 2012;24(25):3326-3332. doi:10.1002/adma.201200359
 - 59. Lee J, Lee P, Lee H, Lee D, Lee SS, Ko SH. Very long Ag nanowire synthesis and its application in a highly transparent, conductive and flexible metal electrode touch panel. *Nanoscale*. 2012;4(20):6408-6414. doi:10.1039/c2nr31254a
 - 60. Lee JH, Lee P, Lee D, Lee SS, Ko SH. Large-scale synthesis and characterization of very long silver nanowires via successive multistep growth. *Cryst Growth Des*. 2012;12(11):5598-5605. doi:10.1021/cg301119d
 - 61. Schwanghart H. Measurement of contact area, contact pressure and compaction under tires in soft soil. *J Terramechanics*. 1991;28(4):309-318. doi:10.1016/0022-4898(91)90012-U
 - 62. SensorsONE Ltd. g/cm² to psi Conversion Table. <https://www.sensorsone.com/g-cm2-to-psi-conversion-table/>. Accessed April 25, 2021.
 - 63. Hwang BU, Zabeb A, Trung TQ, et al. A transparent stretchable sensor for distinguishable detection of touch and pressure by capacitive and piezoresistive signal transduction. *NPG Asia Mater*. 2019;11(1). doi:10.1038/s41427-019-0126-x
 - 64. Liu M, Pu X, Jiang C, et al. Large-Area All-Textile Pressure Sensors for Monitoring Human Motion and Physiological Signals. *Adv Mater*. 2017;29(41):1-9. doi:10.1002/adma.201703700

65. Zhu D, Handschuh-Wang S, Zhou X. Recent progress in fabrication and application of polydimethylsiloxane sponges. *J Mater Chem A*. 2017;5(32):16467-16497. doi:10.1039/c7ta04577h
66. Dan L, Shi S, Chung HJ, Elias A. Porous Polydimethylsiloxane-Silver Nanowire Devices for Wearable Pressure Sensors. *ACS Appl Nano Mater.* 2019;2(8):4869-4878. doi:10.1021/acsanm.9b00807
67. Chen M, Zhang L, Duan S, Jing S, Jiang H, Li C. Highly stretchable conductors integrated with a conductive carbon nanotube/graphene network and 3D porous poly (dimethylsiloxane). *Adv Funct Mater.* 2014;24(47):7548-7556. doi:10.1002/adfm.201401886
68. Poupyrev I, Gong NW, Fukuhara S, Karagozler ME, Schwesig C, Robinson KE. Project Jacquard: Interactive digital textiles at scale. *Conf Hum Factors Comput Syst - Proc.* 2016:4216-4227. doi:10.1145/2858036.2858176